

The influence of environmental toxins on the pulmonary system

By

Kimberly C. McCrae

A thesis
Submitted to the Faculty of Graduate Studies
in partial fulfillment of the requirements
for the Degree of

Ph.D.

Department of Oral Biology
Faculty of Dentistry
University of Manitoba
Winnipeg, Manitoba

© November, 2004

THE UNIVERSITY OF MANITOBA
FACULTY OF GRADUATE STUDIES

COPYRIGHT PERMISSION

The influence of environmental toxins on the pulmonary system

BY

Kimberly C. McCrae

**A Thesis/Practicum submitted to the Faculty of Graduate Studies of The University of
Manitoba in partial fulfillment of the requirement of the degree**

Of

Doctor of Philosophy

Kimberly C. McCrae © 2004

Permission has been granted to the Library of the University of Manitoba to lend or sell copies of this thesis/practicum, to the National Library of Canada to microfilm this thesis and to lend or sell copies of the film, and to University Microfilms Inc. to publish an abstract of this thesis/practicum.

This reproduction or copy of this thesis has been made available by authority of the copyright owner solely for the purpose of private study and research, and may only be reproduced and copied as permitted by copyright laws or with express written authorization from the copyright owner.

Table of contents

Acknowledgements.....	3
Abstract.....	5
Abbreviations list.....	6
<u>General introduction</u>	
Part 1: The lungs.....	7
Part 2: Alterations to the respiratory system.....	11
Part 3: Novel techniques used for analyses.....	18
Section 1: Lung Cancer	
Chapter 1: Lung cancer: occurrence and new possibilities for detection.....	35
Chapter 2: Analysis of neoplastic changes in mouse lung using FTIR.....	67
Chapter 3: FTIR analysis of human lung tissue DNA.....	91
Section 2: Pulmonary surfactant	
Chapter 4: The effects of hypercholesterolemia on pulmonary surfactant function.....	111
Chapter 5: Altered airway surfactant composition and function in hypercholesterolemic mice with pre-existing lung adenocarcinoma.....	135
Section 3: <i>Stachybotrys chartarum</i>	
Chapter 6: Analysis of pulmonary surfactant by FTIR spectroscopy following exposure to <i>Stachybotrys chartarum</i> (atra) spores.....	165
Chapter 7: DNA fragmentation in developing lung fibroblasts exposed to <i>Stachybotrys chartarum</i> (atra) spores.....	194
<u>General conclusions</u>	217

Acknowledgements

Baruch Atah Adonai, Elhoheinu Melech Ha'Olam, Oseh Ma'aseh B'reishit

Blessed are You, Eternal One our God, Universal Presence, who makes the works of Creation

I am grateful and thankful to the Lord for giving me the opportunity of a lifetime—to study Your creation; You have been my Help, my Teacher, all along. I trust in You Lord with all my heart and lean not on my own understanding; in all my ways I acknowledge You and You will direct my paths (Prov 3:6), grazie Signore!

To my Mom and Dad (my community), I cannot be grateful enough for your support and encouragement. To Brady and Lisa and my nieces and nephew; Rebekah, Emily, and Tanner, may you accomplish so much more than your ol' Auntie Bim! (Baby and Beanie—see you soon). And to the many people who prayed—thank you!

To my fellow students (Caroline, Rick, Rana, John, Mike, Craig, Jenny, Olga, etc), it was a pleasure learning with you; all the best in your future endeavors. To the many technicians ('botton-dweller' Bev, Lynn, Karol, Paul, Sarah, Angie, etc), it was a pleasure learning from you. To the many administrative assistants at U of M and NRC (Linda, Bev, Yvonne, Pauline, Nancy, Nicole, etc) your help was invaluable. To the animal care staff at U of M (Sandy, Kathy, Stephanie, Shirley, etc), your help was vital. To the 'computer people' at NRC (Randy, Gord, Kristy, Walter, Shelly, Larry, Kim, etc) your help was essential. To the library staff at NRC (Liane, Vera, CISTI, etc) you made the quest for knowledge even easier. To the Commissionaires at NRC (Mel, Terri, Mak, Bob, Gerald, Carol, Dale, Geoff, Larry, Rick, etc) you made coming to work a pleasure.

To Dr. J.E. Scott (or just Dr. Scott), you took a risk in your willingness to take me on as a student when other faculty members said I "didn't have the skills [or] the smarts to be a grad student." Hmmm, seven papers (published/submitted) later and two entirely new research directions...You once said we were a 'deadly combination' and I think *because of* that we accomplished so much. Your method of teaching me was brilliant, you emphasized independence early in my program and you pretty much left me alone to

figure things out, which that made all the difference. This thesis comes from my heart, so I say thanks—with much gratitude.

To Dr. Thliveris (or just Dr. T), you once took the time to listen to my concerns. You also gave me some worthwhile advice at a particularly ‘rough time’ during my program, you quoted a Latin phrase, which loosely translated was “don’t let the turkeys get you down” (sorry, I cannot remember the Latin version). You also called me “colleague”—that made a difference—thank you.

To Dr. Shaw (or just Tony) you taught me about infrared spectroscopy, thank you. To Dr. Sowa (or just Mike) I had the opportunity to observe your leadership qualities, specifically your commitment to your staff, and I appreciated your straightforward comments—thank you.

To Dr. Mantsch (former committee member), your enthusiasm for research was contagious. To Dr. Rand, your research inspired me to be creative—thank you. To Dr. David Gregory (former nursing supervisor, Faculty of Nursing) you inspired me to work hard—thank you!

To the granting agencies for much needed financial support: University of Manitoba Fellowship, Health Sciences Center Foundation Studentship, Western Canada Dental Society Scholarship, Manitoba Institute of Child Health (Biology of Breathing Group), and Dr.Scott.

Abstract

The lungs are composed of an architectural framework, conducting airways, and alveolar sacs. To prevent collapse of lung tissue, alveolar type II (AT II) cells produce pulmonary surfactant (PS), an amphipathic material composed mostly of saturated phospholipids and cholesterol that lines the air/water interface. Alterations to lung cells (neoplastic transformation) or the PS system (composition and function) may result in respiratory complications. We studied the biochemical composition of urethane-induced AT II neoplasms, the role of cholesterol in PS function, and the effect of exposure to pulmonary toxins produced by the mold *S. chartarum*. To assess biochemical alterations of neoplastic mouse lung and excised human lung neoplasms, we used a novel technique called Fourier-transform infrared spectroscopy (FTIR), which provides information based on absorption patterns of molecules. Results showed unique biochemistry of mouse neoplasms compared to normal mouse lung. Analyses of human lung lesions revealed also unique but subtle biochemical differences between neoplasms. To study PS function we used capillary surfactometry (CS), which analyzes the ability of a surface-active material to ensure free airflow, thus simulating the small airways. Results demonstrated that excess cholesterol within PS obtained from healthy and tumor-bearing hypercholesterolemic mice had diminished ability to maintain free airflow. Finally, FTIR analyses of PS from mice exposed to *S. chartarum* spores demonstrated alterations to PS phospholipids. *S. chartarum*'s epigenetic properties were revealed by through analyses of lung fibroblast DNA fragmentation. Alterations to DNA biochemistry, excess PS cholesterol, and epigenetic properties of *S. chartarum* spore toxins may contribute to the development of reversible and/or irreversible respiratory disorders and diseases.

Abbreviations list (alphabetical order)

Alkali-labile sites (A-LS); Alveolar macrophages (AM); Alveolar Type I (AT I); Alveolar Type II (AT II); Adenocarcinoma (AC); Bronchoalveolar lavage (BAL); Capillary surfactometry (CS); Computed tomography (CT); Deoxyribonucleic acid (DNA); Dipalmitoylphosphatidylcholine (DPPC); Extracellular matrix (ECM); Fourier-transform infrared spectroscopy (FTIR); Lamellar bodies (LB); Large cell carcinoma (LCC); Linear discriminant analysis (LDA); Lung adenocarcinoma (LA); Lung liquid lining (LLL); Magnetic Resonance Imaging (MRI); Non-small cell lung carcinoma (NSCLC); Optimal region selection (ORS); Organizing pneumonia (OP); Phosphatidylcholine (PC); Phosphatidylethanolamine (PE); Phosphatidylglycerol (PG); Phosphatidylinositol (PI); Polymerase chain reaction (PCR); Positron emission tomography (PET); Pulmonary surfactant (PS); Reactive oxygen species (ROS); Ribonucleic acid (RNA); Single cell gel electrophoresis (SCGE); Single strand breaks (SSB); Small cell lung carcinoma (SCLC); Squamous cell carcinoma (SCC); Surface-active film (SAF); Surfactant-associated proteins (SAP); Surfactant proteins-A, B, C, & D (SP); Surfactant reservoir (SR); Terminal airways (TA); Tubular myelin (TM); World Health Organization (WHO)

General introduction

Part 1: The lungs

The lungs present the largest surface area of the human body exposed to the environment, roughly 150 m² [48], and function primarily in absorbing oxygen and releasing carbon dioxide. This occurs in the gas exchange units or alveolar sacs. Alveolar sacs are composed of flattened alveolar type I (AT I) cells attached to endothelial cells via thin basement membranes [6,] creating the thin filter (1/50 the thickness of paper) through which carbon dioxide and oxygen are exchanged [17]. Dispersed throughout the walls of the alveoli are alveolar type II (AT II) cells that synthesize and secrete pulmonary surfactant (PS), an amphipathic material that decreases the surface tension [125] generated by the intermolecular attraction of the ‘lung liquid’ (or fluid) lining (LLL) the alveoli to move into the “bulk” phase [118].

Lungs are composed also of an irregular branching system of conducting airways called the tracheobronchial tree [17,77], which ventilates the lungs. The caliber of the conducting airways becomes increasingly smaller from the trachea to the terminal airways (approximately 2.0 cm to 0.2 mm diameter, respectively) [77]. Attached to the ends of the smallest conducting airways, called terminal airways (TA), are the alveolar sacs. To ensure patency and unobstructed ventilation, the larger airways are composed of structural rudiments such as cartilage and/or smooth muscle cells. The smaller TA however, lack such elements to varying degrees and are therefore prone to physical collapse or formation of liquid occlusions by the LLL [77,90].

The lungs have an architectural framework flexible enough to withstand dynamic mechanical forces during the breathing cycle, yet composed of a minimal amount of very

strong structural material [17]. The alveolar septal fibrous network, most of which form post-natally, separates and connects the alveolar sacs [17,119]. This delicate architectural support system is comprised of extracellular matrix (ECM) elements such as collagen, elastin, fibronectin, proteoglycans, and basement membranes along with a variety of cells including lymphatic, immune, endothelial, and fibroblast [119].

Fetal lungs develop by arborization of conducting airways (and vascular system), until formation of terminal sacs, which give rise to alveolar ducts, is complete—usually by the end of the third trimester [10,80]. By the end of the gestational period, the lungs consist of some physiologically functional gas exchange units and a functional PS system. There is rapid growth of alveolar sacs post-natally and lung tissue surface area continues to expand for at least eight to ten years (in humans) [80]. Lung tissue develops and is maintained by cooperative efforts of mesenchymal cells, epithelial cells, and phagocytic/immune cells.

Fibroblasts are the largest, in number and volume, of the mesenchymal cells [119]. Traditional thinking is that pulmonary fibroblasts function primarily to maintain the integrity of lung tissue, under normal and injurious conditions, through deposition, maintenance, degradation, and remodeling of ECM material [80,119]. Under injurious conditions, e.g. inflammation, fibroblasts interact intimately with phagocytic and immune cells, thereby stimulating fibroblast proliferation, migration, and formation of fibrotic tissue [80]. They play important roles also in lung development. During lung growth, fibroblasts construct the delicate fibrous skeleton on which alveolar sacs are attached. Fibroblasts also function to enhance AT II cell development [50] and may serve as reservoirs for PS substrates (e.g. triglycerides) [87].

AT II cells comprise approximately 16% of total lung cells whereas AT I only roughly 8% [31]. Yet AT I cells are the largest in volume and cover the largest surface area compared to AT II cells, ~93% and 7%, respectively [31,48], which is not surprising since about 92-97% of lung tissue is involved in gas exchange [17,48]. AT II cells serve as stem cells that terminally differentiate into type I cells [10,17], e.g. during development and following injury [10]. AT II cells function as the source of PS. PS is composed of 90% lipids and 10% proteins [92,116]. Surfactant-associated proteins (SAP) are SP-A, B, C, and D [54,92]. PS lipids consist of 80% phosphatidylcholine (PC), 40-50% occurs in a unique saturated form, dipalmitoylphosphatidylcholine (DPPC), 8-15% phosphatidylglycerol (PG) and phosphatidylinositol (PI), approximately 3-5% phosphatidylethanolamine (PE) and about 10% neutral lipids, most of which is free cholesterol (90%) [89,116].

PS is synthesized and secreted by AT II cells and exists in four characteristic forms that may be isolated readily by bronchialveolar lavage and sequential centrifugation techniques (see Section two: Chapters 4 & 5). Most constituents, except cholesterol, are synthesized *de novo* and packaged into concentric membrane bound storage units called lamellar bodies (LB), which is referred to as intracellular surfactant [98,123]. LB are exocytosed into the LLL and rearranged into a lattice-like structure called tubular myelin (TM) [55,98,123] and oligolamellar vesicles [55]. Once secreted, PS material is referred to as extracellular surfactant. TM is reorganized into aggregates for efficient dispersal through the LLL to the surfactant reservoir (SR) [102]. At the SR, SAP play important roles in rapid adsorption of the PS constituents into the air/water interface, called the surface-active film SAF [54,92]. The lipid components, mostly DPPC and some

cholesterol, orientate naturally and rapidly into a compact layer with hydrophobic tails directed to the air phase and hydrophilic heads in the water phase [62].

The water molecules in the LLL create surface tension in the lungs. Due to the strong attraction forces between them, water molecules at the surface of the LLL are pulled toward the interior of the LLL, which creates the surface tension of water [reviewed in 28]. As the surface of the LLL becomes smaller, due to the surface tension, there is a tendency to collapse the tissue lined by the LLL, e.g. atelectasis of the alveolar sacs [17] or occlusion of the small airways [77].

Surface tension is minimized by carefully choreographed collaboration of PS constituents, since individual components *per se* do not make good surfactants. To illustrate, the long saturated acyl chains of DPPC compact easily, giving DPPC films the compressibility or stability at high surface pressures [68]. However because the DPPC film exists in a gel state at physiological temperatures, it does not re-adsorb into the air/water layer rapidly after over-compression [reviewed in 125]. Cholesterol imparts fluidity to the saturated phospholipid film by intercalating between the acyl chains, which interestingly facilitates collapse of the phospholipid film [36,37,111]. Concomitantly, other phospholipids play important roles in fluidizing the film and the SAP are critical for adsorption of SR aggregates into the interface layer [116].

PS components are re-adsorbed into the SR for re-entry into the SAF [125] or exist as oligolamellar vesicles [55] awaiting recycling [55,98,123]. A small number of AT II cells (~30%) recycle a large portion of PS (~60-80%) [91,97] whereas, most of the alveolar macrophages (AM) (~70%) take up a smaller proportion of PS (~20-30%) for degradation [91].

Alterations to the lung cells, ventilation, gas-exchange, or the PS system may result in any number of reversible or non-reversible respiratory conditions. The present work describes (i) urethane-induced AT II neoplasm biochemistry and the effect of neoplasms on PS composition and function, (ii) hypercholesterolemia influence on PS composition and function in TA, and (iii) the impact of a highly toxic mold, *Stachybotrys chartarum*, on PS and genetic material of developing lung fibroblasts. The next part provides some background information about alterations to the pulmonary system and a brief description of techniques, while the next section describes experiments in detail (introduction, methodology, results, discussion, and conclusions), and finally, a summary of findings are presented.

Part 2: Alterations to the respiratory system

[1] The effect of urethane on AT II cells: the Mouse-Urethane Model

Urethane (ethyl carbamate) is a known pulmonary carcinogen. Catabolism (metabolism and elimination) of urethane and the mechanism(s) of action of urethane and/or its derivatives are not completely understood. Once administered to adult mice, urethane is distributed throughout the body [85]. 50% of the urethane may be catabolized within 5 hours [25] and 90% of the dose is catabolized within 24 hours [16]. Roughly 6% of urethane is eliminated in urine [16,25], 90% as CO₂ in expired air within 24 hours of administration [16,120,121], while about 6% remains in the body [16]. Urethane is metabolized by *N*-hydroxylation [12,13,72,85,121]. The urethane molecule itself is believed to be most carcinogenic to lung cells *in vivo* [5,13,5,85], while derivatives such as *N*-methylethylcarbamate and *N*-hydroxyurethane, although carcinogenic *in vitro* have

less carcinogenic activity on lung cells *in vivo* [13,72,82,85]. Other urethane metabolites have no apparent carcinogenicity [reviewed in 5].

Studies using radioactive-labeled urethane demonstrated that some urethane remained attached to DNA, RNA, and cytoplasmic proteins *in vivo* [8,9,14,21]. Bhide et al. [9] demonstrated maximum binding of urethane to DNA within the lungs (as opposed to kidney for example) for up to 12 hours after one intraperitoneal injection. With chronic exposure, urethane may be bound to DNA for a prolonged period, possibly up to two weeks [70-71,94]. The carcinogenic action is believed due to modification of nucleic acids by urethane [12], perhaps alteration of gene sequence or expression [121]. Urethane inhibits initially synthesis of DNA, RNA, and proteins [94]. Two to three weeks following urethane exposure, cell proliferation was markedly increased for a few weeks until nodules are visible then tumor growth slows down [41]. In keeping with these findings, energetic metabolism (e.g. Embden-Meyerhof pathway, Krebs cycle, etc) is higher in early urethane-induced lesions than in the mature neoplasms [3].

The development of urethane-induced lung tumors may depend upon age (carcinogenic potency decreases with age [25]) and sex (tumor incidence higher in male mice and castrated female mice [21]). Although treatment dosage, schedule, and method give variable results in terms of susceptibility of tumor-formation and maximum number/size of tumors [25,41,69-71,88,93,105,120]. Having said that, studies have shown that administration of urethane induces tumors in a variety of tissues, the lungs in particular.

Histologically most researchers describe the tumors as peripherally located, discrete small pearly-white nodules derived mostly from AT II cells (non-ciliated

cuboidal or columnar). Ultrastructurally, the neoplasms resemble morphologically normal AT II cells, e.g. numerous microvilli at the apical surface, an assortment of organelles (e.g. mitochondria, endoplasmic reticulum, Golgi apparatus) with round or oval-shaped nuclei, abundant cytoplasm, and numerous LB [for reviews see 1,15,60,84,104,109,112].

Previous investigations of the effect of urethane on PS involved analyses of homogenates and dissections of normal and neoplastic lung tissues, which provided insight into the synthesis of intracellular surfactant components. Voelker et al. [117] demonstrated that adenomas were capable of maintaining elevated fatty acid production (compared to normal lung cells) by altering levels of key enzymes, acetyl-CoA carboxylase and fatty acid synthase, involved in fatty acid biosynthesis. Klass et al. [73] and Snyder et al. [106-107] found increased quantities of saturated phospholipids within adenomas, while Stoner et al. [108] reported decreased amounts of anionic phospholipids along with elevated quantities of saturated phospholipids. In terms of protein synthesis and PS secretion, Mason et al. [79] demonstrated that cells of urethane-induced lung tumors expressed messenger RNAs for all four surfactant proteins, although Fabio et al. [44] found that SP-A mRNA levels were three to five times higher in tumors. Bocking et al. [11] analyzed lung tissue from urethane-treated mice and found increased activity of esterase-7, an enzyme associated with extrusion of LB into the alveolar space.

AM and/or AT II cells of urethane-treated lungs may be altered, as a result PS may accumulate within the lungs. Dobbs et al. [38] found surfactant components, particularly surfactant proteins (SP-A), inhibited surfactant secretion by normal AT II cells *in vitro*. Since in normal lungs approximately 60-80% of surfactant clearance is by AT II cells and about 20-30% by AM [91], it is possible that the surfactant feedback

system may be altered in neoplastic AT II cells and/or normal AT II cells from urethane-treated lungs, with consequent accumulation of PS. Concomitantly, AM may have diminished capacity to take up efficiently the excess PS; in fact studies have demonstrated AM susceptibility to urethane-induced injury [23,29,30,49].

Altogether, the mouse-urethane lung adenocarcinoma model is an important tool for understanding the effect of a genotoxic substance on AT II cells and PS. This method was used to induce lung adenocarcinoma in mice for the purpose of analyzing the biochemistry of neoplastic tissue with Fourier-transform infrared spectroscopy (discussed in Section 3 and Chapter 2). The function of PS from tumor-bearing lungs was analyzed by capillary surfactometry (discussed in Section 3 and Chapter 4-5).

[2] Hypercholesterolemia influences the PS composition and function in TA

99% of the cholesterol within PS is derived from the blood [57]. It is not clear though which of the 40 plus types of lung cells [74] take up cholesterol and which secrete it as a constituent within PS. Hass & Longmore [56] demonstrated that at least 20% of the cholesterol taken up by AT II cells is destined for release into the LLL for incorporation into extracellular surfactant. Darrah et al. [32] showed that cholesterol was distributed throughout many lung cells but concentrated mostly within lipid vacuoles of septal cells.

Nonetheless, cholesterol is a vital component within surfactant because it enhances the fluidity of the phospholipid film [36-37,89,111,125]. While doing so however, cholesterol tends to facilitate collapse of the film under pressure. Although, cholesterol is most notably associated with heart disease (high serum cholesterol) or cancer (low serum cholesterol) [24], the effect of hypercholesterolemia in lung disease is

not well established. For these reasons, the effect of excess cholesterol on PS composition and function was investigated using a highly innovative hypercholesterolemia mouse model. PS was obtained from healthy and tumor-bearing hypercholesterolemic mice by bronchoalveolar lavage and function was analyzed by capillary surfactometry (discussed in Section 3 and Chapters 4-5).

[3] *Stachybotrys chartarum* influence on PS and genetic material of lung fibroblasts

Thus far the current investigation has focused on non-inhalation substances (urethane and cholesterol) that influence the lungs, particularly the AT II cells and the PS system. However, as mentioned, the lungs function primarily in gas exchange, (i.e. ventilation), consequently substances small enough to enter the lungs may deposit within the lung tissue, perhaps deep within the periphery of the lungs [110]. One example of such materials is *S. chartarum*.

S. chartarum (atra) is a highly toxic black to greenish-black mold that appears slimy when wet and sooty or powdery when dry [67,114]. *S. chartarum* is commonly found worldwide in soil and decaying plant material (such as compost). It has three requirements for colonization: appropriate temperature, proper nutrients, and adequate amount of water. Optimal growth for *S. chartarum* occurs at normal indoor temperatures (20-23°C), although it may tolerate a range of 15 to 30°C [81]. Since it is considered saprotrophic [86], meaning it obtains nutrients from dead moist organic material, it will thrive on water-saturated, low-nitrogen, high-cellulose materials such as hay, straw, and a variety of common paper-based building products (fiber board, wallpaper, books) [51].

S. chartarum requires an unusually large amount of water, approximately 91-98% relative humidity with optimal growth occurring at 94% [81]. Water damage is the most

significant cause of high moisture levels. A variety of situations such as flooding, sewage back-up, roof leaks, and defective plumbing installations may cause water damage. Some homes and buildings may have chronic water damage and subsequent mold problems. The Canada Mortgage and Housing Corporation studied chronic mold problems on the Roseau River Anishinabe First Nation Reserve in southern Manitoba, Canada [18]. In the spring of 1997, this community of approximately 1,000 people was evacuated due to flooding from the Red River. At least 114 houses suffered flood damage due mainly to basement seepage and sewage back-up and of these houses approximately 34 were contaminated with *S. chartarum*.

S. chartarum samples may be collected via bioaerosol, swab, and bulk sampling methods, and cultured on malt extract agar and/or corn meal agar media plates [114]. Air sampling however, may result in false negatives because spores may not be readily aerosolized under very moist conditions [114]. Identification of *S. chartarum* (and other microorganisms) relies on cultural and microscopic methods, however new DNA-based techniques are currently being developed and tested such as fungus-specific PCR that may detect low levels of spores with greater accuracy in a timely fashion [122,126].

S. chartarum gained notoriety in the last century beginning in the 1930-40s and in the mid-nineties for being the cause of health problems, termed stachybotryotoxicosis. This term was coined in the 1930s by a team of Russian scientists when they discovered *S. chartarum* appeared to cause illnesses or deaths of thousands of horses that consumed *S. chartarum*-infested hay [40]. The scientists noted *S. chartarum*'s effect on humans after volunteers(?) rubbed the mold on to their skin and subsequently developed skin rash, coughing, pain in the throat, burning in the nose along with bloody exudate, and

congestion in the chest [40]. In the mid-nineties, *S. chartarum* was thought to be the cause of public health problems (even deaths), especially in infants, e.g. this headline from a major newspaper “Families plagued by home-wrecking mold” [63]. Secondary metabolites produced by this mold, contained in the spores, have been implicated also as a potential biological weapon, apparently as part of Iraq’s biological weapons program [78].

S. chartarum produces spores that contain several highly toxic secondary metabolites called mycotoxins, e.g. satratoxins F, G, H (and isotoxins of the same), roridin A, verrucarins A, stachylysin, stachyrase A, and tricoverrals A & B [65,81]. Research demonstrated that inhalation exposure to the spores, especially those containing mycotoxins, resulted in changes to respiratory epithelium [reviewed in Chapter 7: Table 1]. Indeed, several studies by Rand et al. have shown the effects of *in vivo* exposure to the spores in mice, e.g. uptake of toxins by AM [52,53], inflammatory response to low spore doses [46], changes to lung tissue after long-term exposure (decreased alveolar space) [96], and prelethal oncotic changes to AT II cells [95].

A well-known study reported the health effects, e.g. pulmonary hemorrhage/hemosiderosis, in infants from exposure to *S. chartarum* (Cleveland, OH) [33,83]. Consequently, the American Academy of Pediatrics issued statements on the toxic properties of molds and warned physicians of the potential for indoor molds to cause respiratory illnesses, especially in infants [2]. Interestingly, the Centers for Disease Control (CDC), after reviewing data from the Cleveland study, reported serious flaws in the methodology of that study and concluded that although there was not enough evidence for causal connections between cases of respiratory illnesses and *S. chartarum*,

the plausibility warrants further scientific investigations [20]. For these reasons, the effect of *S. chartarum* on the PS system was studied using FTIR (see Chapter 6) and epigenetic effects on developing lung fibroblasts were investigated using a DNA fragmentation assay called single cell gel electrophoresis (Chapter 7).

Part 3: Novel techniques used for analyses

[1] Fourier-transform infrared spectroscopy (FTIR)

FTIR spectroscopy is based on the interaction between infrared radiation and molecules. Essentially all molecules have a rich spectrum of infrared absorptions and virtually any substance may be characterized based on absorption patterns using FTIR. Consequently this technique has been used extensively to provide biochemical information of a number of biological materials, e.g. biological fluids, blood, tissue, cells, and even teeth [reviewed in 64 and Chapter 1]. Spectra obtained from biological tissues reflect the total biochemical composition of the sample and contain a dizzying array of peaks, which represent functional groups of molecules that comprise lipids, proteins, and DNA [64]. Furthermore, spectra from biological tissues may also look quite similar to each other [101], which sometimes make comparisons very difficult.

However, qualitative and quantitative analyses of spectra yield much information about biological specimens. Infrared measurements may be made in transmission (Chapters 2 & 6) or reflectance (Chapter 3) mode [100]. Acquired spectra are usually processed, e.g. corrected for water vapor and/or background and normalized to avoid differences in absorbances [75]. Once spectra have been processed, the most useful task is to assign the peaks or absorption bands to functional groups, e.g. absorptions at $\sim 1540\text{ cm}^{-1}$ corresponds to the amide II (N-H bending vibration) and $\sim 1650\text{ cm}^{-1}$ signifies the

amide I (C=O stretching vibration) that are believed to reflect protein [64]. Once assignments are made, the next task is to decide on the best approach for the particular research endeavor. The focus of the research may be detecting the presence or absence of a particular analyte within the sample or it may involve complex pattern recognition methods [64].

Complex pattern recognition methods were used to analyze lung adenocarcinomas from mice (Chapter 2). Pattern recognition involves comparing variables within a set of data, e.g. intensity of absorptions or the position of an absorption band, or a combination of any number and type of variable [64,100]. These variables may show distinct patterns within the spectra of a particular specimen, which may characterize biochemically that particular biological tissue [64,100]. The characteristic spectral patterns from the biological specimen may be used to identify similar tissues or distinguish from other tissues. In the current study, two techniques were employed: Optimal Region Selection (ORS) combined with Linear Discriminant Analysis (LDA). ORS searched for subregions within the spectra that may serve to distinguish two sets of point spectra, e.g. 930-935 and 958-968 cm^{-1} , (signifies DNA absorption bands), and LDA was first used to classify the subsets as neoplastic or normal tissue and secondly to predict the classification of an unknown set of spectra from a known lung specimen. These techniques may be helpful diagnostically to distinguish cancerous tissues from healthy tissues with great accuracy (64).

Based on the accuracy of classification (or pattern recognition) in the previous study involving mouse lung neoplasms, another study was launched to analyze human lung lesions (Chapter 3). In this preliminary investigation however, a rather simplified

method of qualitative spectral analysis was chosen. The research endeavor was to identify the presence of particular structural characteristics of the DNA, since FTIR gives information regarding the conformation of molecules [7,35,39,64,113]. The large DNA molecule has characteristic absorption bands, also known as marker bands, that correspond to the particular conformations, e.g. rigid A-form, relaxed B-form, and left-handed Z-form [34,39,113]. The significance of different forms of DNA is not clearly established, however modifications to the structure may affect key cell functions, e.g. gene silencing due to aberrant methylation [4,66]. Alterations to the DNA structure appear to be one hallmark of neoplastic transformation [115,66] including lung cancers [127]. Intratumoral variations within subtypes of lung cancers may arise from multiple changes to genetic material [19,103] and these variations may be useful indicators to study lung cancers and perhaps classify lung neoplasms based on unique DNA architecture.

[2] Capillary surfactometer (CS)

The CS is a novel instrument designed originally to study the surface tension of pure fluids by observing capillary attraction [28]. In principle, due to the strong attraction forces of water molecules to each other, a liquid is pulled into the narrow tube thereby occluding it [reviewed in 42 & 76]. The CS may be used to simulate the small airways and analyze the ability of a liquid to ensure free airflow. Briefly, a fluid occluding a narrow capillary tube is pushed out when air pressure is great enough. A fluid like water, which has high surface tension due to intermolecular attractive forces, will continually flow back into the tube thereby obstructing airflow [76]. However when an amphipathic material like PS is suspended in the water, the lipid molecules, driven by hydrophobicity,

orientate naturally and rapidly forming a layer between the air and water phases. This interface layer with the polar hydrophilic heads oriented into the aqueous layer bind the water molecules preventing the collapse of water back into the narrow tube thus ensuring continuous airflow. This unique method of PS analysis has been used extensively to study substances that may disrupt the surfactant film thereby decreasing the ability to maintain patent airflow [reviewed in 43]. In the following studies, CS was used to analyze the ability of PS with excess cholesterol, obtained from BAL from healthy and lung tumor-bearing mice, to decrease resistance to airflow and maintain patent airways.

[3] Single cell gel electrophoresis (SCGE)

SCGE assay demonstrates the ability of negatively charged DNA to migrate through agarose under an electrical field (principle assumptions of SCGE are discussed in Chapter 7). Rydberg and Johanson developed this technique roughly 20 years ago to detect DNA damage in individual cells [reviewed in 99]. Two versions of SCGE have been established, alkaline (pH>13) and neutral methods (pH 7 or 12.3). This technique has been tested extensively against other DNA analysis methods, e.g. chromosome aberration test [59], flow cytometry [124], micronucleus test [58], alkaline DNA unwinding [47], and alkaline elution of DNA [47]. The advantages of SCGE in detecting DNA damage include sensitivity to detect DNA single and double strand breaks and alkali-labile sites in individual cells, rapid results without being labor-intensive, and requires very little sample (which may be cell suspension or tissues) [reviewed also in 26 & 27].

The information obtained from SCGE depends on the research endeavor. The focus may be to determine the relative amount of DNA damage in cells, in which case

evaluation requires only a light microscope to measure the extent of DNA damage in terms of high, medium, low, or none [45]. More sophisticated computer automated image analysis systems are available as well as lesion-specific enzyme SCGE assays to detect particular kinds of DNA damage [reviewed in 26]. SCGE has been used extensively as a biomonitoring tool to test genotoxicity of many environmental substances [22,27,61]. In the current study SCGE was used to evaluate the effect of *S. chartarum* on developing fetal lung cells.

The following sections are divided into: (1) Lung cancer: lung neoplastic tissue studies using FTIR; (2) Pulmonary surfactant: the role of hypercholesterolemia on PS composition and function using CS; and (3) *Stachybotrys chartarum*: the impact of *S. chartarum* on PS and lung tissue using FTIR and SCGE.

References

1. Amaral-mendes, J.J. (1969). Histopathology of primary lung tumors in the mouse. *J Pathol*, 97, 415-427.
2. American Academy of Pediatrics. (1998). Toxic effects of indoor molds. *Pediatrics*, 101, 712-714.
3. Azzopardi, A., & Thurlbeck, W.M. (1969). The oxidative enzyme pattern of urethane-induced pulmonary adenoma. *Am Rev Respir Dis*, 100, 801-812.
4. Baylin, S.B., Herman, J.G., Graff, J.R., Vertino, P.M., & Issa, J-P. (1998). Alterations in DNA methylation: a fundamental aspect of neoplasia. *Adv Cancer Res*, 72, 141-196.
5. Berenblum, I., Ben-Ishai, D., Haran-Ghera, N., Lapidot, A., Simon, E., & Trainin, N. (1959). Skin initiating action and lung carcinogenesis by derivatives of urethane (ethyl carbamate) and related compounds. *Biochem Pharmacol*, 2, 168-176.
6. Bertalanffy, F.D. (1964). Respiratory tissue: structure, histophysiology, cytodynamics. II New approaches and interpretations. *Int Rev Cytol*, 17, 213-297.
7. Bertrand, H-O., Ha-Duong, T., Fermandjian, S., & Hartmann, B. (1998). Flexibility of the B-DNA backbone: effects of local and neighboring sequences on pyrimidine-purine steps. *Nucleic Acids Res*, 26, 1261-1267.
8. Bhide, S.V., & Ranadive, K.J. (1966). Effect of urethan on nucleic acids. *Nature*, 2, 82-83.
9. Bhide, S.V., Premkumar, E., Siddiqui, M.A., & Bhargava, P.M. (1971). Preliminary observations on the binding of urethane to DNA in various tissues of mice and rats. *Indian J Cancer*, 8, 172-175.
10. Bishop, A.E. (2004). Pulmonary epithelial stem cells. *Cell Proliferation*, 37, 89-96.
11. Bocking, B., Mittermayer, C., & von Deimling, O. (1981). Urethane-induced lung hyperplasia: carboxylesterase isozymes as markers in lung pathology. *Lab Invest*, 44, 138-143.
12. Boyland, E. (1968). The biochemistry of urethane. *NZ Med J*, 67, suppl 4-7.
13. Boyland, E., & Nery, R. (1965). The metabolism of urethane and related compounds. *Biochem J*, 94, 198-208.
14. Boyland, E., & Williams, K. (1969). Reaction of urethane with nucleic acids in vivo. *Biochem J*, 111, 121-127.

15. Brooks, R.E. (1968). Pulmonary adenoma of Strain A mice: an electron microscopic study. *J Natl Cancer Inst*, 41, 719-742.
16. Bryan, C.E., Skipper, H.E., & White, L. (1949). Carbamates in the chemotherapy of leukemia. IV. The distribution of radioactivity in tissues of mice following injection of carbonyl-labeled urethan, *J Biol Chem*, 177, 941-950.
17. Burri, P.H. (1985). Morphology and respiratory function of the alveolar unit. *Int Archs Allergy Appl Immun*, 76, 2-12.
18. Canadian Mortgage and Housing Corporation of Canada (1998). A study of recurring mold problems on the Roseau River Reserve, Manitoba. 1-73.
19. Carey, F.A., Lamb, D., & Bird, C.C. (1990). Intratumoral heterogeneity of DNA content in lung cancer. *Cancer*, 65, 2266-2269.
20. CDC/MMWR. (2000). Update: pulmonary hemorrhage/hemosiderosis among infants—Cleveland, OH, 1993-1996. *JAMA*, 283, 1951-1954.
21. Chavon, B.G., & Bhide, S.V. (1972). Interaction of urethan with macromolecules in male and female newborn, adult, and tumor-bearing mice. *J Natl Cancer Inst*, 49, 1019-1025.
22. Chauvel-Lebret, D.J., Auroy, P., Tricot-Dolauz, S., & Bonnaure-Mallet, M. (2001). Evaluation of the capacity of the SCGE assay to assess the genotoxicity of biomaterials. *Biomaterials*, 22, 1795-1801.
23. Cheng, M., Conner, M.K., & Alarie, Y. (1981). Multicellular in vivo sister-chromatid exchanges induced by urethane. *Mutat Res*, 88, 223-231.
24. Cirillo, D.J., Agrawal, Y., & Cassano, P.A. Lipids and pulmonary function in the Third National Health and Nutrition Examination Survey. *Am J Epidemiol*, 155 (2002) 842-848.
25. Cividalli, G., Mirvish, S.S., & Berenblum, I. (1965). The catabolism of urethan in young mice of varying age and strain, and in x-irradiated mice, in relation to urethan carcinogenesis. *Cancer Res*, 25, 855-858.
26. Collins, A.R. (2004). The comet assay for DNA damage and repair. *Mol Biotech*, 26, 249-261.
27. Collins, A., Dusinska, M., Franklin, M., Somorovska, M., Petrovska, H., Suthie, S., Fillion, L., Panayiotidis, M., Raslova, K., & Vaughan, N. (1997). Comet assay in human biomonitoring studies: reliability, validation, and applications. *Env Mol Mutagen*, 30, 139-146.

28. Comroe, J.H. (1977). Premature science and immature lungs. Part 1. Some premature discoveries. *Am Rev Respir Dis*, 116, 127-135.
29. Conner, M.K. (1986). Induction of sister chromatid exchange by ethyl carbamate and vinyl carbamate. *IARC Sci Publ*, 70, 313-320.
30. Conner, M.K., & Cheng, M. (1983). Persistence of ethyl carbamate-induced DNA damage in vivo as indicated by sister chromatid exchange analysis. *Cancer Res*, 43, 965-971.
31. Crapo, J.D., Barry, B.E., Gehr, P., Bachofen, M., & Weibel, E.R. (1982). Cell number and cell characteristics of the normal human lung. *Am Rev Respir Dis*, 126, 332-337.
32. Darrach, H.K., & Hedley-Whyte, J. (1971). Distribution of cholesterol in lung. *J Appl Physiol*, 30, 78-90.
33. Dearborn, D.G., Smith, P.G., Dahms, B.B., Allan, T.M., Sorenson, W.G., Montana, E., & Etzel, R.A. (2002). Clinical profile of 30 infants with acute pulmonary hemorrhage in Cleveland. *Pediatrics*, 110, 627-637.
34. Dickerson, R.E., & Ng, H-L. (2001). DNA structure from A to B. *PNAS*, 98, 6986-6988.
35. Diem, M., Boydston-White, S., & Chiriboga, L. (1999). Infrared spectroscopy of cells and tissues: shining light onto a novel subject. *Appl Spect*, 53, 148A-161A.
36. Discher, B.M., Maloney, K.M., Grainger, D.E., & Hall, S.B. (2002). Effect of neutral lipids on coexisting phases in monolayers of pulmonary surfactant. *Biophys Chem*, 101-102, 333-345.
37. Discher, B.M., Maloney, K.M., Grainger, D.W., Sousa, C.A., & Hall, S.B. (1999a). Neutral lipids induce critical behavior in interfacial monolayers of pulmonary surfactant. *Biochem*, 38, 374-383.
38. Dobbs, L.G., Wright, J.R., Hawgood, S., Gonzales, R., Venstrom, K., & Nellenbogen, J. (1987). Pulmonary surfactant and its components inhibit secretion of phosphatidylcholine from cultured rat alveolar type II cells. *Proc Natl Acad Sci USA*, 84, 1010-1014.
39. Dohy, D., Ghomi, M., & Taillandier, E. (1989). Interpretation of DNA vibration modes: III, the behavior of the sugar pucker vibration modes as a function of its pseudorotation parameters. *J Biomol Structure & Dynamics*, 6, 731-754.
40. Drobotko, V.G. (1945). Stachybotryotoxicosis a new disease of horses and humans. *American Review of Soviet Medicine*, 2, 238-242.

41. Dyson, P., & Heppleston, A.G. (1976). Cell kinetics of urethane-induced murine pulmonary adenomata: the growth fraction and cell loss factor. *Br J Cancer*, 33, 105-111.
42. Enhorning, G. (2001). Pulmonary surfactant function studied with the pulsating bubble surfactometer (PBS) and the capillary surfactometer (CS). *Comp Biochem Physiol A Mol Integr Physiol*, 129, 221-226.
43. Enhorning, G., & Holm, B.A. (1993). Disruption of pulmonary surfactant's ability to maintain openness of a narrow tube. *J Appl Physiol*, 74, 2922-2927.
44. Fabio, R.C., Manenti, G., Borrello, M.G., Colombo, M.P., Fisher, J.H., Pierotti, M.A., Dell Porta, G., & Dragani, T.A. (1992). Multiple molecular alterations in mouse lung tumors. *Molecular Carcinogenesis*, 5, 155-160.
45. Faust, F., Kassie, F., Knasmuller, S., Boedecker, R., Mann, M., & Mersch-Sundermann, V. (2004). The use of the alkaline comet assay with lymphocytes in human biomonitoring studies. *Mutat Res*, 566, 209-229.
46. Flemming, J., Hudson, B., & Rand, T.G. (2004). Comparison of inflammatory and cytotoxic lung responses in mice after intratracheal exposure to spores of two different *Stachybotrys chartarum* strains. *Toxicol Sci*, 78, 267-275.
47. Gabelova, A., Slamenova, D., Ruzekova, L., & Horvathova, E. (1997). Measurement of DNA strand breakage and DNA repair induced with hydrogen peroxide using single cell gel electrophoresis, alkaline DNA unwinding and alkaline elution of DNA. *Neoplasma*, 44, 380-388.
48. Gehr, P., Bachofen, M., & Weibel, E.R. (1978). The normal lung: ultrastructure and morphometric estimation of diffusion capacity. *Resp Physiol*, 32, 121-140.
49. Goon, D., & Conner, M.K. (1984). Simultaneous assessment of ethyl carbamate-induced SCES in murine lymphocytes, bone marrow, and alveolar macrophage cells. *Carcinogenesis*, 5, 399-402.
50. Grant, M.M., Cutts, N. R. & Brody, J. S. (1983). Alterations in lung basement membrane during fetal growth and type 2 cell development. *Dev. Biol.*, 97,173-83.
51. Gravesen, S., Nielsen, P.A., Iversen, R., & Fog-Nielsen, K. (1999). Microfungal contamination of damp buildings—examples of risk constructions and risk materials. *Environ. Health Persp.*, 107, 505-508.
52. Gregory, L., Pestka, J.J., Dearborn, D.G., & Rand, T.G. (2004). Localization of satratoxin-G in *Stachybotrys chartarum* spores and spore-impacted mouse lung using immunocytochemistry. *Toxicol Pathol*, 32, 26-34.

53. Gregory, L., Rand, T.G., Dearborn, D., Yike, I., & Vesper, S. (2002). Immunocytochemical localization of stachylysin in *Stachybotrys chartarum* spores and spore-impacted mouse and rat lung tissue. *Mycopathologia*, 156, 109-117.
54. Haagsman, H.P., & Diemel, R.V. (2001). Surfactant-associated proteins: function and structural variation. *Comp Biochem Physiol*, 129, 91-108.
55. Haller, T., Dietl, P., Stockner, H., Frick, M., Mair, N., Tinhofer, I., Ritsch, A., Enhorning, G., & Putz, G. (2004). Tracing surfactant transformation from cellular release to insertion into an air-liquid interface. *Am J Physiol Lung Cell Mol Physiol*, 286, L1009-L1015.
56. Hass, M.A., & Longmore, W.J. (1979). Surfactant cholesterol metabolism of the isolated perfused rat lung. *Biochim Biophys Acta*, 573, 166-174.
57. Hass, M.A., & Longmore, W.J. (1980). Regulation of lung surfactant cholesterol metabolism by serum lipoproteins. *Lipids*, 15, 401-406.
58. Hartmann, A., Elhajouji, a., Kiskinis, E., Poetter, F., Marus, H-J., Fjallman, A., Friauff, W., & Suter, W. (2001). Use of the alkaline comet assay for industrial genotoxicity screening: comparative investigation with the micronucleus test. *Food and Chem Toxicol*, 39, 843-858.
59. Hartmann, A., Plappert, U., Poetter, F., Suter, W. (2003). Comparative study with the alkaline comet assay and the chromosome aberration test. *Mutat Res*, 536, 27-38.
60. Hattori, S., Matsuda, M., & Wada, A. (1965). An electron microscopic study of pulmonary adenomas in mice. *GANN*, 56, 275-280.
61. Henderson, L., Wolfreys, A., Fedyk, J., Bourner, C., & Winderbank, S. (1998). The ability of the comet assay to discriminate between genotoxins and cytotoxins. *Mutagen*, 13, 89-94.
62. Hills, B.A. (2002). Surface-active phospholipid: a Pandora's box of clinical applications. Part 1. The lung and air spaces. *Internal Medicine J*, 32, 170-178.
63. Holloway, L. (1997). Families plagued by home-wrecking mold. *New York Times*, November 9, Section 1, p. 39.
64. Jackson, M., Sowa, M.G., & Mantsch, H.H. (1997). Infrared spectroscopy: a new frontier in medicine. *Biophys Chem*, 68, 109-125.
65. Jarvis, B., & Mazzola, E.P. (1982). Macrocyclic and other novel tricothescenes: Their structure, synthesis and biological significance. *Acc. Chem. Res.*, 15, 388-395.

66. Jones, P.A., & Baylin, S.B. (2002). The fundamental role of epigenetic events in cancer. *Nature Rev*, 3, 415-428.
67. Jong, S.C., & Davis, E.E. (1976). Contribution to the knowledge of *stachybotrys* and *memnoniella* in culture. *Mycotaxon*, III, 409-485.
68. Kaganer, V.M., Möhwald, H., & Dutta, P. (1999). Structure and phase transitions in Langmuir monolayers. *Rev Mod Phys*, 71, 779-819.
69. Kauffman, S.L. (1969). Alterations in cell proliferation in mouse lung following urethane exposure. 1. The nonvacuolated alveolar cell. *Am J Pathol*, 54, 83-93.
70. Kauffman, S.L. (1971). Alteration in cell proliferation in mouse lung following urethane exposure. II Effects of chronic exposure on terminal bronchiolar epithelium. *Am J Pathol*, 64, 531-538.
71. Kauffman, S.L. (1972). Alterations in cell proliferation in mouse lung following urethane exposure. 3. Effects of chronic exposure on type 2 alveolar epithelial cells. *Am J Pathol*, 68, 317-326.
72. Kaye, A.M., & Trainin, N. (1966). Urethan carcinogenesis and nucleic acid metabolism: factors influencing lung adenoma induction. *Cancer-Res*, 26, 2206-2212.
73. Klass, D., Lesperance, E., & Naimark, A. (1975). Phospholipid metabolism in lung adenomas: a model of surface active material synthesis. *Chest*, 67, 37S-39S.
74. Kuhn, C. (1982). The cytology of the lung: ultra-structure of the respiratory epithelium and extracellular lining layers. In *Lung Development: Biological and Clinical Perspectives*, Vol I. Ferrel, P.M. (Ed). Academic Press:NY NY, 27-55.
75. Liu, K-Z., Jia, L., Kelsey, S.M., Newland, A.C., & Mantsch, H.H. (2001). Quantitative determination of apoptosis on leukemia cells by infrared spectroscopy. *Apoptosis*, 6, 269-278.
76. Liu, M., Wang, L., Li, E., & Enhorning, G. 1991. Pulmonary surfactant will secure free airflow through a narrow tube. *J Appl Physiol*, 71, 742-748.
77. Macklem, P.T. (1971). Airway obstruction and collateral ventilation. *Physiological Reviews*, 51, 368-436.
78. Madsen, J.M. (2001). Toxins as weapons of mass destruction: a comparison and contrast with biological-warfare and chemical-warfare agents. *Laboratory Aspects of Biowarfare*, 21, 593-605.

79. Mason, R.J., Kalina, M., Nielsen, L.D., Malkinson, A.M., & Shannon, J.M. (2000). Surfactant protein C expression in urethane-induced murine pulmonary tumors. *Am J Pathol*, 156, 175-182.
80. McGowan, S.E., & Torday, J.S. (1997). The pulmonary lipofibroblast (lipid interstitial cell) and its contributions to alveolar development. *Annu Rev Physiol*. 59:43-62.
81. Miller, J.D., Rand, T.G., & Jarvis, B.B. (2003). *Stachybotrys chartarum*: cause of human disease or media darling? *Medical Mycology*, 41, 271-291.
82. Mirvish, S.S., Chen, L., Haran-Ghera, N., & Berenblum, I. (1969). Comparative study of lung carcinogenesis, promoting action in leukaneogenesis and initiating action in skin tumorigenesis by urethane, hydrazine and related compounds. *Int J Cancer*, 4, 318-326.
83. Montana, E., Etzel, R.A., Allan, T., Horgan, T.E., & Dearborn, D.G. (1997). Environmental risk factors associated with pediatric idiopathic pulmonary hemorrhage and hemosiderosis in a Cleveland community. *Pediatrics*, 99, 5-18.
84. Mostofi, F.K., & Larsen, C.D. (1951). The histopathogenesis of pulmonary tumors induced in Strain A mice by urethane. *J Natl Cancer Inst*, 11, 1187-1222.
85. Nery, R. (1968). Some aspects of the metabolism of urethane and N-hydroxyurethane in rodents. *Biochem J*, 106, 1-13.
86. Nikulin, M., Reijula, K., Stjernvall, T., Hintikka, E-L. (1997). Ultrastructure of conidia and hyphae of *Stachybotrys chartarum*. *Karstenia*, 37, 57-64.
87. Nunez, J., & Torday, J. (1995). The developing rat lung fibroblast and alveolar type II cell actively recruit surfactant phospholipids substrate. *J Nutr*, 125, 1639S-1644S.
88. O'Flatory, E.J., & Sichak, S.P. (1983). The kinetics of urethane elimination in the mouse. *Toxicol and Appl Pharmacol*, 68, 354-358.
89. Orgeig, S., & Daniels, C.B. (2001). The roles of cholesterol in pulmonary surfactant: insights from comparative and evolutionary studies. *Comp Biochem Physiol*, 129A, 75-89.
90. Otis, D.R., Johnson, J.M., Pedley, T.J., & Kamm, R.D. (1993). Role of pulmonary surfactant in airway closure: a computational study. *J Appl Physiol*, 75, 1323-1333.
91. Poelma, D.L.H., Zimmermann, L.J.I., Scholten, H.H., Lachmann, B., & van Iwaarden, J.F. (2002). In vivo and in vitro uptake of surfactant lipids by alveolar type II cells and macrophages. *Am J Physiol Lung Cell Mol Physiol*, 283, L648-L654.
92. Possmayer, F., Nag, K., Rodriguez, K., Qanbar, R., & Schurch, S. (2001). Surface activity in vitro: role of surfactant proteins. *Comp Biochem Physiol*, 129, 209-220.

93. Pound, A.W. (1972). Tumor formation in mice by urethane administered with related carbamates. *British J Cancer*, 26, 216-225.
94. Prodi, G., Rocchi, P., & Grilli, S. (1970). *In vivo* interaction of urethan with nucleic acids and proteins. *Cancer Res*, 30, 2887-2892.
95. Rand, T.G., Mahoney, M., White, K., & Oulton, M. (2002). Microanatomical changes in alveolar type II cells in juvenile mice intratracheally exposed to *Stachybotrys chartarum* spores and toxins. *Toxicol Sci*, 65, 239-245.
96. Rand, T.G., White, K., Logan, A., & Gregory, L. (2002). Histological, immunohistochemical and morphometric changes in lung tissue in juvenile mice experimentally exposed to *Stachybotrys chartarum*. *Mycopathologia*, 156, 119-131.
97. Reed, J.A., & Whitsett, J.A. (1998). Granulocyte-macrophage colony-stimulating factor and pulmonary surfactant homeostasis. *Proc Assoc Am Physicians*, 110, 321-332.
98. Rooney, S.A., Young, S.L., & Mendelson, C.R. (1994). Molecular and cellular processing of lung surfactant. *FASEB J*, 8, 957-967.
99. Rojas, E., Lopez, M.C., & Valverde, M. (1999). Single cell gel electrophoresis assay: methodology and applications. *J Chromat*, 722, 225-254.
100. Salzer, R., Steiner, G., Mantsch, H.H., Mansfield, J., & Lewis, E.N. (2000). Infrared and Raman imaging of biological and biometric samples. *J Analyt Chem*, 366, 712-716.
101. Schultz, C.P., Liu, K-Z., Kerr, P.D., & Mantsch, H.H. (1998). In situ infrared histopathology of keratinization in human oral/oropharyngeal squamous cell carcinoma. *Oncol Res*, 10, 277-286.
102. Schurch, S., Qanbar, R., Bachofen, H., & Possmayer, F. (1995). The surface-associated surfactant reservoir in the alveolar lining. *Biol Neonate*, 67 Suppl 1 61-76.
103. Sekido, Y., Fong, K.M., & Minna, J.D. (1998). Progress in understanding the molecular pathogenesis of human lung cancer. *Biochim Biophys Acta*, 1378, F21-F59.
104. Shimkin, M.B., & Polissar, M.J. (1955). Some quantitative observations on the induction and growth of primary pulmonary tumors in strain A mice receiving urethan. *J Natl Cancer Inst*, 16, 75-97.
105. Shimkin, M.B., Sasaki, T., McDonough, M., Baserga, R., Thatcher, D., & Wieder, R. (1969). Relation of thymidine index to pulmonary tumor response in mice receiving urethan and other carcinogens. *Cancer Res*, 29, 994-998.

106. Snyder, C., Malone, B., Nettesheim, P., & Snyder, F. (1973). Urethan-induced pulmonary adenoma as a tool for the study of surfactant biosynthesis. *Cancer Res*, 33, 2437-2443.
107. Snyder, F., & Malone, B. (1975). Acyltransferase and the biosynthesis of pulmonary surfactant lipid in adenoma alveolar type II cells. *Biochem Biophys Res Commun*, 66, 914-919.
108. Stoner, G.D., Hallman, M., & Troxell, M.C. (1978). Lethithin biosynthesis in a clonal line of lung adenoma cells with type II alveolar cell properties. *Exp Mol Pathol*, 29, 102-114.
109. Stoner, G.D. (1998). Introduction to mouse lung tumorigenesis. *Exp Lung Res*, 24, 375-385.
110. Subramaniam, R.P., Feijer, J.L., Miller, F.J., & Anjilvel, S. (2003). Analysis of lobar differences in particle deposition in the human lung. *Inhalation Toxicol*, 15, 1-21.
111. Sugahara, M., Urugami, M., & Regen, S.L. (2003). Selective association of cholesterol with long-chain phospholipids in liquid-ordered bilayers: support for existence of lipid rafts. *J Am Chem Soc*, 125, 13040-13041.
112. Svoboda, D.J. (1962). Ultrastructure of pulmonary adenomas in mice. *Cancer Res*, 22, 1197-1201.
113. Taillandier, E., & Liquier, J. (1992). Infrared spectroscopy of DNA. *Methods Enzymol*, 211, 307-335.
114. Tiffany, J.A., & Bader, H.A. (2000). Detection of *Stachybotrys chartarum*: the effectiveness of culturable-air sampling and other methods. *J Environ Health*, 62, 9-11.
115. Tsou, J.A., Hagen, J.A., Carpenter, C.L., & Laird-Offringa, I.A. (2002). DNA methylaiton analysis: a powerful new tool for lung cancer diagnosis. *Oncogene*, 21, 5450-5461.
116. Veldhuizen, R., Nag, K., Orgeig, S., Possmayer, F. (1998). The role of lipids in pulmonary surfactant. *Biochim Biophys Acta Molecular Basis of Disease*, 1408, 90-108.
117. Voelker, D.R., Lee, T-C., & Snyder, F. (1976). Fatty acid biosynthesis and dietary regulation in pulmonary adenomas. *Archives of Biochemistry and Biophysics*, 176, 753-756.
118. Walters, D.V. (2002). Lung liquid lining—the hidden depths. *Biol-Neonate*, 81, 2-5.

119. Weibel, E.R., & Crystal, R.G. (1991). Structural organization of the pulmonary interstitium. In *The Lung*, R.G. Crystal, J.B. West, et al. (Eds). Raven Press, Ltd:New York, 369-380.
120. White, M.R., Grendon, A., & Jones, H.B. (1970). Tumor incidence and cellularity in lungs of mice given various dose schedules of urethane. *Cancer Res*, 30, 1030-1036.
121. Williams, K., & Nery, R. (1971). Aspects of the mechanism of urethane carcinogenesis. *Xenobiotica*, 1, 545-550.
122. Williams, R.H., Ward, E., & McCartney, H.A. (2001). Methods for integrated air sampling and DNA analysis for detection of airborne fungal spores. *Appl Environ Microbiol*, 67, 2453-2459.
123. Wright, J.R., & Hawgood, S. (1989). Pulmonary surfactant metabolism. *Clin Chest Med*, 10, 83-93.
124. Yasuhara, S., Zhu, Y., Matsui, Tipirneni, N., Yasuhara, Y., Kaneki, M., Rosenzweig, A., & Jeevendra Martyn, J.A. (2003). Comparison of comet assay, electron microscopy, and flow cytometry for detection of apoptosis. *J Histochem Cytochem*, 51, 873-885.
125. Zasadzinski, J.A., Ding, J., Warriner, H.E., Bringezu, F., & Waring, A.J. (2001). The physics and physiology of lung surfactants. *Current Opinions in Colloid and Interface Science*, 6, 506-513.
126. Zhou, G., Whong, W.Z., Ong, T., & Chen, B. (2000). Development of a fungus-specific PCR assay for detecting low-level fungi in an indoor environment. *Mol Cell Probes*, 14, 339-348.
127. Zochbauer-Muller, S., Minna, J.D., & Gazdar, A.F. (2002). Aberrant DNA methylation in lung cancer: biological and clinical implications. *The Oncologist*, 7, 451-457.

Section 1: lung cancer

The following section consists of three chapters pertaining to lung cancer. The first chapter is a literature review that defines lung cancer, provides an overview of some causes of lung cancer, highlights current diagnostic techniques, and introduces new emerging technologies, e.g. Fourier-transform infrared spectroscopy (FTIR), that may be useful for diagnosing lung cancer. The second chapter describes a preliminary investigation of the potential of FTIR to analyze excised lung adenocarcinomas from mice. Based on information learned from the previous study, the FTIR investigation was extended to include analyses of human lung lesions. The third chapter describes the application of FTIR as a method of characterizing excised human lung lesions. The insight gained from FTIR analyses of lung lesions suggested that FTIR may be useful as an ancillary technique to light microscopy in the classification of neoplastic tissue.

Chapter 1

Lung cancer: occurrence and new possibilities for detection*

K.C. McCrae,¹ R.A. Shaw,³ H.H. Mantsch,³ J.A. Thliveris,² R.M. Das,¹ K. Ahmed,¹
J.E. Scott,^{1,2} Departments of Oral Biology,¹ Human Anatomy & Cell Science,² Faculties
of Dentistry and Medicine, University of Manitoba, the National Research Council,
Institute for Biodiagnostics,⁴ Winnipeg, Manitoba

*(1999). Lung cancer. Occurrence and new possibilities for detection. *International Journal of Health Care Quality Assurance* 12, I - XIII. **2000 Literati Club (London England) MCB University Press Award for Excellence, Most Outstanding paper.**

Abstract

Lung cancer is the leading cause of death worldwide. Physical and chemical agents such as tobacco smoke are the leading cause of various lung cancers. The intrinsic heterogeneity of normal lung tissue may be affected in different ways, giving rise to different types of lung cancers classified as either small-cell lung cancer (SCLC) or non-small cell lung cancer (NSCLC). Adenocarcinoma, a NSCLC, accounts for 40% of all lung cancer cases and the incidence is increasing worldwide especially among women. The survival rate and prognosis is poorest for adenocarcinoma. Therefore diagnosis at the earliest stage (Stage I, localized) is critical for increasing survival rates of those suffering from lung cancer. However many factors affect early diagnosis including variable natural growth of tumors plus technological and human factors associated with manipulation of tissue samples and interpretation of results. This article reviews potential problems associated with diagnosing lung cancer and considers future directions of diagnostic technology.

Lung cancer trends

Lung cancer is the leading cause of cancer-related deaths among Canadian men and women. In Canada, an estimated 17,400 deaths and 20,500 new cases of lung cancer occurred in 1999 [43]. Men continue to outnumber women in terms of incidences and deaths due to cancer (fig 1), including lung cancer, which accounts for approximately 30% of all cancer deaths in men and 20% in women [18,43].

For men, the incidence of lung cancer ranks second to prostate cancer (fig 2). For example, in 1999 there were an estimated 12,000 newly diagnosed cases of lung cancer compared to 16,600 cases of prostate cancer. Although lung cancer remains the leading cause of death among men, both incidence and mortality rates have been declining since the mid-1980s [18,43].

However incidence and mortality rates of lung cancer in women continue to rise (fig 3). Interestingly for 1999 the estimated incidence of lung cancer is less than half the incidence of breast cancer, 8,500 and 18,700, respectively (fig 3). Yet given previously observed death rates, lung cancer will account for an estimated 6,800 deaths compared to 5,400 deaths from breast cancer [43].

The lifetime probability of developing lung cancer for women is 1 in 21 [43]. Among men, the probability of developing lung cancer during their lifetimes is 1 in 11. Although cancer primarily afflicts Canadians over age 60, lung cancer is the leading cause of cancer deaths among men aged 35-84 and women aged 50 or older (fig 4). The incidence of lung cancer among women aged 45-74 ranks second to breast cancer, and among men aged 70 or older ranks second to prostate cancer. However lung cancer is the most common type of cancer in men aged 45-69 [18,43].

Internationally, lung cancer incidence and mortality rates for Americans are similar to Canadians [1]. Lung cancer is a major concern worldwide. According to the World Health Organization [62], the top five leading types of cancer which results in death include lung, stomach, colon and rectal, liver, and breast.

Causes of lung cancer

Lung cancer trends follow those of cigarette smoking prevalence, which accounts for at least 80% of all new cases in women and 90% of those in men [11,18]. The risk of developing lung cancer is dose-related, meaning that the risk is higher with increased number of cigarettes per day and with increased number of years of smoking [11,16,18]. However the risk decreases in proportion to the number of years after quitting smoking [16].

There is also a lag time of approximately 15-20 years between smoking and development of lung cancer [11,16-18]. Consequently if current smokers quit smoking, lung cancer and mortality rates will continue to increase well into the 21st century due to the increase of cigarette smoking in younger people, especially young women [17,49].

Environmental tobacco smoke inhaled by non-smokers increases their risk for developing lung cancer. In fact the carcinogenic substance from tobacco smoke “inhaled by non-smokers has a similar chemical composition to that inhaled by smokers, but has higher *N*-nitros-amine levels and smaller size particles which remains suspended in air and can more easily penetrate the bronchial tree” [16]. This remains a concern especially for children and adolescents exposed to cigarette smoke because even if they choose not to smoke, their risk of developing lung cancer is higher than non-smokers [16,49].

Several other environmental factors are associated with an increased risk of developing lung cancer. For example, carcinogens such as polycyclic aromatic hydrocarbons, which are released from motor vehicle exhaust and contribute to air pollution [16,18,35]. Other industries expose workers to particular chemicals during the manufacturing process that are associated with an increased risk of lung cancer (Table 1).

Recent research has revealed other potential causes of lung cancer that are genetic- or hormone-related and/or associated with previous lung injuries or diseases. Accumulations of genetic mutations, specifically involving *K-ras* and *p53* genes, have been suggested to play a role in the development of lung cancer [25,27,33,37,38,52]. However familial lung cancers are rare in comparison to colon or breast cancers [34].

There is evidence that development of lung cancer in women may be associated with the estrogen hormone. For instance, an early onset of menopause may be associated with decreased risk, whereas use of estrogen replacement therapy may be associated with increased risk [17]. A previous lung injury or disease in both women and men may also increase the risk of developing lung cancer [17]. In short it appears that exposure to a combination of multiple risk factors over the years contributes to the development of lung cancer.

Heterogeneity of lung cancer

The heterogeneous nature of lung cancer is associated with the heterogeneous nature of normal lung tissue. Lung cancer cells develop from normal lung cells that have been transformed by genetic mutations or by using a variety of physical or chemical agents. The lung is the most heterogeneous tissue in the body [29]. It is composed of different populations of cells possessing unique morphology, biochemistry and function.

Centrally located squamous cells line the respiratory tract of the trachea and bronchi, while secretory cells are found throughout the bronchioles and secrete mucous. Alveolar sacs lined with extremely attenuated epithelium function in air exchange and are located at the periphery [41]. In total, some 40 different cell types have been identified in the mature lung [5].

Therefore different cell populations give rise to different cancers. Furthermore, given that some lung cell populations may be exposed repeatedly to inhaled carcinogens more so than others, lung cancer may develop unequally. Consequently some areas of lung tissue may not be affected while others bear the majority of the exposure [41,44].

Multiple carcinogens affect lung tissue in different ways, many of which are not yet understood. The WHO classified different types of lung cancers, which can be affected by a variety of physical and chemical agents yielding a variety of different diseases [16,31,34,41]. These different lung cancers are clinically and biologically classified into two distinct types: small-cell lung carcinoma (SCLC) and non-small cell lung carcinoma (NSCLC). Squamous-cell carcinoma, adenocarcinoma, and large-cell carcinoma are included within the NSCLC category.

SCLC accounts for approximately 10-20% of lung cancers. This rapid growing lung cancer was originally referred to as oat-cell carcinoma because it resembled a grain of oat seed. SCLC tend to occur as nests of small round or oval cells of neuroendocrine origin lying in the bronchial mucosa [31]. Therefore the majority of SCLC is considered a central carcinoma and rarely occurs in the peripheral lung. SCLC is usually associated with smoking and is more common in men than women [22,31].

Squamous-cell carcinoma accounts for approximately 30% of all lung cancers. It is associated with smoking and shows increased incidence among men. This tumor, also considered a central carcinoma, typically arises from segmental bronchi as stratified squamous epithelium and is progressively replaced by malignant squamous cells. Although squamous-cell carcinomas are rapid growing, three to four years are required for development from earliest stages to clinical manifestation. As the tumor grows, it extends into the lumen of the bronchial tube obstructing the passage of air, thereby inducing occurrence of the characteristic coughing, wheezing, hemoptysis, atelectasis, dyspnea, or post-obstructive pneumonia [16,31].

Adenocarcinoma, which accounts for approximately 40% of all lung cancer cases, does not appear to be significantly associated with smoking. These slow-growing tumors originate in the peripheral lung tissue arising from alveoli and bronchial mucosal glands. As well this type of lung cancer is associated with a high percentage of *K-ras* genetic mutations (80-90%) [38]. Adenocarcinoma may manifest in various forms and be localized or spread throughout both lungs. This lung cancer is usually asymptomatic but some patients may suffer from pain due to chest wall involvement [17,31].

Large cell carcinoma is the least common lung cancer and accounts for only about 15% of all lung cancers. This lobular group of cancerous cells resembles both adenocarcinoma and squamous-cell carcinoma, therefore distinction is made by exclusion when no squamous or glandular differentiation is detected by light microscopy. However with the use of electron microscopy and immunohistochemical staining, many previously diagnosed large-cell carcinomas are now classified as adenocarcinoma or squamous-cell carcinoma [17,31]. In short, lung cancers exhibit characteristic histological patterns in

addition to clinical signs and symptoms associated with lung tumors arising from the particular lung tissue.

Survival rates and prognosis

Regardless of the type of lung cancer, the disease is most often fatal even though it is potentially curable. Moreover, patients who survive the occurrence of initial primary lung tumors are at increased risk of second primary tumors [20]. The five-year survival rate has not changed significantly in the past 30 years. The best survival rates are for patients who are diagnosed with lung cancer in clinical Stage I (Table 2) [17,32,33,44].

A patient's prognosis depends on the type of lung cancer, tumor staging and metastatic spread. *K-ras* genetic mutations, associated mainly with adenocarcinoma, tend to give a poor prognosis [37,38]. In fact, adenocarcinoma has a poor prognosis at any tumor stage (except T1, N0) compared to squamous-cell carcinoma [17]. Although squamous-cell carcinoma may grow rapidly, tumors tend to remain within the thoracic cavity thereby facilitating a cure more often than with other NSCLC [17]. Tumors diagnosed at the earliest stage, defined as Stage I (localized), are considered resectable and therefore provide the best prognosis and chance for cure [25,32,38].

Diagnosis

Problems affecting the diagnosis of lung tumors include the natural growth of tumors and the anatomical nature of the thoracic cavity. The nature of tumor growth (particularly doubling time, size, and shape of lesions) may hinder diagnoses in early stages and may prohibit distinction between benign and malignant tumors. Presumably, tumors begin as single cells that divide and amass at a constant rate, which is referred to as a tumor's doubling time. The size of the tumor is associated with its doubling time,

e.g. after 20 doublings, a tumor measures one millimeter in diameter and after 30 doublings it measures approximately one centimeter in diameter [10,24,30]. A tumor approximately two centimeters in diameter is considered an early lesion, but may contain an estimated 500 million cells [24].

Additionally, growth may be fast or slow depending on the type of cancer. For example, SCLC doubling time may be one month whereas the doubling time for adenocarcinoma may be six months [10]. Lung tumors that remain asymptomatic or mimic other respiratory illnesses may grow for 10-15 years before detection, thereby delaying diagnosis [10,30]. The occurrence of lung tumor metastases is not surprising considering the number of cells, length of growing time and the highly vascular nature of the lungs which could distribute cancerous cells throughout the body and contribute to poor prognosis and death.

Controversy exists over the reliability of using tumor size and shape as the crucial distinction between benign and malignant lesions. Both malignant and benign tumors may share characteristics that may not be reliable for diagnoses [24,65]. A lesion that is less than three centimeters in diameter is usually considered benign, however malignant lesions may be greater than or less than three centimeters in diameter [24,45,48]. In fact the smallest reported peripheral lung carcinomas measure one centimeter in diameter or less [64]. Lesions with smooth regular edges are likely to be benign, although edges of malignant tumors may range from well defined to fuzzy and multi-spiculated [24,30,45]. Also, both malignant and benign lesions may be round, oval, irregular or lobulated [24,30,48].

To complicate matters, cancerous nodules may be confused also with normal pulmonary lymph nodules of similar size and shape. Small intrapulmonary lymph nodes (IPLN) that measure approximately one centimeter or less in diameter are scattered throughout lung tissue within the thoracic cavity [63,64]. These IPLNs may be confused also with small benign or malignant lesions [63].

The anatomical nature of the thoracic cavity contributes also to problems with diagnoses. The pulmonary hilum (composed of connective tissue, blood vessels and lymph nodes) connects both lungs to the mediastinum and may conceal carcinomas arising from bronchi or parenchyma [19]. Many tumors remain hidden also by connective tissue of major blood vessels or bony structures such as the ribs [19,24].

Ultimately, an early diagnosis depends on a patient's initiative to consult a physician. However early lung cancer often presents itself with no pulmonary symptoms, and symptoms of later stages may be mistaken for other respiratory illnesses [16,31,44]. Therefore, physical examination of the patient by a physician becomes critical since the myriad of presentations makes lung cancer a challenge to diagnose.

A variety of diagnostic tools are at a physician's disposal when lung cancer is suspected. Once a physician can be relatively sure of the possibility of lung cancer, a definitive diagnosis is sought using cytological and histological methods. However the initial diagnosis of lung cancer may be missed due to technological factors associated with the ability to detect and to human factors associated with manipulation of tissue and interpretation of results. The remainder of this article reviews potential problems associated with diagnosing lung cancer and future directions for application of new diagnostic technology.

Diagnostic technology

Chest radiography

Chest radiography is a valuable and powerful diagnostic tool that is relatively easy to perform and generally inexpensive [16,24]. Most lung cancers, usually located in the periphery, are diagnosed using this method, either intentionally or incidentally. Chest radiography offers the ability to detect changes in a patient's respiratory condition by comparing old and new x-ray films [16]. Chest radiography is the diagnostic tool of choice by physicians whose patients are suspected of having lung cancer, hence ruling out lung cancer if the radiograph is normal [16].

Despite the wide spread use of chest radiography, many problems exist. The technical quality of films is poor which limits interpretation because of the inability to view adequately both mediastinum and lungs on the same film [24]. This problem is due to differences in densities of the tissues and intensities of radiation required to transmit through these tissues [24]. Consequently, over-penetration is required to view the mediastinum but over-exposes lung tissue, while under-penetration to view lung parenchyma under-exposes the mediastinum [24].

Appropriate exposure of these tissues is necessary to view abnormalities. Therefore new film (Insight Chest Systems, Kodak Canada, Inc Toronto, ON) of better quality has been developed with a high-contrast screen on one side along with standard low-contrast screen on the other. As a result, the mediastinum and lungs may be viewed simultaneously on one radiograph. Furthermore, this new film does not require new radiography equipment [24].

Another problem with chest radiography stems from human misinterpretation of films. Lesions are often missed [24,56]. A review of Mayo Lung Project screening study found 90% of peripheral lesions and 65% of central lesions went undetected after the first radiograph reading [39]. In fact peripheral lung cancers such as adenocarcinoma were most often missed by radiography particularly when tumor were located in the right upper lobe region [24]. Interestingly, women under age 40 appear to have a higher incidence of upper lobe lung cancers [9].

Frequent discrepancy exists in interpretation of films by radiologists thereby contributing to missed diagnoses of lung cancer. Austin et al., [2] found 18 out of the 27 radiologists studied missed potentially resectable bronchogenic carcinomas. Furthermore, most of the missed lung cancers were in female patients with tumors located in the right upper lobe [2].

The accuracy of interpretation depends also on the radiologist's knowledge of factors such as the patient's gender, age, history of smoking, clinical signs and symptoms. On the other hand, cues suggestive of cancer (e.g. symptomatic male smoker) may bias the radiologist's interpretation of the films and result in false positives. Whereas, increase in false-negatives may result when cues are not suggestive of lung cancer (e.g. asymptomatic female non-smoker) [24]. Double readings by trained physicians or technologists may be recommended to increase sensitivity of interpretation [56].

Another problem associated with chest radiography is heavy reliance on tumor-size, resulting in poor differentiation not only between benign and malignant tumors but also between questionable lesions and normal ILPNs [56,63]. Zerhouni [65] reported

nearly 70% of lung tumors are misdiagnosed as solitary lung nodules. A tumor measuring one centimeter in diameter is the lower limit detectable by chest x-ray, whereas three centimeters in diameter is the usual size that is detected [10,24]. Consequently, when tumors are allowed to progress and accumulate large numbers of cells, resectability and possibility of cure decreases while risk of metastases and eventual death increases.

Therefore, detection of lung cancer in the earliest stage is necessary to increase chance of survival. Presently, cancer agencies do not advocate the use of chest x-rays for mass screening, except during yearly examinations for high-risk individuals. However, during the 1970-80s, the National Cancer Institute launched three randomized controlled trials using chest radiography to screen thousands of male smokers (Table 3).

The purpose was to investigate the possibility of chest radiography as a cost-effective screening regimen that would detect lung cancer early in order to increase survival rates. The end results from all three trials were clear and consistent; even though chest radiography was relatively inexpensive and diagnosed lung cancer more often in screened subjects than in control subjects, the use of radiographs as well as sputum cytological analysis for diagnosis did not result in increased survival rates of participants [14,36,60].

Mass screening is not recommended. Unfortunately, an effective screening tool that could accurately detect all forms of lung cancer at low cost, thereby improving survival rates, has not been found. Interestingly, controversy exists over the results obtained by screening studies. Although the results of the Mayo Lung Project (MLP) do not justify recommending large-scale programs of radiological or cytological screening for lung cancer, neither do the results of the MLP mean that testing high-risk patients for

lung cancer by chest x-ray or sputum cytology is not useful as some have claimed (14). Strauss [57] suggests the proper question is not, "does screening reduce mortality?" the critical question is: "does screening save lives?" Indeed, screening trials did identify individuals with lung cancer who may not have otherwise been diagnosed. Thus, a potentially effective treatment program and chance of survival were possibilities for those who were diagnosed with lung cancer.

Some screening studies included sputum cytology as part of the regimen. However, with or without chest radiography, this strategy did not prove to be an effective method. Despite recommendations against sputum cytology as a screening method, it may be used to diagnose positively suspected lung cancers, especially in high-risk individuals, because it is a relatively simple non-invasive procedure [16]. In fact a three-day collection of early morning sputum samples appears to be effective in diagnosis of approximately 80% of central tumors such as squamous-cell carcinoma [16,44]. However, the ability to detect peripherally located tumors is hampered by the low representation of distal lung regions in any sputum sample. Therefore, the ability to detect lung cancers such as adenocarcinoma is less likely [16,44].

One drawback in using sputum cytology is that once the presence of lung cancer has been shown, the location or origin of the tumor remains unknown and requires further follow-up [44]. Another problem stems from inexperience of cytopathologists to distinguish malignancies from infections, inflammations or severe dysplasia of the lung [44]. However, monoclonal antibody staining techniques, which are currently under investigation, may prove useful in detecting the presence of malignancies [44].

Computed tomography

Computed tomography (CT) may not be an effective strategy for screening because of the expense [65]. Interestingly, in an ongoing mass-screening study of about 5000 Japanese people, using a mobile CT scanner, ten times as many cancers were revealed using CT compared to standard chest x-ray. Sone et al. [53] have yet to determine the effect this ongoing screening project has on mortality rates.

Not only is CT the gold standard of non-invasive diagnosis and staging of lung cancer, abnormalities undetected by chest radiography may be visible on CT scans [16,24,65]. CT scans reveal the presence and number of lesions. Lymph node metastases are identified also [44]. A unique feature of CT scans is the ability to “blur” overlying structures, such as bone or blood vessels, thereby clarifying the environment underneath [65]. As well, this modality is able to establish mediastinal and chest wall involvement in lung cancer [19,47].

CT scans reveal also segmental and subsegmental bronchial lesions [47]. In fact Munden et al., [42] found at least one of every four lesions one centimeter or smaller at CT, represented primary bronchogenic carcinoma. Therefore, CT scanning has the ability to detect extremely small lesions with great accuracy.

Interpretation of CT scans relies heavily on size of suspected lung lesions to differentiate these from lymph nodes. In this case, IPLNs may be mistaken for lung cancer [63]. As well, CT scans reveal size and not histological characteristics thus further diagnostic follow-up is required [24]. Therefore, CT may be used to direct bronchoscopic techniques in tissue sampling for diagnostic confirmation [46].

Bronchoscopic biopsy techniques

Tissue samples are required when non-invasive diagnostic techniques are unable to determine accurately the presence of lung cancer. A variety of different sampling techniques and instruments are required to obtain samples directly from suspected lung lesions located in different areas of the lung [15,59]. For example, forceps biopsy is most frequently used to sample tissue from central airway lesions. This technique requires at least three biopsies to increase sensitivity of detecting lung cancer [15]. For peripheral pulmonary lesions, transbronchial needle aspiration (TBNA) can be considered the most accurate bronchoscopic sampling instrument for biopsy [15]. TBNA is used also for sampling tissue in the hilar and mediastinal regions of the lungs [15].

There are some advantages of using TBNA. Mainly, information regarding lung cancer may be obtained in a less invasive fashion compared to thoracotomy. Consequently, the procedure may be performed on an out-patient basis thereby possibly eliminating lengthy hospitalization and increased medical expenses [59]. This procedure is reported to have fewer complications, such as pneumothorax, than other sampling techniques such as percutaneous pulmonary biopsy (46).

However, reliability of this procedure is dependent upon the experience of the radiologist. Tao (59) reports that in most cases, representative samples were obtained on the first attempt by experienced radiologists. However 7% of cases did not yield representative material even when the radiologists were quite sure that the needle was in the x-ray lesion. Consequently, this may result in increased potential for false-negatives.

Tissue samples obtained by biopsy techniques are cytomorphologically examined. Tao [59] reports problems associated with interpretation of tissue under the microscope.

Malignant cells may be easy to detect. However even the most experienced cytologists report that the interpretation is not straightforward, so practical experience becomes the only guide. The so-called 'cytologic criteria of malignancy' (as generally described in pathology books) is not applicable in the interpretation of aspirate preparations because malignant cells from some tumors appear benign-looking, and the irritated epithelial cells and reactive cells may meet the cytologic criteria of malignancy [59].

Future direction of diagnostic technology

Molecular genetics

Research had revealed genetic links to cancer. Lung cancer cells accumulate multiple genetic changes [27]. Studies have found at least three genetic mutations associated with adenocarcinoma. Mutations in tumor suppressor genes *p53* [27,58] and *p16* [3] and oncogene *K-ras* [33,37,52] are retained as tumors grow. Identification of genetic mutations holds opportunities to detect early molecular changes thereby facilitating early diagnosis of lung cancer.

Genetic mutations may serve as potential biomarkers in sputum samples and tumor biopsies. However, due to the great cellular heterogeneity of the lung and lung cancer, Mulshine et al. [41] point out that it would be both medically and economically impractical to have 1,000 different early detection markers.

Magnetic Resonance Imaging

Considerable attention has focused on the role of magnetic resonance imaging (MRI) in thoracic imaging. Sostman et al. [54] suggest that MRI may have a role in diagnosis of chest wall and mediastinal invasion by tumors. Heitzman [19] pointed out distinct advantages of MRI compared to CT radiography when imaging the pulmonary

hilus. He stated that ionizing radiation is not employed and the negative signal arising from rapidly flowing arterial blood allows ready distinction of a prominent pulmonary artery from a hilar mass without the necessity of contrast injection. However, when comparing the two modalities, there were no significant differences in the accuracy of detecting mediastinal lymph node metastases [24]. Also, CT scans are generally preferred over MRI because of the lower cost and general availability [24].

Positron Emission Tomography

Positron emission tomography (PET) is a unique non-invasive imaging technique that characterizes biochemical and physiological processes of tissue [21]. PET measures tissue distribution and biologic behavior of a variety of compounds labeled with positron-emitting isotopes [21]. Furthermore, PET has the ability to distinguish between benign and malignant lesions [16,21,55]. Thus using glucose analog-2[fluorine-18] fluoro-2-deoxy-D-glucose (FDG), increased uptake by malignant lung cells can be measured [16,21,55]. However, a differential diagnosis must be made between lung cancer and other respiratory illnesses because the increased uptake of glucose may also be due to infection or inflammation [21].

Fourier-transform Infrared spectroscopy

Fourier-transform Infrared (FTIR) spectroscopy is a technique used traditionally for studying physical, organic and atmospheric chemistry [23]. While FTIR spectroscopy has been often employed in the study of isolated biological material such as proteins, lipids, and membranes, only recently has the range of applications been expanded to include the study of diseased tissues [12,23,28].

Infrared spectroscopy is based on the interaction between infrared radiation and molecules. Infrared radiation is of lower energy than high frequency ultraviolet radiation, which is known to induce irreversible electronic changes in molecules. The result of infrared adsorption by a substance is molecular vibration since the energy of radiation is insufficient for electronic transitions [50]. While infrared radiation is not perceived by the human eye, instrumental measurements nevertheless reveal rich color patterns characteristic of the sample. Essentially all molecules have a rich spectrum of infrared absorptions; the absorption pattern may be viewed as a 'fingerprint' characteristic of the sample.

Virtually any substance in any state may be characterized using FTIR spectroscopy. The resulting spectrum provides information regarding the molecular structure of the substance and in the case of a mixture, the relative amounts of the various constituents [23]. In the case of tissues, the spectrum in principle reflects the biochemical makeup of the specimen. The biochemical characterization is latent in the infrared absorption spectrum (fig 5).

Recently, FTIR spectroscopy has been used to investigate respiratory disease. Knells et al. [28] used this method to characterize surfactant subfractions of bronchoalveolar lavage (BAL) collected from adult rabbit lungs. Pulmonary surfactant may further provide useful information regarding diseased states such as adult respiratory distress syndrome. Therefore, FTIR spectroscopic analysis of BAL may provide important clinical clues to respiratory illnesses [28]. Similarly, FTIR spectroscopy of lung tissue sections or cells may prove useful in a diagnostic role. For example, a

preliminary study has suggested that cancerous cells may be distinguishable from normal lung cells on the basis of their infrared spectra [61].

One potential advantage of FTIR compared to classical histological and cytological technologies is that it does not require the addition of reagents used for fixation and staining techniques [23]. FTIR may therefore provide useful diagnostic information without the difficulty associated with manipulation of tissue and misinterpretation of results.

Conclusions

Lung cancer is a disease with high mortality rates, which affects men and women equally. The incidence of lung cancer continues to rise worldwide yet survival rates remain unchanged. Physical and chemical agents such as tobacco smoke and industrial pollutants are the leading causes of lung cancer. Carcinogenic substances may enter and penetrate the airways easily thereby affecting lung tissue in a variety of ways causing different forms of lung cancer. Often lung cancer is diagnosed too late because the disease either mimicked other respiratory illnesses or remained asymptomatic, consequently increasing the risk of tumor growth and metastases. Therefore early diagnosis along with treatment is necessary to decrease the number of deaths.

Many diagnostic radiographic or cytologic modalities are at the disposal of physicians. However, despite the widespread use and advancement in research of these techniques, many problems exist for diagnosing lung cancer. Chest radiography and computed tomography remain the preferred diagnostic methods. Potential problems affecting these modalities include misinterpretation of results plus the inability to determine accurately malignancy and to differentiate adequately lesions from normal

pulmonary lymph nodes. Lung cancer diagnosis via bronchoscopic biopsy may be dependent upon radiologists' experiences and abilities to obtain representative samples of lesions and provide accurate interpretation of cytologic results.

Future directions of lung cancer diagnostic technology have expanded to include research involving molecular genetics, magnetic resonance imaging, positron emission tomography and infrared spectroscopy. Further investigation of lung cancer detection methods may result in discovery of diagnostic procedures that could detect precisely all forms of lung cancer in the earliest stages, thereby increasing significantly the survival rates of those suffering from this disease.

References

1. American Cancer Society (1998). Cancer statistics, 1998: a cancer journal for clinicians, 48, 6-30.
2. Austin, J.H., Romney, B.M., & Goldsmith, L.S. (1992). Missed bronchogenic carcinoma: radiographic findings in 27 patients with a potentially respectable lesion evident in retrospect. *Radiology*, 182, 115-122.
3. Belinsky, S.A., Nikula, K.J., Palmisano, W.A., Michels, R., Saccommano, G., Gabrielson, E., Baylin, S.B., & Herman, J.G. (1998). Aberrant methylation of p16ink4a is an early event in lung cancer and a potential biomarker for early diagnosis. *Proc Natl Acad Sci*, 95, 11891-11896.
4. Berndt, R., Nischan, P., & Ebeling, K. (1990). Screening for lung cancer in the middle-aged. *International J of Cancer*, 45, 229-230.
5. Bertalanffy, F.D. (1964). Respiratory tissue: structure, histopathology, cytodynamics I, review and basic cytomorphology. *International Rev Cytol*, 16, 233-328.
6. Bertalanffy, F.D. (1964). Respiratory tissue: structure, histopathology, cytodynamics II new approaches and interpretations. *International Rev Cytol*, 17, 213-297.
7. Boucot, K.R., & Weiss, W. (1973). Is curable lung cancer detected by semi-annual screening? *JAMA*, 224, 1361-1365.
8. Brett, G.A. (1969). Earlier diagnosis and survival in lung cancer. *Brit Med J*, 4, 260-262.
9. Byers, T.E., Vena, J.E., & Rzepka, T.F. (1984). Predilection of lung cancer for the upper lobes: an epidemiological inquiry. *J Natl Cancer Inst*, 72, 1272-1275.
10. Christensen, E.D., Harvald, T., Jendersen, M., Aggestrup, S., & Petterson, G. (1997). The impact of delayed diagnosis of lung cancer on the stage at the time of operation. *Eur J Cardio-Thoracic Surgery*, 12, 880-884.
11. Christiano, L. (1997). Public health concerns about lung cancer: a case report. *Chest*, 112, 214S-125S.
12. Das, R.M., Ahmed, M.K., Oulton, M.R., Mantsch, H.H., Tsubai, T., & Scott, J.E. (1997). Methylmercury-induced alterations in lung and pulmonary surfactant properties of adult mice. *Chem Phys Lipids*, 89, 107-117.
13. Dragini, T.A., Maneti, G., & Pierotti, M.A. (1995). Genetics of murine lung tumors. *Advances in Cancer Research*, 67, 83-112.

14. Fontana, R.S., Sanderson, D.R., Woolner, L.B., Taylor, W.F., Miller, W.E., & Muhm, J.R. (1986). Lung cancer screening: the Mayo program. *J Occupational Medicine*, 28, 746-750.
15. Gasparini, S. (1997). Bronchoscopic biopsy techniques in the diagnosis and staging of lung cancer. *Monaldi Archives of Chest Disease*, 52, 392-398.
16. Ginsberg, R., Vokes, E., & Raben, A. (1997). Cancer of the lung: non-small cell lung cancer. In Devita, V.T., Hellman, J.S., & Rosenberg, S.A. (Eds). *Cancer: Principles & Practice of Oncology*, Lippincott-Raven Publishers:Philadelphia, 858-907.
17. Healey-Baldini, E., & Strauss, G.M. (1997). Women and lung cancer: waiting to exhale. *Chest*, 112, 229S-234S.
18. Health Canada (1998). Facts on cancer. Cancer Bureau: Laboratory Center for Disease Control, Health Protection Branch, Ottawa.
19. Heitzman, E.R. (1986). The pulmonary hilus and lung cancer. *Chest*, 89, 320S-321S.
20. Huber, M.H., & Soo-Lee, J. (1995). Long-term survivors of lung cancer. In Johnson, B.E., & Johnson, D.H. (Eds). *Lung Cancer*, Wiley Liss, Inc: NY, 1-14.
21. Hughes, J.M.B., & Coates, G. (1993). Radionucleotide imaging: positron camera. In Potchen, E.J., Grainger, R.G., & Greene, R. (Eds). *Pulmonary Radiology*. W.B. Saunders Company:Philadelphia, 315-328.
22. Ihda, D.C. (1995). Small-cell lung cancer: state-of-the-art therapy, 1994. *Chest*, 107, 243S-248S.
23. Jackson, M., Sowa, M.G., & Mantsch, H.H. (1997). Infrared spectroscopy: a new frontier in medicine. *Biophys Chem*, 68, 109-125.
24. Janower, M.L., & Kono, M. (1993). Radiographic diagnosis of lung carcinoma: state of the art. In Potchen, E.J., Grainger, R.G., & Greene, R. (Eds). *Pulmonary Radiology*. W.B. Saunders Company:Philadelphia, 315-328.
25. Johnson, B.E. (1995). Biology of lung cancer. In Johnson, B.E., & Johnson, D.H. (Eds). *Lung Cancer*, Wiley Liss, Inc: NY, 1-14.
26. Johnston, M.R. (1997). Curable lung cancer: how to find it and treat it. *Postgraduate Medicine*, 3, 155-165.
27. Kishimoto, Y., Murakami, Y., Shiraishi, M., Hayashi, K., & Sekiya, T. (1992). Aberrations of the p53 tumor suppressor gene in human non-small cell carcinomas of the lung. *Cancer Res*, 52, 4799-4804.

28. Knells, G., Ahmed, M.K., Das, R.M., Oulton, M.R., Mantsch, H.H., & Scott, J.E. (1997). Fourier-transform infrared spectroscopic analysis of rabbit lung surfactant: subfraction-associated phospholipid and protein profiles. *Chem Phys Lipids*, 77, 193-201.
29. Kuhn, C. (1982). The cytology of the lung: ultrastructure of the respiratory epithelium and extracellular lining layers. In *Lung Development: Biological and Clinical Perspectives*, Vol I, Farrell, P.M. (Ed). Academic Press, Inc:NY, 27-55.
30. Lillington, G.A. (1997). Management of solitary pulmonary nodules, *Post Graduate Medicine*, 10, 145-150.
31. Linnoila, R.I., Aisner, S.C. (1995). Pathology of lung cancer: an exercise in classification. In Johnson, B.E., & Johnson, D.H. (Eds). *Lung Cancer*, Wiley Liss, Inc: NY, 1-14.
32. Luketich, J.D., & Ginsber, R.J. (1995). Diagnosis and staging of lung cancer. In Johnson, B.E., & Johnson, D.H. (Eds). *Lung Cancer*, Wiley Liss, Inc: NY, 1-14.
33. Mao, L., Hruban, R.H., Boyle, J.O., Tockman, M., & Sidransky, D. (1994). Detection of oncogene mutations in sputum precedes diagnosis of lung cancer. *Cancer Research*, 54, 1634-1637.
34. Mathews, M.J. (1986). World Health Organization lung cancer classification. *Chest*, 89, 315A.
35. McCalla, D.R., Kaiser-Farrell, C., Quilliam, M.A., Lant, M., Sheldrake, C.P., Kerr, A., Lockington, J.N., Gibson, E.S. (1986). Lung cancer in a steel foundary: a search for causation. *Chest*, 89, 313S.
36. Melamed, M.R., Flehinger, B.J., Zaman, M.B., Heelan, R.T., Perchick, W.A., & Martini, N. (1984). Screening for early lung cancer: results of the Memorial Sloan-Kettering study in New York. *Chest*, 86, 44-53.
37. Mills, N.E., Fishman, C.L., Rom, W.N., Dubin, N., & Jacobson, D.R. (1995). Increased prevalence of K-ras oncogene mutations in lung adenocarcinoma. *Cancer Research*, 55, 1444-1447.
38. Minna, J.D., Sekido, Y., Fong, K.M., & Gazdar, A.D. (1997). Cancer of the lung: molecular biology of lung cancer. In Devita, V.T., Hellman, J.S., & Rosenberg, S.A. (Eds). *Cancer: Principles & Practice of Oncology*, Lippincott-Raven Publishers:Philadelphia, 858-907.
39. Muhm, J.R., Miller, W.E., Fontana, R.S., Sanderson, D.R., & Uhlenhopp, M.A. (1983). Lung cancer detected during a screening program using four-month chest radiographs. *Radiology*, 148, 60-615.

40. Muller, J. (1986). Environmental carcinogens. *Chest*, 89, 312S-313S.
41. Mulshine, J.L., & Scott, F. (1995). Molecular markers in early cancer detection. *Chest*, 107, 280S-286S.
42. Munden, R.F., Pugatch, R.D., Liptay, M.J., Sugarbaker, D.J., & Le, L.U. (1997). Small pulmonary lesions detected at CT: clinical importance. *Radiology*, 102, 105-110.
43. National Cancer Institute of Canada: Canadian Statistics, 1999, Toronto, Canada.
44. Potchen, E.J., Austin, J.H. (1993). Problems and pitfalls in the diagnosis of early lung cancer. In Potchen, E.J., Grainger, R.G., & Greene, R. (Eds). *Pulmonary Radiology*. W.B. Saunders Company: Philadelphia, 315-328.
45. Pugatch, R.D. (1995). Radiographic evaluation in chest malignancies: a review of imaging modalities. *Chest*, 107, 294S-297S.
46. Rong, F., & Cui, B. (1998). CT scan directed transbronchial needle aspiration biopsy for mediastinal nodes. *Chest*, 114, 36-38.
47. Sagal, S.S. (1986). Computed tomography in the evaluation of lung cancer. *Chest*, 89, 318S-319S.
48. Shaffer, K. (1997). Radiographic evaluation in lung cancer: diagnosing and staging. *Chest*, 112, 235S-238S.
49. Shopland, D.R. (1995). Effects of smoking on the incidence and mortality of lung cancer. In Johnson, B.E., & Johnson, D.H. (Eds). *Lung Cancer*, Wiley Liss, Inc: NY, 1-14.
50. Skoog, D.A., & West, D.M. (1976). *Fundamentals of analytical chemistry* (3rd Ed), Holt, Rinehart & Winston, New York.
51. Sobue, T., Suzuki, T., & Naruke, T. (1992). A case-control study for evaluating lung-cancer screening in Japan: Japanese Lung-Cancer-Screening Research Group. *International J Cancer*, 50, 230-237.
52. Somers, V.A., Pietersen, A.M., Theunissen, P.H., & Theunissen, F.B. (1998). Detection of K-ras point mutations in sputum from patients with adenocarcinoma of the lung by Point-EXACCT. *J Clin Oncol*, 16, 3061-3068.
53. Sone, S., Takashima, S., Li, F., Yang, Z., Honda, T., Manuyama, Y., Hasegawa, M., Yamanda, T., Kubo, K., Hanamura, K., & Asakura, K. (1998). Mass screening for lung cancer with mobile spiral computed tomography scanner. *The Lancet*, 351, 1242-1245.

54. Sostman, H.D., & Webb, W.R. (1993). Magnetic resonance imaging in thoracic diseases. In Potchen, E.J., Grainger, R.G., & Greene, R. (Eds). *Pulmonary Radiology*. W.B. Saunders Company:Philadelphia, 315-328.
55. Steinert, H.C., Hauser, M.A. Allemann, F., Engel, H., Berthold, T., von Schulthess, G.K., & Weder, W. (1997). Non-small cell lung cancer: nodal staging with FDG PET versus CT with correlative node mapping and sampling. *Radiology*, 202, 441-446.
56. Stitik, F.P. (1986). Early radiologic detection of lung cancer. *Chest*, 89, 319S-320S.
57. Strauss, G.M. (1997). Measuring effectiveness of lung cancer screening: from consensus to controversy and back. *Chest*, 112, 216S-227S.
58. Takahasi, T., Nau, M.M., Chiba, I., Birrer, M.J., Rosenberg, R.K., Vinocour, M., Levitt, M., Pass, H., Gazdar, A.F., & Minna, J.D. (1989). A frequent target for genetic abnormalities in lung cancer. *Science*, 246, 491-494.
59. Tao, L.C. (1986). Transthoracic fine-needle aspiration biopsy: cytomorphicologic interpretation and its histological bases. *Chest*, 89, 328S-330S.
60. Tockman, M.S. (1986). Survival and mortality from lung cancer in a screened population. *Chest*, 89, 324S-325S.
61. Wang, H.P., Wang, H.C., & Huang, Y.J. (1997). Microscopic FTIR studies of lung cancer cells in pleural fluid. *Science of the Total Environment*, 204, 283-287.
62. World Health Organization (1998). *World Health Report 1998: life in the 21st century—a vision for all*, published by WHO.
63. Yokomise, H., Mizuno, H., Wada, H., Hitomi, S., & Itah, H. (1998). Importance of intrapulmonary lymph nodes in the differential diagnosis of small pulmonary nodular shadows. *Chest*, 113, 703-706.
64. Yoshida, J., Nagai, K., Yokose, T., Takahashi, K., Nishimura, M., Goto, K., & Nishiwaki, Y. (1998). Primary peripheral lung carcinoma smaller than 1 cm in diameter. *Chest*, 114, 710-712.
65. Zerhouni, E. (1986). The diagnosis of peripheral nodules. *Chest*, 89, 327S-328S.

Table 1: Occupational exposure to known carcinogens

Chemical carcinogen	Occupation/industry
Asbestos	Shipyard; construction; miners; insulation workers
Arsenic	Vineyard; sheep dip; goldmines; smelters
Polycyclic aromatic hydrocarbons	Generating plants; steelworkers
Chromate & chromium	Industry; chromium platers
Silica	Steel founding
Mustard gas; nickel; uranium (radon)	Industry; mines

Refs 11, 16, 18, 35, 40

Table 2: Five-year survival rates for stages of lung cancer

Stage	Definition	Rate %
I (T1-2, N0, M0)	Positive malignant cell < 3cm diameter; no nodal involvement, no metastases	45-70
II (T1-2, N0, M0)	Positive malignant cell > 3cm diameter; no nodal involvement, no metastases	25
III (T3-4, N0-2, M0)	Nodal involvement; extension to pleura, chest wall, diaphragm, or pericardium	10-15
IV (any M0)	Metastases present (pleura, lung, bone, brain, pericardium, or liver)	1

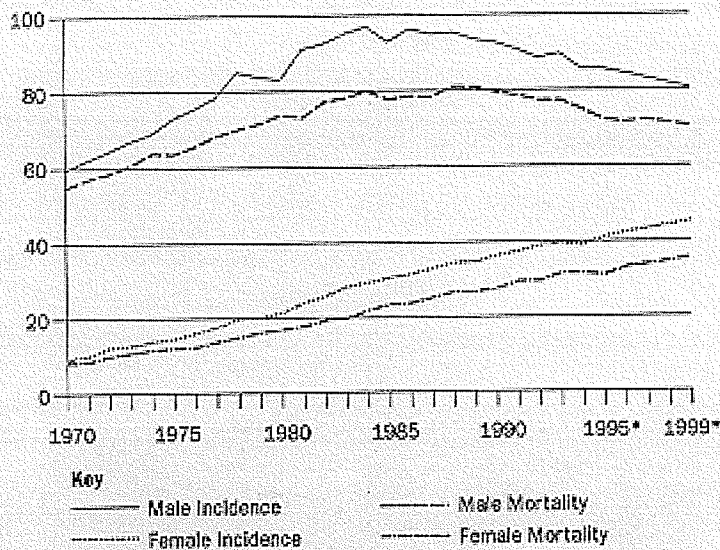
Refs 16, 32, 33, 44

Table 3: Results of screening studies worldwide

Project	Diagnostic method (*cxr, sc)	Incidence	Mortality rates	Ref
Mayo Lung	Screen: initial+quarterly cxr/sc	5.5/1000/yr	3.2/1000/yr	14
	Control: no intervention	4.3/1000/yr	3.0/1000/yr	
Hopkins Lung	Screen: annual cxr +quarterly sc	3.4/1000/yr	60
	Control: no intervention		3.8/1000/yr	
Memorial Lung	Screen: annual cxr+quarterly sc	No difference	No difference	36
	Control: no intervention			
Philadelphia Neoplasm	Semi-annual cp (10 yrs)	Increased	No difference	7
North West London	Screen: semi-annual cxr	Increased	No difference	8
	Control: initial/final cxr			
Germany	Cxr every 2 yrs (10 yrs)	No difference	4
Japan	Annual cxr for all participants + sc for high risk participants	Increased	No difference	51
Czechoslovakia	Trial 1 (3 yrs): Screen: semi-annual cxr	Increased	No difference	57
	Trial 2 (3 yrs): Annual cxr	Increased	No difference	

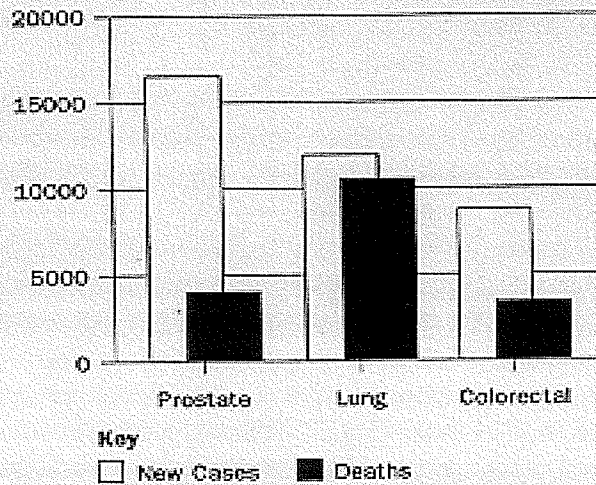
*cxr=chest x-ray; sc=sputum cytology; cp=chest photofluorograms

Figure 1
Age-standardized incidence and mortality rates for lung cancer, males and females, Canada, 1970-1999



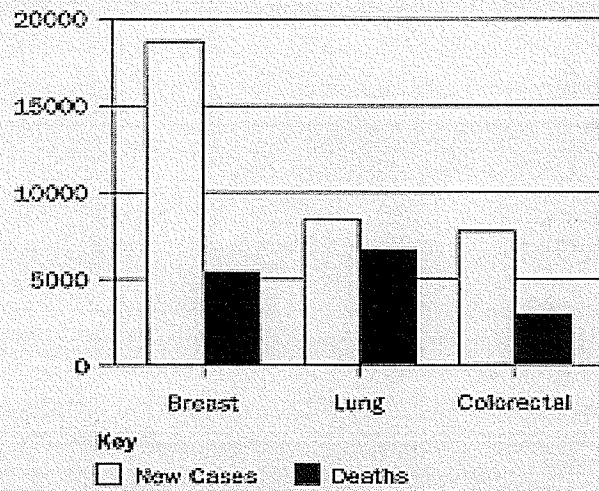
* Estimated Rates 1995-1999
Source: National Cancer Institute of Canada: Canadian Cancer Statistics, 1999, Toronto, Canada, 1999.

Figure 2
Estimated new cases and deaths for selected cancer sites, male, Canada, 1999 (rate per 100,000)



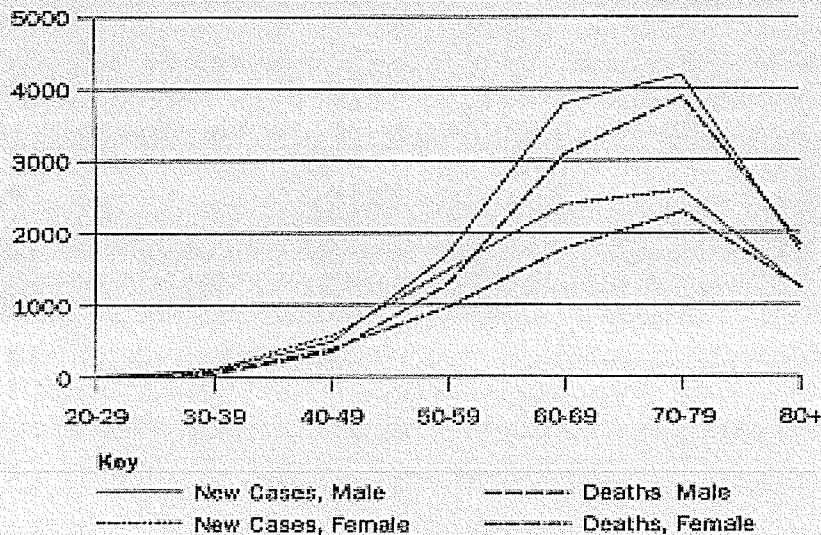
Note: the number of new prostate cases was estimated based on data years, 1980-1989.
Source: National Cancer Institute of Canada: Canadian Cancer Statistics, 1999, Toronto, Canada, 1999.

Figure 3
 Estimated new cases and deaths for selected cancer sites, female, Canada, 1999 (rate per 100,000)



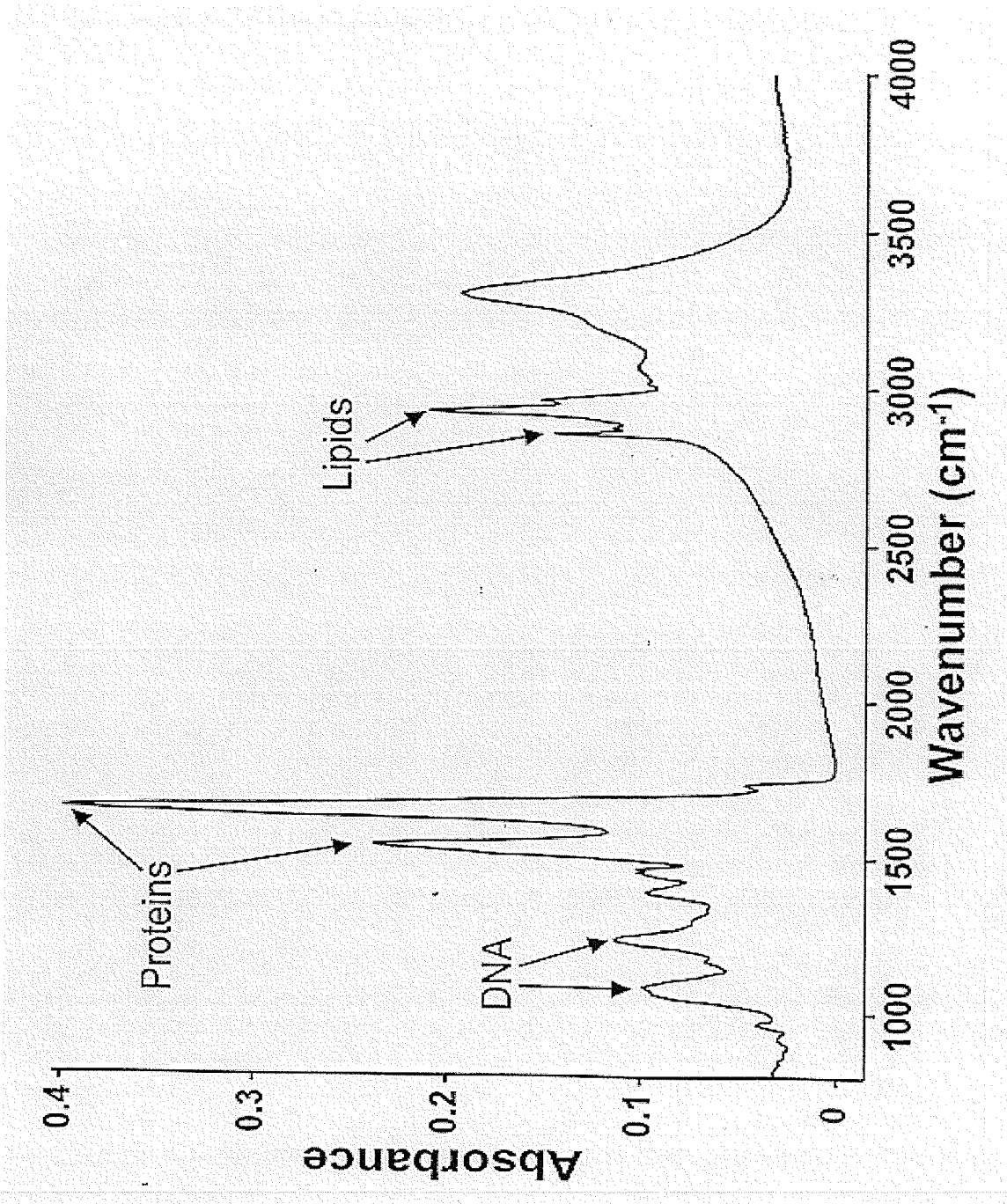
Source: National Cancer Institute of Canada: Canadian Cancer Statistics, 1999, Toronto, Canada, 1999.

Figure 4
 Distribution of lung cancer by age group and sex, Canada, 1999



Source: National Cancer Institute of Canada: Canadian Cancer Statistics, 1999, Toronto, Canada, 1999.

Figure 5: Representative IR spectra of lung tissue showing various peaks associated with different molecule types.



Chapter 2

Analysis of neoplastic changes in mouse lung using Fourier-transform infrared microspectroscopy*

Kimberly C. McCrae¹, Henry H. Mantsch³, James A. Thliveris², J.Elliott Scott^{1,2}, and R.
Anthony Shaw^{3*}

Departments of Oral Biology¹ and Anatomy², Faculties of Dentistry and Medicine,
University of Manitoba, Winnipeg, Manitoba, and National Research Council, Institute
for Biodiagnostics³, Winnipeg, Manitoba

*(2002). Analysis of neoplastic changes in mouse lung using Fourier-transform infrared
microspectroscopy. *Vibrational Spectroscopy* 28, 189-197.

Abstract

Methods based on infrared microspectroscopy were explored as a means to distinguish normal from neoplastic lung tissue. Mice were exposed to urethane, a known environmental carcinogen. After 3-8 months, lungs were removed, snap-frozen, sectioned and analyzed by standard histological methods and by infrared microspectroscopy. Neoplasms were readily observed in mice treated with urethane. Ultra-structurally, the neoplasms were composed entirely of type II alveolar cells displaying intracellular lamellar bodies. A fusion of two spectral preprocessing techniques, optimal region selection and linear discriminant analysis, was used to search for infrared spectral signatures distinguishing normal from neoplastic tissue. These techniques showed clear and reproducible differences between the complex spectra of these tissue types, suggesting that infrared microspectroscopy in conjunction with spectral processing technology may be useful to reveal subtle spectral differences occurring following induction of neoplastic changes and to interpret their biochemical origins.

Introduction

The epithelial lining within the lungs is the largest and most attenuated body surface exposed to the environment. Inhalation exposure to various environmental contaminants or known carcinogens, such as tobacco products [1-5], radiation [6], urethane [7], asbestos fibers [5,6,8], radon [9] asphalt constituents [10], or toxigenic molds [11,12] may induce changes in lung, potentially initiating neoplastic transformation. Accurate identification of lung neoplasms is problematic as neoplasms may be difficult to distinguish from hyperplastic or normal lung tissue [13].

Histological and cytological analysis of lung neoplasms is based largely on the appearance of the tissue and cells. For example an increased nucleocytoplasmic ratio may be characteristic of a hyperplastic or neoplastic cell population [13,14]. Other assessment criteria may include cell size and shape, as well as apparent over-crowding, disorganization and lack of cohesion among cells within the tissue [13]. Such identification is clearly subjective and interpretation under the microscope may lead to incorrect assessment of the lung tissue [15].

For this reason, we explored a method based on infrared (IR) microspectroscopic analysis, followed by application of spectral processing techniques, as an approach to analyze normal and neoplastic lung tissue. IR microspectroscopy is an established method used to determine the structure and biochemical composition of magnified images [16]. Recently, the range of applications has expanded to include analysis of diseased tissue (for a review, see e.g. reference 17). One important area of research is whether this technique, in combination with spectral processing techniques, could be

used to characterize neoplastic tissue, thereby distinguishing it from non-neoplastic tissue (see e.g. Refs. 18-21).

Spectral absorption patterns may be viewed as a tissue 'fingerprint' with band intensities reflecting the structure, conformation, and interactions among the constituent molecules. The spectra represent an average of all the constituents within the normal and neoplastic tissue, which may complicate visual interpretation of the spectra. Therefore, an algorithm combining optimal region selection algorithm with linear discriminant analysis (LDA) was employed to seek spectral patterns distinguishing neoplastic from normal tissue. This technique successfully identified spectral subregions whose intensity patterns provided the basis for distinguishing the two histological classes.

Materials and Methods

Urethane-induced lung neoplasms

Female CD1 mice, aged 4-6 weeks, were obtained from Animal Care Services at the University of Manitoba. Mice were approximately 25 grams in weight at the beginning of this study. Throughout the study they were housed in plastic boxes with aspen chip bedding and maintained in a temperature-controlled room (20°C) with a constant cycle of 12 h light and 12 h dark. All mice were fed a diet of Rat Mouse Hamster Chow pellets and received drinking water *ad libitum*. All procedures using animals were approved by the Canadian Council on Laboratory Animals.

Lung neoplasms were induced by a combination of previously described methods [22,23]. Urethane (ethyl carbamate) was dissolved in sterile normal saline at a concentration of 0.1 g/ml. Mice were treated by an intraperitoneal injection (1 mg/g body weight). Control mice received an equal volume of sterile saline injected by the same

route. Urethane was dissolved in drinking water to make a 1% solution and given to treated mice until day of sacrifice; control mice received regular water. Water consumption and body weights were monitored regularly for a period of three months.

On the day of sacrifice, mice were euthanized by IP injection with Euthanyl (sodium pentobarbital, 240 mg/ml, 1 ml per mouse). Lungs were removed, snap-frozen in liquid nitrogen and stored in a -85°C freezer. A portion of lung tissue was fixed in 2% buffered glutaraldehyde followed by post-fixation in 1% osmium tetroxide for examination by electron microscopy. Samples were dehydrated and embedded in Epon 812 using standard procedures. Thin sections were prepared and viewed on a Phillips 201 electron microscope.

IR spectroscopy and spectral classifications

Frozen lung tissue was mounted using optimal cutting medium and sectioned at 10 μm at -21°C. Alternate serial sections were placed onto glass slides, which were stained with hematoxylin and eosin for light microscopy, while the remaining sections were placed on circular IR-transparent BaF₂ disks (13 mm diameter x 2 mm thick) for infrared microspectroscopy.

Infrared spectra were acquired with a Bruker Equinox 55 infrared spectrometer equipped with an IR Scope II infrared microscope accessory. The microscope accessory includes a liquid nitrogen-cooled mercury cadmium telluride detector and a motorized mapping stage. All spectra were acquired with an aperture of 100 x 100 μm . For each pixel, 128 interferograms were collected, signal averaged and Fourier-transformed to generate spectra with a nominal resolution of 4 cm^{-1} .

Spectra were acquired for two different tissue sections. Each section included both normal tissue and neoplastic regions. For one section, IR spectra were acquired at 60 distinct points corresponding to normal tissue and 60 points corresponding to neoplastic tissue (as confirmed by the adjacent H & E stained serial section). The second section was mapped by acquiring spectra at each point in a 12 x 15 (1200 x 1500 μ m) grid that encompassed both normal and neoplastic regions.

The experiments were designed with the goal of answering three specific questions:

1. On average, do the IR spectra of neoplastic tissue differ from the IR spectra of normal tissue?
2. Can a region selection algorithm find spectral patterns to identify individual spectra as normal or neoplastic?
3. Are diagnostic spectral patterns identified in 2) generally applicable, i.e. can the same spectral features be used to classify correctly spectra from a separate section?

The simplest analysis involved averaging all point spectra for neoplastic tissue and comparing that average to the corresponding control tissue spectra. This search for a diagnostic spectral pattern to designate individual point spectra as normal or neoplastic was carried out using an algorithm, written in-house, that fuses two techniques, optimal region selection and LDA [24,25]. The set of spectral subregions thus identified was used as the basis to predict classifications (normal or neoplastic) for the spectra making up the map grid.

Results

Electron microscopic analysis

Water consumption and weight changes were unaffected by exposure to urethane (Fig. 1). Following urethane exposure for three months, neoplasms were readily

observable in mouse lungs. Electron microscopy revealed several differences between the lung structures of animals treated with saline or urethane (Fig. 2). Well-defined capillary structure was apparent in both saline-exposed lung and in normal areas of lung from animals exposed to urethane. Typical type II alveolar cells containing conspicuous lamellar bodies with good preservation of internal lamellae were observed (Fig. 2C). Lungs of urethane-exposed mice displayed many neoplasms, some of which were located within the lung parenchyma and did not infringe on the pleural surface. As a result, these tumors were not apparent upon surface inspection (Fig. 2A). Cells of neoplasms showed many lamellar bodies arranged within the cytosol.

Cells within the neoplasms were of an extremely uniform nature, with copious numbers of lamellar bodies and mitochondria visible within the cytoplasm. Neoplastic type II cells displayed a reduced cytoplasmic-nuclear ratio in comparison to control type II cells, apparently due to a reduction in the volume occupied by the cytoplasm. In addition, neoplastic lesions displayed a clear increase in heterochromatic character of the nuclei compared to controls.

IR microspectroscopic analysis

Spectra of normal and neoplastic lung tissue are shown in Figure 3, and their second derivatives in Figure 4 (Note: the second derivative spectra have been inverted so that positive features correspond to positive absorptions in the original spectra). The absorption profiles are typical of tissue infrared spectra, which are dominated by protein amide I and amide II absorptions in the 1500-1700 cm^{-1} range. Lipids and DNA constituents also contribute prominently. For example, absorptions within the 2800-3000 cm^{-1} range are assigned to lipid CH_2 and CH_3 groups, along with weaker protein CH

stretching bands, and the 1060-80 and 1220-1240 cm^{-1} regions encompass the PO_2^- stretching modes of DNA.

The clearest differences between the spectra in Fig. 3 are the decreased intensity in the protein absorptions and increased intensity in the lipid C=O stretching absorption at 1740 cm^{-1} for the neoplastic tissue relative to control tissue. To illustrate more subtle differences in the class average spectra, the second derivative spectra appear in Fig. 4 as three segments to illustrate the changes in bands corresponding to lipids (2800-3000 cm^{-1}), proteins (1400-1800 cm^{-1}), and DNA (800-1400 cm^{-1}). Prior to derivation, the individual spectra contributing to these average spectra were normalized to a common intensity in the amide I and II absorptions over the 1500-1700 cm^{-1} range; the spectra are therefore normalized to a common protein content. This procedure ensured that any successful discrimination between the spectra in different histological classes would be based upon differences in the spectral pattern rather than differences in overall intensity. In the 800-1400 cm^{-1} region, neoplasia promoted obvious changes in the two absorptions ascribed to the DNA phosphate stretching modes, at 1087 cm^{-1} (symmetric PO_2^- stretch) and at 1220-1240 cm^{-1} (asymmetric PO_2^- stretch). The neoplastic tissue showed increased intensity in the 1087 cm^{-1} absorption, and splitting of two component bands in the 1220-1240 cm^{-1} range that are nearly coincident in the spectrum of normal tissue.

While the second derivative spectra in the 1400-1800 cm^{-1} range show approximately equal intensities in the amide I and amide II regions (not surprisingly since the spectra are normalized to these absorptions), there is a clear change in the amide I absorption profile. The spectrum of neoplastic tissue is less intense at 1659 cm^{-1} and more intense at 1638 cm^{-1} than its control tissue counterpart. These changes suggest a loss of

α -helical structure and increase in random coil structure in neoplastic as compared to control tissue [26]. The difference spectrum (neoplastic – control) further reveals a positive band at 1740 cm^{-1} indicating increased lipid levels in the neoplastic tissue. This suggestion is corroborated by the difference spectrum in the $2800\text{-}3000\text{ cm}^{-1}$ range, which shows positive bands at 2848 and 2916 cm^{-1} corresponding to lipid CH_2 symmetric and asymmetric stretching modes. These difference bands are shifted to low frequency relative to the absorptions at 2850 and 2920 cm^{-1} in the spectrum of normal tissue.

Spectral classifications

The trials to seek an LDA classifier distinguishing normal point spectra from neoplastic point spectra provided success based upon only two spectral subregions. The integrated intensities within the two subregions identified by the region selection algorithm ($930\text{-}935$ and $962\text{-}972\text{ cm}^{-1}$) served to distinguish the two sets of point spectra with an accuracy of 99.2% (Table 1). Figure 5 further illustrates the success in partitioning the two sets of spectra, each of which is represented by a point defined by the integrated intensity in the $930\text{-}935\text{ cm}^{-1}$ region (X-coordinate) and in the $962\text{-}972\text{ cm}^{-1}$ region (Y-coordinate). It is of interest that this pair of regions is not unique in distinguishing neoplastic from control tissue. Equally effective alternatives were identified by employing the same algorithm to seek the optimal regions within restricted spectral ranges. For example, when only the region $1400\text{-}1800\text{ cm}^{-1}$ was available to the routine, the two subregions $1530\text{-}1555$ and $1640\text{-}1655\text{ cm}^{-1}$ were selected; within the $1100\text{-}1400\text{ cm}^{-1}$ range, the optimal subregions were $1130\text{-}1155$ and $1240\text{-}1255\text{ cm}^{-1}$.

The spectra collected in mapping unstained tissue were classified as either neoplastic or normal on the same basis, i.e. by re-expressing each spectrum as a pair of

integrated intensities over the pair of spectral ranges previously identified, and predicting their class memberships using the same LDA classifier. The classification results are shown pictorially in Figure 6, where regions predicted to be neoplastic are dark, and regions designated as normal are light. The border between normal and neoplastic tissue was completely consistent with histological assessment of the adjacent hemotoxylin/eosin stained serial section.

Discussion

The internal surface of the lungs represents the largest body surface exposed to the environment, approximately $1 \text{ m}^2/\text{kg}$ body weight [27,28]. The biological barrier presented by the pulmonary epithelium, which is exposed to environmental toxigenic agents is extremely complex and varied. From a multi-cellular layer lining the trachea and primary bronchi, this barrier becomes attenuated to the point that only a thin trilaminar membrane which averages about $1.5 \text{ }\mu\text{m}$ or less in thickness [29] separates the air and its various constituents from the vascular system. Tobacco products, asbestos fibers, urethane, radon, mold spores and any other inhalable gas or particle may reach the terminal air-exchange regions of the lung, potentially altering metabolic functions and thus inducing pathological changes such as neoplastic alterations [10].

This study confirmed that infrared spectroscopy may play a role both in detecting lung neoplasia and in delineating the structural and biochemical changes accompanying the change from normal to neoplastic tissue. One indicator emerged from a set of point spectra measured for an unstained lung section using an IR microscope. The class average of spectra acquired for neoplastic regions (as confirmed by a stained serial section) was clearly different from the corresponding class average for normal tissue. A

non-subjective classification approach (optimal region selection/linear discriminant analysis) further revealed that each of the individual neoplastic spectra shared common traits (regional intensities) distinguishing them from all the normal spectra. Finally, the same spectral regions provided a basis to assign points on a spectroscopic map grid as normal or neoplastic. A gray scale image based upon those classifications clearly demarcated the regions corresponding to neoplastic and normal tissue, as confirmed by a serial section stained in the conventional fashion.

The differences between the class average spectra for neoplastic and unaffected lung tissue were clear and substantial. Obvious differences were observed in the nucleic acid PO_2^- stretching (1087 and 1240 cm^{-1}) absorptions, which are more intense for neoplastic than for normal lung tissue. This observation is consistent with previous studies of colon tissue [18], lymph cells [19], leukemia cells [20], and cervical tissue [21]. One possible explanation for the increased DNA contribution is that the features arise due to increased somatic cell DNA content or increased heterochromatic DNA.

A second distinguishing feature is the elevated lipid/protein ratio in neoplastic tissue. This finding was also implicit from the spectra of neoplastic and normal colon [18], but the opposite trend appears for the spectra of lymph cells [19] where trends in the CH stretching absorption intensities ($2800\text{-}3000 \text{ cm}^{-1}$) region indicate a decrease in the CH_2/CH_3 ratio with the onset of neoplasia. Reduction in lipid content relative to their normal counterparts has also been observed in leukemic lymphocytes [20].

In order for spectral differences cited above to be useful generally in identifying neoplasia, it must be shown that variations within each class of spectra do not obscure the features distinguishing the class average spectra. The question is whether discriminatory

patterns distinguishing random neoplastic/normal pairs of spectra can provide a basis to distinguish all possible pairs of spectra, i.e. are there rules that can correctly assign each of the individual spectra as neoplastic or normal. Three broad approaches have been employed to address this question in previous studies, namely cluster analysis, regression, and classification. In its simplest form, cluster analysis partitions spectra into subgroups according to their Euclidean distance from the mean spectrum. The hope in using this approach is that spectra in one diagnostic group (e.g. neoplasia) will cluster in a subgroup that is well displaced from the cluster of normal spectra. This method successfully partitioned the spectra of lymphocytes according to whether they were leukemic or not [20]. One regression approach, as exemplified by Haaland's study of lymph cells [19], is to assign to each spectrum a dummy variable indicating the degree of neoplasia. A partial-least-squares regression may then be carried out in the normal fashion, with the ideal result being that the resulting PLS calibration model predicts high values for neoplastic spectra and low values for normals, with a clear demarcation separating the two groups of spectra.

The approach we have adopted here was first introduced with examples classifying NMR spectra from colon biopsies as normal or neoplastic, and NMR spectra of brain tissue as meningioma or astrocytoma [24]. It has since been employed to classify breast tumours according to their grade and steroid receptor status [30], to seek features distinguishing the IR spectra of dysplastic from normal cervical cell preparations [31], and to identify basal cell skin carcinoma on the basis of the mid-IR spectrum of skin [32]. Perhaps the most appealing feature of this approach is that it yields specific spectral regions that provide the basis for the LDA classification, and hence the possibility of

interpreting the biochemical underpinnings of successful classification. For example, the two spectral subregions $930\text{-}935\text{ cm}^{-1}$ and $962\text{-}972\text{ cm}^{-1}$ encompass DNA absorptions [33] that presumably contribute to the spectral distinctions separating neoplastic from normal tissue in the LDA classification. Similarly, the alternative diagnostic pairs of spectral regions encompass protein ($1530\text{-}1555/1640\text{-}1655\text{ cm}^{-1}$) or DNA ($1130\text{-}1155/1240\text{-}1255\text{ cm}^{-1}$) absorptions.

In conclusion, this study provides evidence that infrared microspectroscopy is an invaluable tool in characterizing neoplastic tissue. While the tissue used in this study represents an end-stage of disease when neoplastic transformation is well developed and tissues are visually distinguishable, the present data identifies spectral changes that signal transformation at the single cell level. Further study will explore the extent to which these molecular changes might precede morphological evidence of neoplasia.

Acknowledgement

This work was supported by a grant from the Natural Sciences and Engineering Research Council of Canada.

References

1. J. Lukanich, *Chest* 116 (1998) 486S-489S.
2. W.P. Bennett, M.C.R. Alavanja, B. Blomeke, K.H. Vähäkangas, K. Castrén, J.A. Welsh, E.D. Bowman, M.A. Khan, D.B. Flieder, D.B. Harris, *J. Nat. Canc. Inst.* 91 (1999) 2009-2014.
3. P. Boffetta, F. Nyberg, A. Agudo, E. Benhamou, K. Jöckel, M. Kreuzer, F. Merletti, G. Pershagen, H. Pohlabein, L. Simonato, H.E. Wichmann, R. Saracci, *Int. J. Cancer* 83 (1999) 805-806.
4. S. Ha Jee, H. Ohrr, I. Soon Kim, *Int. J. Epidemiol.* 28 (1999) 824-828.
5. M. Kreuzer, H. Pohlabein, W. Ahrens, L. Kreienbrock, I. Brüske-Hohlfeld, K. Jöckel, H.E. Wichmann, *Scand. J. Work Environ. Health* 25 (1999) 422-429.
6. R.A. Rinsky, J.M. Melius, R.W. Hornung, R.D. Zumwalde, R.J. Waxweiler, P.J. Landrigan, P.J. Bierbaum, W.E. Murray, *Am. J. Epidemiol.* 127 (1988) 55-64.
7. A. Barbin, *Mutation Res.* 462 (2000) 55-69.
8. Dufresne, P. Looserrwanich, B. Armstrong, G. Thériault, R. Bégin, *Am. Indust. Hygiene Assoc. J.* 57 (1996) 370-375.
9. L. Tomášek, V. Plaček, *Radiation Res.* 152 (1999) S59-S63.
10. T. Partanen, P. Boffetta, *Am. J. Indust. Med.* 26 (1994) 721-740.
11. K.C. McCrae T. Rand, C. Mason, M.R. Oulton, C. Hastings, T. Cherlet, J.A. Thliveris, R.A. Shaw, H.H. Mantsch, J. MacDonald, J.E. Scott, *Chem. Phys. Lipid* (2000) In press.
12. C.D. Mason, T. Rand, M.R. Oulton, J. MacDonald, J.E. Scott, *Nat. Toxins* 6 (1998) 27-33.
13. W.W. Johnston, C.E. Elson, *Respiratory tract*. In M. Bibbo (Ed.). *Comprehensive Cytopathology*. W.B. Saunders Company: Philadelphia. (1991).
14. L. MacDonald, *Bull. Can. Soc. Cytol.* 16 (2000) 1-3.
15. L-C. Tao, G.L. Weisbrod, F.G. Pearson, D.E. Sanders, E.E. Donat, L. Filipetto, *Cancer* 57 1986 1565-70.

16. J.A. Reffner, P.A. Martoglio, Uniting microscopy and spectroscopy. In H.J. Humecki (Ed.). Practical guide to infrared microspectroscopy. Pp 41-84. Marcel Dekker, Inc: New York. (1995)
17. M. Jackson, M.G. Sowa, H.H. Mantsch, *Biophys. Chem.* 68 (1997) 109-25.
18. Rigas, S. Morgello, I.S. Goldman, P.T. Wong, *Proc. Natl. Acad. Sci. USA.* 87 (1990) 8140-4.
19. D.H. Haaland, H.D.T. Jones, E.V. Thomas, *Appl. Spectrosc.* 51 (1997) 340-5.
20. C.P. Schultz, K-Z. Liu, J.B. Johnson, H.H. Mantsch, *Leukemia Res.* 20, (1996) 649-55.
21. L. Chiriboga, P.H. Xie, D. Yee, D. Zarou, D. Zakim, M. Diem, *Cell. Mol. Biol. (Noisy-le-grand)* 44 (1998) 219-29.
22. B.R. Blakley, *Can. J. Comp. Med.* 48 (1984) 299-302.
23. I.Y.R. Adamson, A.J. Klass, *Canc. Res.* 36 (1976) 1669-73.
24. A. Nikulin, B. Dolenko, T. Bezebah, R.L. Somorjai, *NMR Biomed.* 11 (1998) 209-216.
25. H.H. Eysel, M. Jackson, A. Nikulin, R.L. Somorjai, H.H. Mantsch, *Biospectroscopy* 3, (1997) 161-7.
26. W.K. Surewicz, H.H. Mantsch, D. Chapman, *Biochemistry* 32 (1993) 389-94.
27. E.R. Weibel, In: *Morphometry of the human lung.* Academic Press Inc., New York, NY (1963).
28. J.L. Mauderly, J.M. Samet In: R.G. Crystal and J.B. West (eds.), *The Lung Scientific Foundations.* pp. 1947-60. Raven Press, New York. (1991).
29. S.P. Sorokin, In: L. Weiss (ed.), *The Lung.* 6th edition, Urban & Schwarzenberg, Baltimore MD., pp. 753-813 (1988).
30. M. Jackson, J.R. Mansfield, B. Dolenko, R.L. Somorjai, H.H. Mantsch, P.H. Watson, *Cancer Detect. Prev.* 23 (1999) 245-53.
31. R.A. Shaw, F.B. Guijon, M. Paraskevas, S. Low Ying, H.H. Mantsch, *Anal. Quant. Cytol. Histol.* 21 (1999) 292-302.
32. L.M. McIntosh, M. Jackson, H.H. Mantsch, M.F. Stranc, D. Pilavdzic, A.N. Crowson, *J. Invest. Dermatol.* 112 (1999) 951-6.

33. E. Taillandier, J. Liquier, *Methods Enzymol.* 211 (1992) 307-35.

Table 1. Classification table comparing histology predicted via region selection/LDA of the IR spectra (in columns) to true histology (in rows).

<i>Tissue type</i>	<i>Neoplastic</i>	<i>Normal</i>	<i>Accuracy (%)</i>	<i>Specificity (%)</i>
<i>Neoplastic</i>	59	1	98.3	100
<i>Normal</i>	0	60	100	98.3

Figure 1A: Mean water consumption (mls/day)

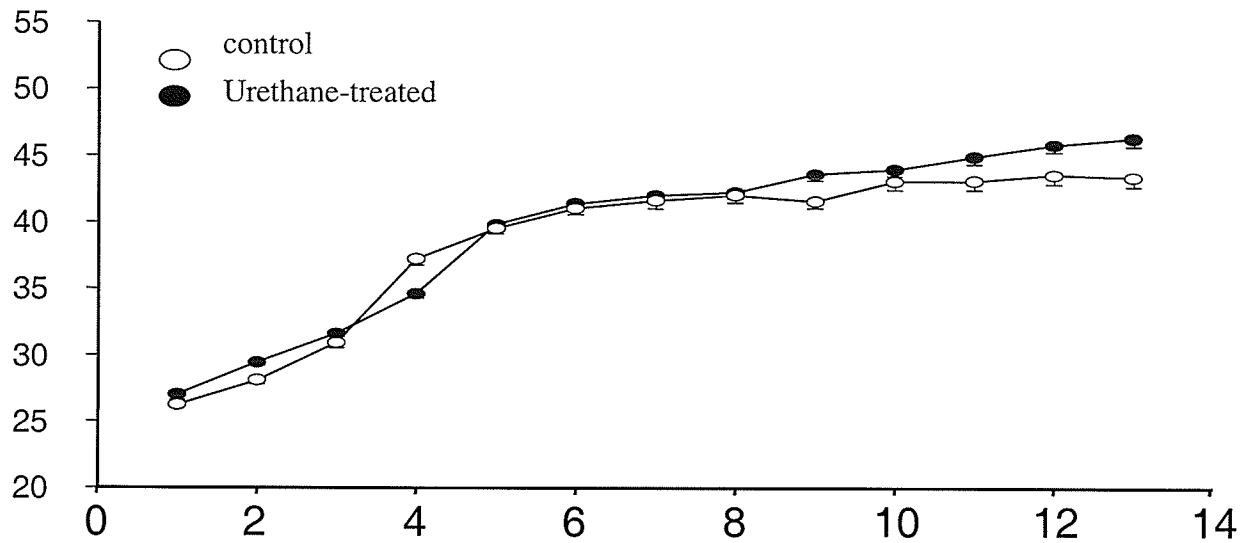


Figure 1B: mean body weight (gm)

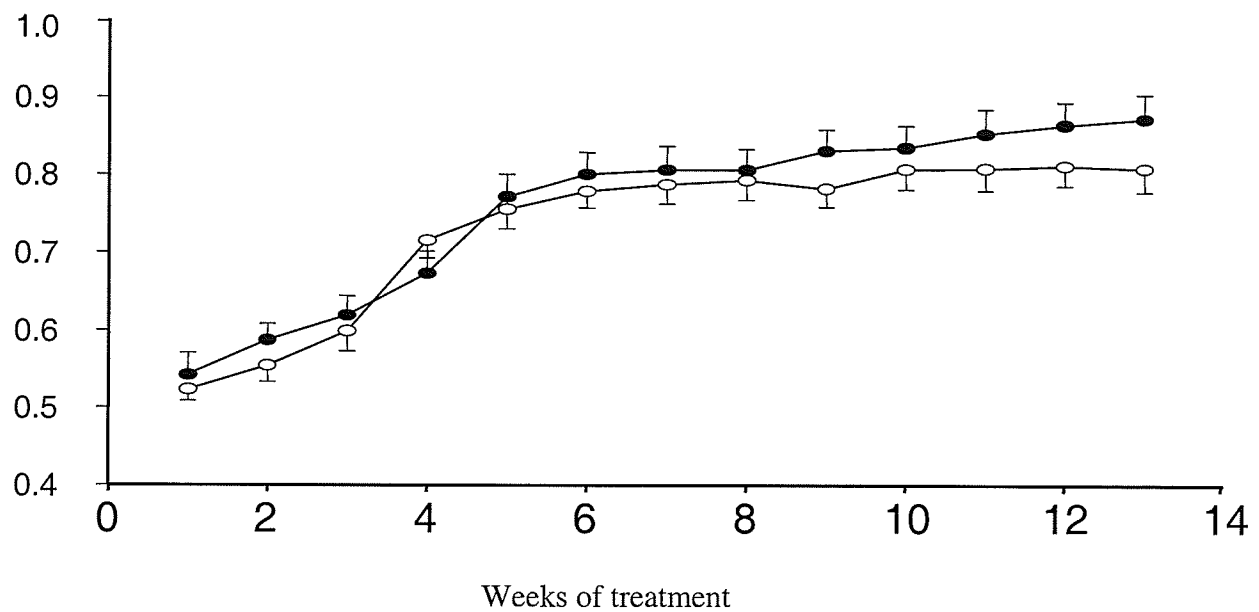
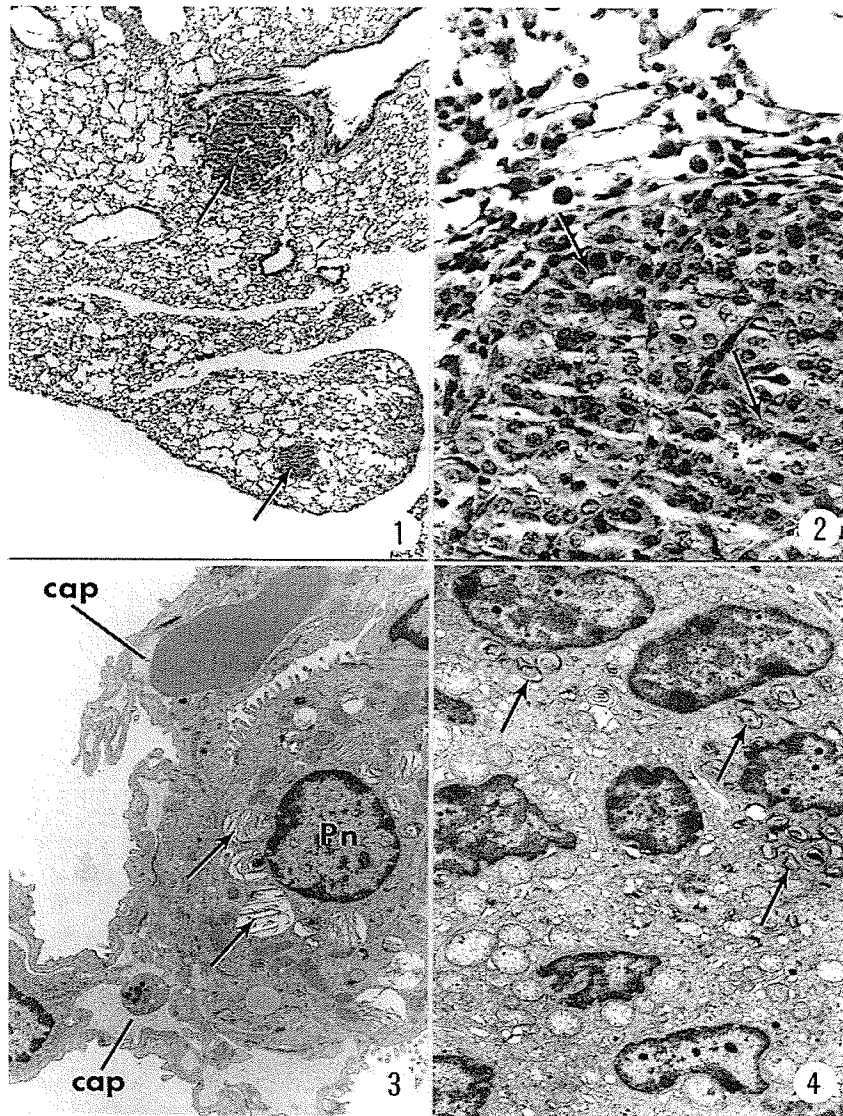


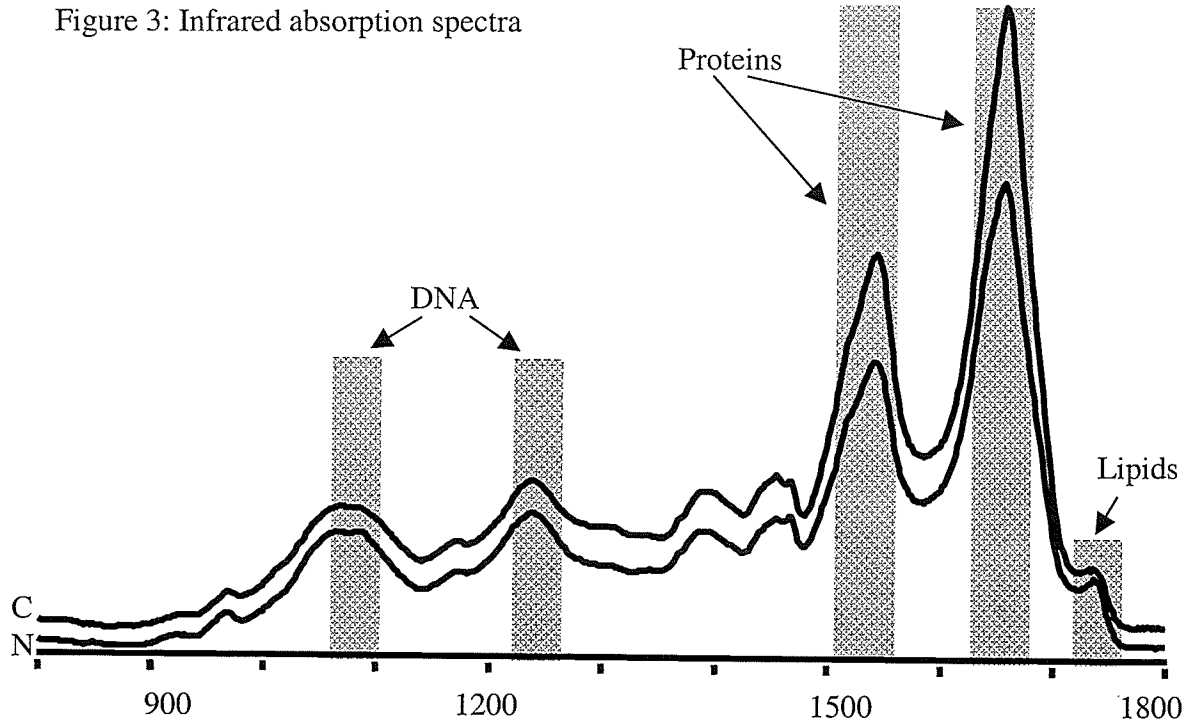
Figure 1A & B. Effect of urethane treatment on mouse body weights and water consumption. Analysis of covariance confirmed that urethane treatment had no significant influence on body weight or water consumption.

Figure 2: Electron micrograph of mouse lung tissue



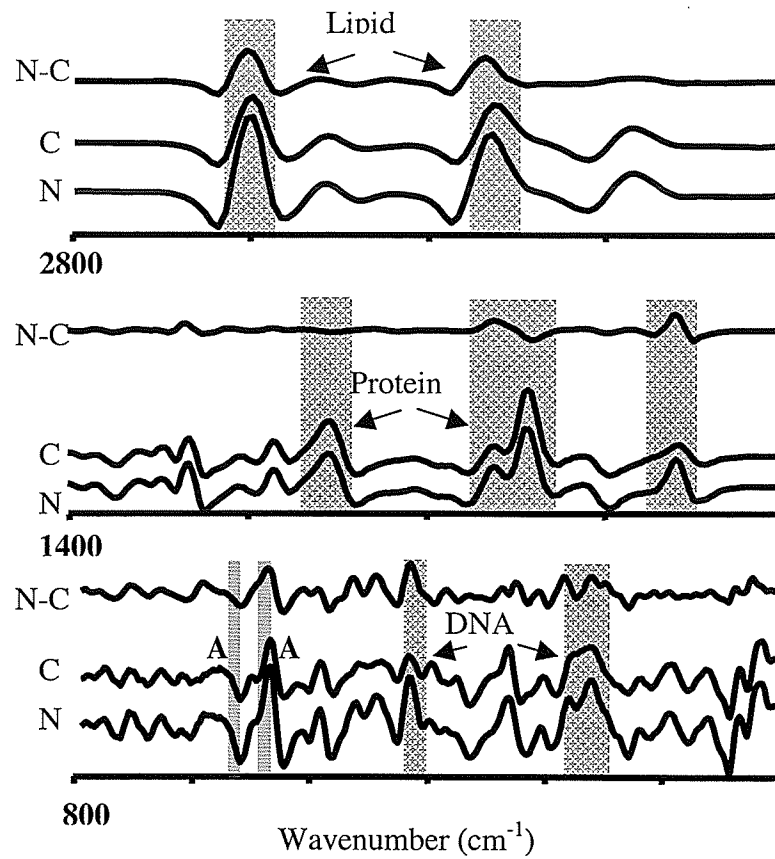
Electron micrographs of normal and neoplastic lung tissue. Panel 1: Low power light micrograph of lung from an animal treated with urethane. Note the presence of two discrete tumors (arrows). Magnification x 20. Panel 2: High power view of tumor in panel 1, showing well differentiated cells in a glandular pattern (arrows). Magnification x 150. Panel 3: Electron micrograph of lung from a control animal. Several lamellar bodies are present in the cytoplasm (arrows) of the type 2 pneumocyte (Pn) cap (capillary). Magnification x 4,700. Panel 4: Electron micrograph of lung tissue from a urethane treated animal. Several tumor cells are present with lamellar bodies (arrows). Magnification x 4,700.

Figure 3: Infrared absorption spectra



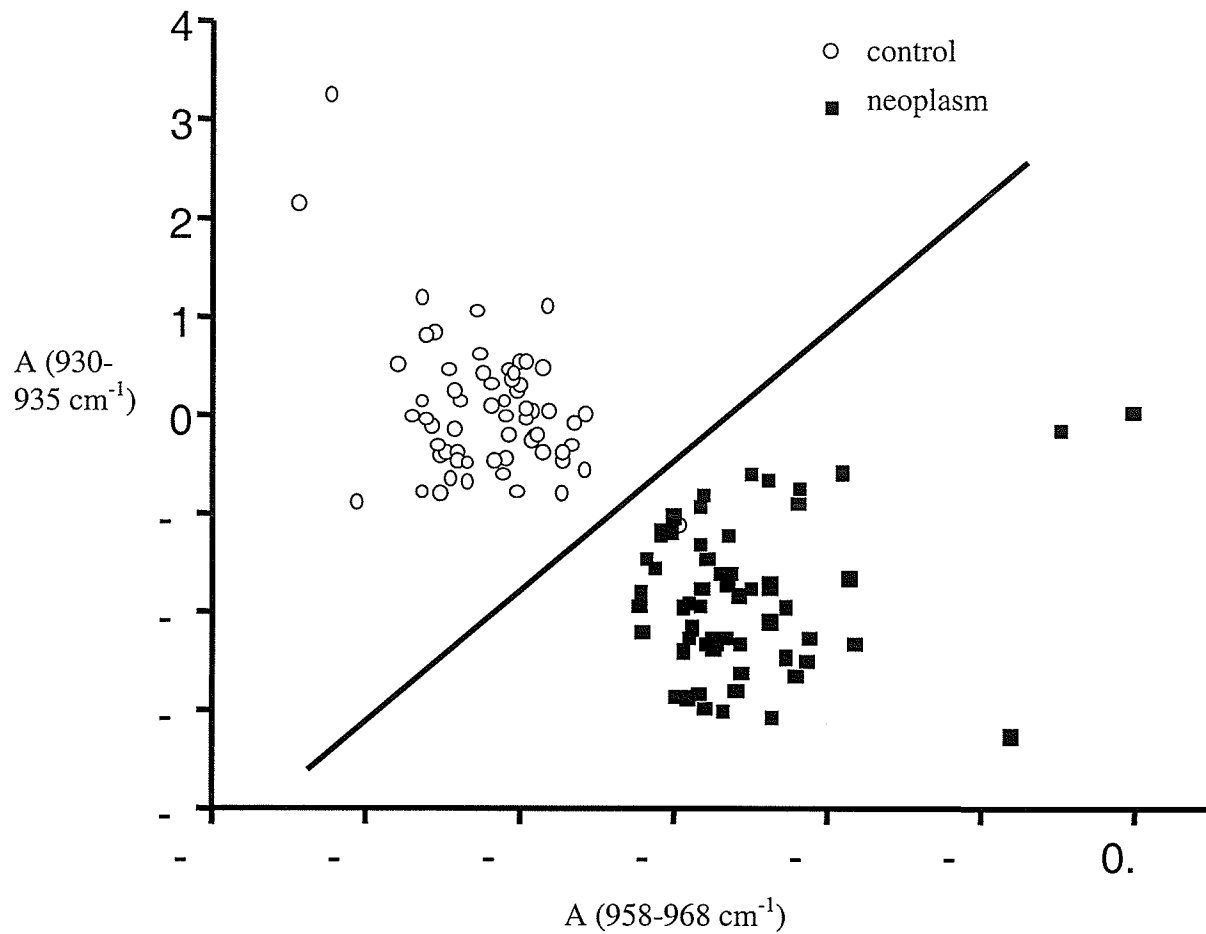
Infrared absorption spectra for neoplastic (N) and control (C) lung tissue. Each trace is the average of 60 spectra.

Figure 4: Second derivatives



Infrared spectra (second derivatives, inverted so that positive features correspond to absorption maxima) for control (C) and neoplastic (N) tissue. Each trace is the average of 60 spectra, with all 120 spectra normalized to a common intensity over the range 1500-1700 cm⁻¹ prior to averaging and derivation.

Figure 5: Scatterplot of bands represented by A from fig 4



Scatterplot wherein each point represents an infrared spectrum for control or neoplastic tissue; the X-coordinate is the integrated intensity over the range 962-972 cm⁻¹ for the second derivative of the absorption spectrum, and the Y-coordinate the integrated intensity over the range 930-935 cm⁻¹.

Figure 6: Lung tissue section analyzed by FTIRM

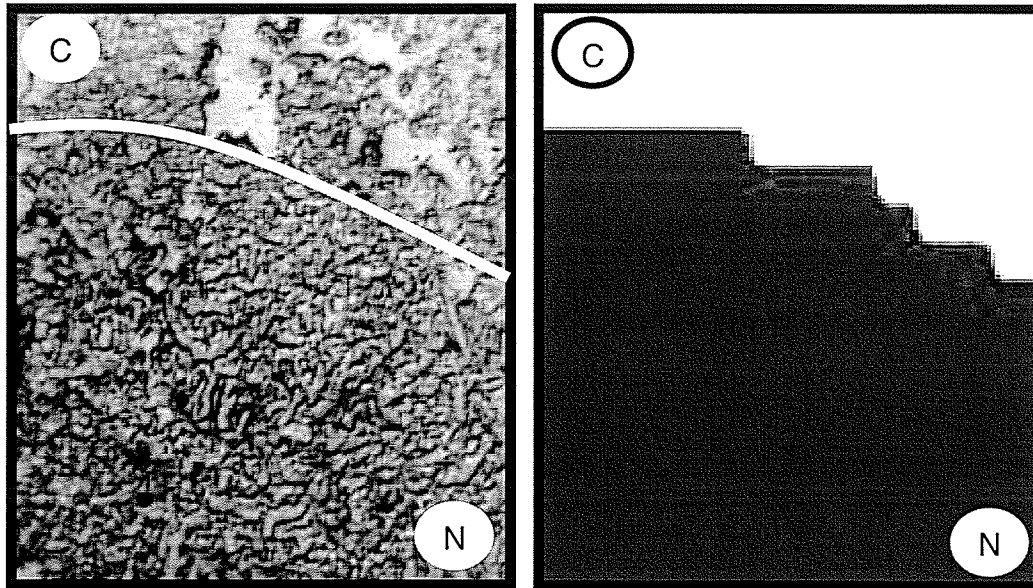


Figure 6. Left panel: Lung tissue section employed for microspectroscopy. The white line separates neoplastic (N) from control (C) tissue, with the border determined through hemotoxylin/eosin staining of an adjacent serial section. Right panel: Gray scale image obtained via optimal region selection/LDA classification of a grid of spectra obtained by IR microspectroscopy of the tissue section shown in the left panel. The dark pixels correspond to spectra classified as neoplastic, and the light pixels to spectra classified as control.

Chapter 3

Fourier-transform infrared microspectroscopic analysis of human lung tissue DNA *

K.C., McCrae¹, H.W., Unruh³, R.A., Shaw⁴, M.G., Sowa⁴, J.A., Thliveris², H.H., Mantsch⁴, J.E. Scott,^{1,2*} Departments of Oral Biology¹, Human Anatomy², and Surgery³, University of Manitoba, and the National Research Council, Institute for Biodiagnostics⁴, Winnipeg, Manitoba, Canada

*(2004) Fourier-transform infrared microspectroscopic analysis of human lung tissue DNA. *Biospectroscopy* (In manuscript).

Abstract

Lung cancer is the leading cause of cancer-related deaths worldwide. It is generally thought that cancers arise from alterations to the genetic material. Previous work from our laboratories, using Fourier-transform infrared microspectroscopy (FTIRM) to analyze mouse lung neoplasms, showed biochemical features in the DNA region ($930\text{-}935\text{ cm}^{-1}$ & $962\text{-}972\text{ cm}^{-1}$) that distinguished neoplastic from normal tissue. In the present study, we used FTIRM to analyze human lung tissue. Samples were obtained during routine surgical excision for lung cancer. Samples were snap-frozen, sectioned onto silver-coated glass reflectance slides, analyzed by FTIRM. Spectral absorptions reflecting DNA geometries, e.g. 965 cm^{-1} (DNA marker band) were identified in all tissue samples. Remarkable similarities were found in the spectra of samples of the same diagnosis (adenocarcinoma and squamous cell carcinoma). Pronounced differences in the $1000\text{-}1200\text{ cm}^{-1}$ region were found in the spectra of mucinous adenocarcinoma compared to spectra from non-mucinous adenocarcinoma, which likely reflects the presence of mucin. Structural changes to the DNA molecule may influence the functional ability of genetic material. The results indicate that FTIR may be used to identify similarities and differences within the DNA regions of neoplastic tissue.

Introduction

Lung cancer remains the leading cause of cancer-related deaths worldwide [1]. There are two major categories of lung cancer: small cell lung cancer, which account for 20-25% of all cases, and non-small cell lung cancer (NSCLC), which accounts for the majority of cases 75-85% [1,2]. The major types of NSCLC include squamous cell carcinoma (SCC), adenocarcinoma (AC), and large cell carcinoma (LCC). Neoplasms are classified currently according to the best-differentiated histological features of the tissues [1,2].

It is generally thought that neoplasms arise from multiple complex changes to the cell's genetic material [reviewed in 3-5]. DNA modification may be direct, e.g. gene mutations [6], or indirect, e.g. aberrant methylation [7]. While mutations may be found at any gene sequence, methylation occurs at specific locations, namely cytosine bases in CpG islands, which are found in proximal promoter regions of most genes [reviewed in 8 & 9]. Both genetic and epigenetic alterations may result in dysfunctional repair mechanisms and/or suppression or activation of some important genes (e.g. tumor-suppressor or oncogenes) [4,11] leading to neoplastic transformation.

The dynamic nature of DNA architecture has been studied extensively. The DNA helix exists in two right-handed forms, a rigid A-DNA and a flexible B-DNA with 13-14 different intermediate structures [12], and in a left-handed Z-form [13,14]. Although the significance of these conformations in normal or diseased cells is not established, it is evident that genomic stability is modulated by chromatin organization [8]. The structure of chromatin may be modified, e.g. by addition of methyl groups, which may subsequently influence accessibility of proteins to the DNA sequence. For example,

unmethylated DNA is accessible to proteins and consequently transcriptionally active whereas methylated DNA is inaccessible and therefore transcriptionally inactive [8]. While the cell's ability to modify the structure of DNA is a vital process to normal cell function, aberrant methylation patterns have been found in many neoplastic cells including lung neoplasms [7,9,11,16,17].

Information about DNA geometry may be obtained from Fourier-transform infrared spectroscopic [FTIR] analyses [14,18-21]. Absorption bands observed within the spectral range 700 to 1800 cm^{-1} , believed to correspond to nucleic acids, provide information about helical conformations [14]. Furthermore, structural changes to the DNA molecule due to methylation have been investigated using FTIR analyses, specifically the conformation-sensitive spectral regions (800-1800 cm^{-1}) [18].

Though it is possible to obtain a large amount of vibrational information characteristic of DNA architecture using purified DNA in aqueous solution or solid state, identifying DNA marker bands in spectra obtained from biological tissue presents a challenge [19]. Spectra reflect the total biochemical composition of the tissue specimen, with absorption patterns representing lipids, proteins, and DNA [21]. For this reason, caution is advised when assigning specific absorptions to particular molecules within whole tissue spectra. Nonetheless, many researchers [21-24,25,27] have assigned absorbances in the spectral region 800-1200 cm^{-1} to nucleic acids and phosphates based on analyses of biological tissue specimens.

Vibrational spectroscopic analyses provide biochemical and conformational information about healthy and diseased biological specimens. Previous work from our laboratory reported clear differences within spectral subregions that encompass DNA

absorptions (930-935 and 962-972 cm^{-1}) between normal and neoplastic mouse lung tissue [22]. The current study used Fourier-transform infrared microspectroscopy (FTIR) to analyze human lung lesions. As a preliminary investigation, we sought to determine if FTIR could provide vibrational information related to the DNA structure (e.g. identification of characteristics such as conformation-sensitive bands) of lung tissue specimens.

Experimental

Lung neoplastic tissue samples ($n=12$) were obtained during routine surgical excision for lung cancer at the Health Sciences Center, Winnipeg, Canada. Samples were placed immediately in sterile phosphate buffered saline, transported on ice, and within approximately 20 minutes of excision, samples were snap-frozen in liquid nitrogen and stored at -80°C . Lung tissue sections were obtained and frozen supported by a small amount of OCT (Optimal Cutting Tool) and sectioned at $12\ \mu\text{m}$ at -21°C . Sections were placed onto silver-coated glass reflectance slides (Kevley Technologies) for infrared microspectroscopy and hematoxylin and eosin for light microscopy.

Silver-coated glass reflectance slides were modified (in house) to subculture a human lung carcinoma A549 cell line (#CCL-185, ATCC, MD). Slides were modified with a removable media chamber (eight wells) (Nunc Lab-Tek II Chamber slide system, Fisher, Canada) adhered to the reflectance slides by silicone adhesive. Cells were dispersed onto the slides within each chamber. Minimum essential medium (MEM) (Gibco, ON) with 10% newborn calf serum (NCS) (Gibco ON) and 1% each of antibiotic/antimycotic and Fungizone (Gibco, ON) was added and the medium was changed after 24 h and 48 h for four days, until cells reached confluence as visualized

through a phase contrast microscope. Cells attached to the slides were washed gently three times with sterile Hanks Balanced Salt Solution (HBSS, Gibco, ON) (pH 7.1) to remove traces of medium and with the media chamber removed, slides were air-dried for 20 min before microspectroscopic analysis.

FTIR measurements were performed in reflectance mode using a Bruker Equinox 55 infrared spectrometer equipped with an IR Scope II infrared microscope accessory, as previously described by our laboratory [22]. The microscope accessory includes a liquid nitrogen-cooled mercury cadmium telluride detector and a motorized mapping stage. Spectra were recorded in the mid-infrared ($800\text{-}4000\text{ cm}^{-1}$). All spectra were acquired with an aperture of $60 \times 60\text{ }\mu\text{m}$. For each tissue sample section, a set of spectra was acquired over a rectangular grid of points (spectra maps). For each pixel, 128 interferograms were collected signal averaged and Fourier-transformed to generate spectra with a normal resolution of 4 cm^{-1} . All IR spectra were normalized to a common intensity over the $900\text{-}1800\text{ cm}^{-1}$ range to ensure successful discrimination based upon differences in the spectral pattern rather than differences in overall intensity [23]. Second derivatives were calculated from these normalized spectra and peaks were marked using spectra processing software (Grams/32 Spectral Notebook, version 4.11, 1999, Galactic Industries). At least 1000-5000 spectra were collected for each lung lesion and results were expressed as averages of those spectra.

Results and Discussion

Diagnoses and patient profiles are shown in Table 1. The average age of the male ($n=8$) and female ($n=4$) patients was 70 and 68, respectively. Figures 1-3 show averages of spectral maps collected for each tissue sample and A549 cells. Partial spectra (800-

1360 cm^{-1}) are shown with second derivatives inverted so that positive features correspond to absorption maxima.

Studies involving FTIR analyses of DNA in aqueous solution or solid state and biological tissues have provided some information about DNA conformation absorptions. A band at 958-968 cm^{-1} represents the C-C and C-O vibrations in deoxyribose, and is generally reported as a 'DNA marker' [23-25], which may indicate both right- and left-handed helices [13]. Absorption bands at 1220-1240 cm^{-1} reflecting PO_2^- symmetric vibrations of phosphate I [19,21-24] and 1080-1090 cm^{-1} signifying PO_2^- asymmetric vibrations of phosphate II [19,21-24] are thought to represent the backbone of B-form DNA [in 15 & 20]. Bands at 920-930 cm^{-1} have been shown to reflect the phosphate-sugar backbone of Z-form of DNA [13]. Absorptions at 860-865 cm^{-1} apparently signify the phosphate-sugar backbone of A-form of DNA [13,20].

Figure 1 compares the averaged spectra from AC lesions. On visual inspection, each spectrum displays the DNA marker band at 965 cm^{-1} , the PO_2^- symmetric and asymmetric bands, reflecting the B-form DNA, and the band signifying the Z-form of DNA (925 cm^{-1}). For the most part, there were remarkable similarities between the spectra of the AC classified lesions. This is interesting because AC is one of the most histologically heterogeneous neoplasms; i.e. most AC lesions are composed of a mixture of cell types, e.g. alveolar type II or Clara cells [1]. A very small absorption at 860 cm^{-1} , which reflects the A-form of DNA, was observed in the spectra from the poorly-differentiated AC specimen. This may reflect intratumoral variations of AC neoplasms [26] since histologically the difference between poorly-differentiated AC and AC is that the

former lesion consists of mostly undifferentiated cells with focal adenocarcinoma, whereas the latter is composed of mostly adenocarcinoma [1].

Figure 2 shows partial spectra obtained from SSC lesions. There was remarkable consistency between the SCC spectra, e.g. each displayed absorptions corresponding to the DNA marker band, PO_2^- symmetric and asymmetric vibrations, and Z-form DNA. However there was an increase in the relative intensity of the PO_2^- asymmetric band (1235 cm^{-1}) in the spectrum of the moderately-differentiated SCC, although the intensity was fairly consistent in the spectra from the mostly undifferentiated SCC specimens. Again, this may again reflect intratumoral variations of SCC lesions [26].

Other features, which may not be associated with DNA absorptions, were observed within the spectra of both AC and SCC lesions (Fig 1 and 2, respectively), e.g. the presence of glycogen (signified by 1045 cm^{-1}). This finding is in good agreement with other reports on FTIR analysis of excised lung lesions [27]. Two other bands prominent only in the spectra from the well-differentiated mucinous AC specimen observed at 1036 and 1120 cm^{-1} are presently unassigned and may reflect the presence of mucin, a glycosylated protein [28,29], which may have overlapped bands within the phosphodiester/carbohydrate region ($1000\text{-}1300\text{ cm}^{-1}$) [30].

Figure 3 shows spectra from organizing pneumonia (OP), LCC, pleomorphic carcinoma (PC), and an adenocarcinoma cell line (A549). All spectra reflected the DNA marker band (965 cm^{-1}), and both phosphate vibrations (1085 and 1235 cm^{-1}). LCC spectra has features similar to spectra from the other lung neoplastic lesions, however the relative intensity of the PO_2^- asymmetric stretch is greater and may indicate an increased nucleocytoplasmic ratio, which is not unexpected since one characteristic of these cells is

the large prominent nuclei and moderate amount of cytoplasm [1]. Pleomorphic carcinoma, a rare kind of neoplasm, is generally thought of as an AC with large cell features with abnormal mitoses [1,31]. The spectra from pleomorphic carcinoma sample differed from AC spectra in the relative intensity of DNA absorptions, which may reflect abnormal nucleocytoplasmic ratios. A particularly intriguing result was the remarkable similarity between the spectra of AC and OP, in terms of DNA band assignments and relative intensities. Interestingly, OP is found frequently within the vicinity of lung neoplasms, particularly adenocarcinomas, and has the potential mimic those lesions in radiographic tests [32]. The A549 cell line was cultured on silver-coated glass reflectance slides and analyzed by FTIR in the same manner as the tissue specimens (Figure 3). The ability to study the cells of a particular histological classification may be necessary to investigate characteristics unique to that neoplastic population, thereby avoiding inherent heterogeneity in excised lesions [1].

There are several important reasons for studying DNA conformation absorption bands in biological tissue specimens. Firstly, it is important to understand that the dynamic nature of the DNA molecule is critical for normal cellular processes, e.g. protein transcription. DNA exists in a rigid A-form, which is heavily methylated, and therefore restricted transcriptionally [8]. DNA exists also as a flexible, unmethylated B-form that is open to gene transcription [8]. The structure of DNA, therefore, is modified and stabilized by methylation, the covalent addition of methyl groups to the 5 position of cytosine bases within CpG dinucleotides. Changes in DNA structure due to aberrant methylation, e.g. hypomethylation or hypermethylation, have been implicated as important epigenetic events in the transformation of neoplastic cells [7,9,10,15]. The

mechanism of transformation, though not clearly understood, is thought to arise from gene silencing due to the rigid, heavily methylated form of DNA which makes the specific gene sequences inaccessible to transcription proteins [11].

Secondly, aberrant DNA methylation patterns have been observed frequently in lung cancers [16]. Many genes have been identified as targets for hypermethylation, or epigenetic inactivation, such as those involved in the cell cycle, DNA repair, or cell adherence, [for review see 33]. The heterogeneity of subpopulations within the primary population of neoplastic cells may be due to multiple genetic changes which precede phenotypic alterations [10]. Furthermore, some molecular alterations may be common to one lung cancer subtype or to all subtypes [16]. Toyooka et al. [34] demonstrated differences in DNA methylation patterns between AC and SCC; specifically the methylation rates were higher for AC than SCC. Altered DNA architecture may reflect in characteristic spectral absorptions that may be useful variables for analyses by sophisticated multivariate pattern recognition methods, which could lead to unique classification strategies.

Thirdly, some alterations may not be reversible, e.g. genetic mutations, whereas methylation is potentially reversible. In fact demethylating agents (5-azacytidine), which inhibit DNA methylation, are currently being tested clinically for treating patients with malignant diseases [9,10]. Taken together, identifying characteristic indicators of change to genetic architecture would be particularly helpful for understanding mechanisms of potentially reversible neoplastic transformation. Furthermore, these indicators could be used to analyze changes to a neoplastic population of cells, cultured on glass reflectance slides, following exposure to a carcinogen(s) and/or cancer-treatment method(s).

In summary, the current results suggest that some information related to DNA structure may be obtained through FTIR analyses of lung tissues. DNA conformations may be assigned according to reported absorption bands, namely the rigid A-form (860 cm^{-1}), the flexible B-form ($1080\text{-}1090$ or $1220\text{-}1225$ and $1235\text{-}1245\text{ cm}^{-1}$), and the Z-form (925 cm^{-1}). Both B- and Z-forms, were apparent in the spectra from all lung lesions, whereas the A-form was observed in one histological classification (poorly-differentiated AC). Spectra from specimens of the same histological classification (e.g. AC or SCC) were remarkably similar, yet presented subtle differences compared to lesions with different diagnoses (e.g. AC vs. mucinous AC). Finally, an adenocarcinoma cell line was cultured on silver-coated glass reflectance slides and analyzed using FTIR microspectroscopy. Identification of DNA structural absorptions within the DNA region of spectra of biological tissues may be useful for exploitation in FTIR analyses using sophisticated automated multivariate pattern recognition techniques. This not only provides valuable information about the genetic material of neoplasms, but may be helpful to classify lung neoplasms based on characteristic biochemical features.

Acknowledgements

This work was supported by a grant from the Natural Sciences and Engineering Research Council of Canada, Manitoba Institute of Child Health (MICH) and a fellowship from MICH to KCM.

References

1. World Health Organization. (1999). International histological classification of tumors. 2nd edn. WHO, Geneva.
2. Beadsmore, C.J., & Screatton, N.J. (2003). Classification, staging and prognosis of lung cancer. *European J of Radiology*, 45, 8-17.
3. Minna, J.D., Fong, K., Zochbauer-Muller, S., & Gazdar, A.F. (2002). Molecular pathogenesis of lung cancer and potential translational applications. *Cancer J*, 8, S41-S46.
4. Sekido, Y., Fong, K.M., & Minna, J.D. (1998). Progress in understanding the molecular pathogenesis of human lung cancer. *Biochim Biophys Acta*, 1378, F21-F59.
5. Zochbauer-Muller, S., Minna, J.D., & Gazdar, A.F. (2002). Aberrant DNA methylation in lung cancer: biological and clinical implications. *The Oncologist*, 7, 451-457.
6. Wistuba, I.I., Berry, J., Behrens, C., Maitra, A., Shivapurkar, N., Michgrub, S., Mackay, B., Minna, J.D., & Gazdar, A.F. (2000). Molecular changes in the bronchial epithelium of patients with small cell lung cancer. *Clinical Cancer Research*, 6, 2604-2610.
7. Baylin, S.B., Herman, J.G., Graff, J.R., Vertino, P.M., & Issa, J-P. (1998). Alterations in DNA methylation: a fundamental aspect of neoplasia. *Cancer Res*, 72, 141-196.
8. Geiman, T.M., & Robertson, K.D. (2002). Chromatin remodeling, histone modifications, and DNA methylation—how does it all fit together? *JBC*, 87, 117-125.
9. Ramsahoye, B.H., Davies, C.S., & Mills, K.I. (1996). DNA methylation: biology and significance. *Blood Reviews*, 10, 249-261.
10. Jones, P.A., & Baylin, S.B. (2002). The fundamental role of epigenetic events in cancer. *Nature Reviews*, 3, 415-428.
11. Virmani, A.K., & Gazdar, A.F. (2003). Tumor suppressor genes in lung cancer. *Methods Mol Biol*, 222, 97-115.
12. Dickerson, R.E., & Ng, H-L. (2001). DNA structure from A to B. *PNAS*, 98, 6986-6988.
13. Dohy, D., Ghomi, M., & Taillandier, E. (1989). Interpretation of DNA vibration modes: III. The behavior of the sugar pucker vibration modes as a function of its pseudorotation parameters. *J Biomol Structure & Dynamics*, 6, 741-754.

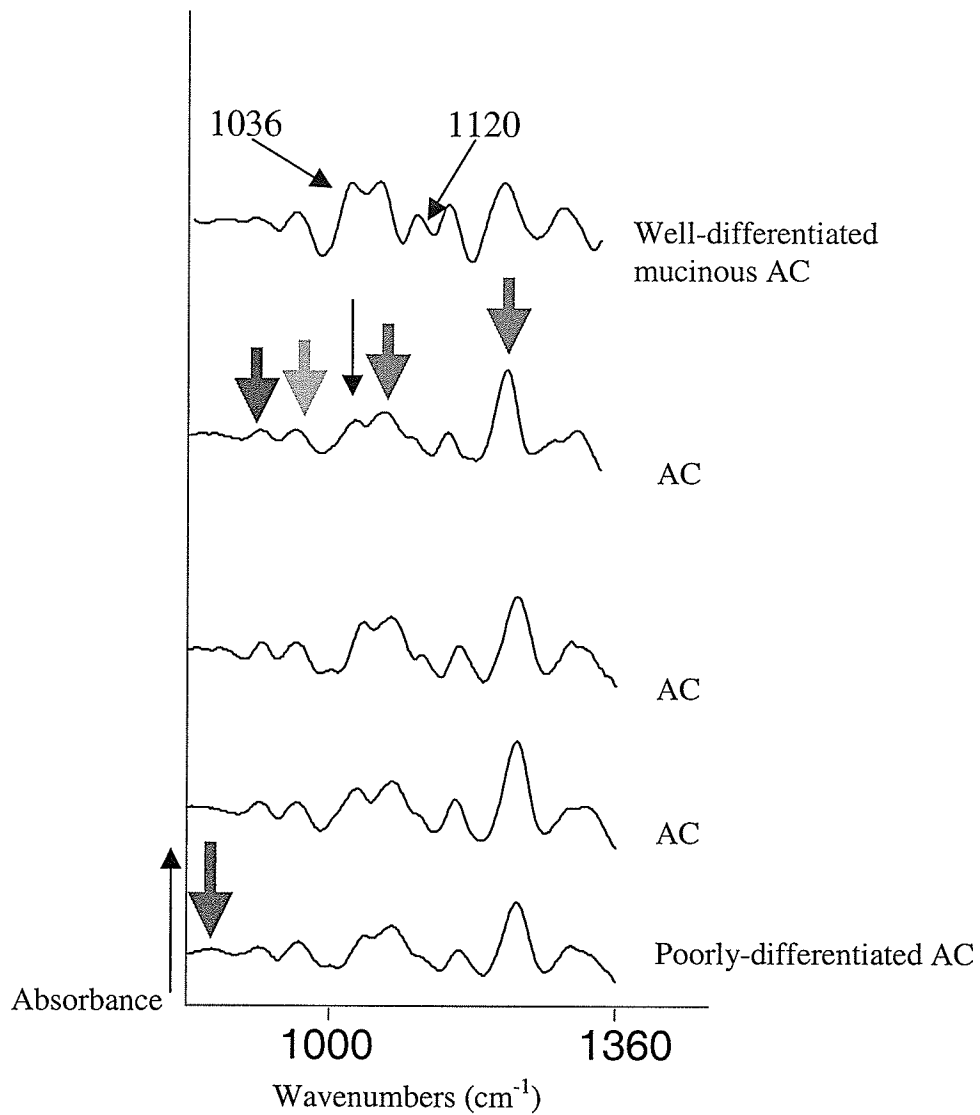
14. Taillandier, E., & Liquier, J. (1992). Infrared spectroscopy of DNA. *Methods Enzymol* 211, 307-335.
15. Baylin, S.B., Esteller, M., Rountree, M.R., Bachman, K.E., Schuebel, K., & Herman, J.G. (2001). Aberrant patterns of DNA methylation, chromatin formation and gene expression in cancer. *Human Mol Genetics*, 10, 687-692.
16. Sekido, Y., Fong, K.M., & Minna, J.D. (2003). Molecular genetics of lung cancer. *Annu Rev Med*, 54, 73-87.
17. Tsou, J.A., Hagen, J.A., Carpenter, C.L., & Laird-Offringa, I.A. (2002). DNA methylation analysis: a powerful new tool for lung cancer diagnosis. *Oncogene*, 21, 5450-5461.
18. Banyay, M., Graslund, A. (2002). Structural effects of cytosine methylation on DNA sugar pucker studied by FTIR. *JMB*, 324, 667-676.
19. Diem, M., Boydston-White, S., & Chiriboga, L. (1999). Infrared spectroscopy of cells and tissues: shining light onto a novel subject. *Appl Spectroscopy*, 53, 148A-161A.
20. Fang, Y., Wei, Y., Bai, C., Tang, Y., Lin, S-B., & Kan, L-S. (1997). Hydrated water molecules of pyrimidine/purine/pyrimidine DNA triple helices as revealed by FTIR spectroscopy: a role of cytosine methylation. *J of Biomolecular Structure & Dynamics*, 14, 485-493.
21. Jackson, M., Sowa, M.G., & Mantsch, H.H. (1997). Infrared spectroscopy: a new frontier in medicine. *Biophysical Chemistry*, 68, 109-125.
22. McCrae, K.C., Mantsch, H.H., Thliveris, J.A., Scott, J.E., & Shaw, R.A. (2001). Analysis of neoplastic changes in mouse lung using Fourier-transform infrared microspectroscopy. *Vibrational Spectroscopy*, 28, 189-197.
23. Liu, K-Z., Jia, L., Kelsey, S.M., Newland, A.C., & Mantsch, H.H. (2001). Quantitative determination of apoptosis on leukemia cells by infrared spectroscopy. *Apoptosis*, 6, 269-278.
24. Dovbeshko, G.I., Chegel, V.I., Gridina, N.Y., Repnyska, P., Shirshov, Y.M., Tryndiak, V.P., Todor, I.M., & Solyanik, G.I. (2002). Surface enhanced IR absorption of nucleic acids from tumor cells: FTIR reflectance study. *Biopolymers*, 67, 470-486.
25. Schultz, C.P., Liu, K-L., Kerr, P.D., & Mantsch, H.H. (1998). In situ infrared histopathology of keratinization in human oral/oropharyngeal squamous cell carcinoma. *Oncology Research*, 10, 277-286.
26. Carey, F.A., Lamb, D., & Bird, C.C. (1990). Intratumoral heterogeneity of DNA content in lung cancer. *Cancer*, 65, 2266-2269.

27. Yano, K., Ohoshima, S., Gotou, Y., Kumaido, K., Moriguchi, T., & Katayama, H. (2000). Direct measurement of human lung cancerous and noncancerous tissue by Fourier Transform infrared microscopy: can an infrared microscope be used as a clinical tool? *Analytical Biochemistry*, 287, 218-225.
28. Lopez-Ferrer, A., Barrano, C., & de Bolos, C. (2002). Differences in the O-glycosylation patterns between lung squamous cell carcinoma and adenocarcinoma. *Anatomic Pathology*, 118, 749-755.
29. Tsutsumida, H., Goto, M., Kitajima, S., Kubota, I., Hirotsu, Y., & Yonezawa, S. (2004). Combined status of MUC1 mucin and surfactant apoprotein A expression can predict the outcome of patients with small-size lung adenocarcinoma. *Histopathology*, 44, 147-155.
30. Wood, B.R., Quinn, M.A., Tait, B., Ashdown, M., Hislop, T., Romeo, M., & Mcnaughton, D. (1998). FTIR microspectroscopy study of cell types and potential confounding variables in screening for cervical malignancies. *Biospectroscopy*, 4, 75-91.
31. Przygodzki, R.M., Koss, M.N., & O'Leary, T.J. (2001). Pleomorphic (giant and/or spindle cell) carcinoma of lung shows a high percentage of variant CYP1A1*2. *Molecular Diagnosis*, 6, 109-115.
32. Romeo, S., Barroso, E., Rodriguez-Paniagua, M., Aranda, F.I. (2002). Organizing pneumonia adjacent to lung cancer: frequency and clinico-pathologic features. *Lung Cancer*, 35, 195-201.
33. Esteller, M., Corn, P.G., Baylin, S.B., & Herman, J.G. (2001). A gene hypermethylation profile of human cancer. *Cancer Research*, 61, 3225-3229.
34. Toyooka, S., Maruyama, R., Toyooka, K.O., McLerran, D., Feng, Z., Fukuyama, Y., Virmani, A.K., Zochbauer-Muller, S., Tsukuda, K., Sugio, K., Shimizu, N., Shimizu, K., Lee, H., Chen, C-Y., Fong, K.M., Gilcrease, M., Roth, J.A., Minna, J.D., & Gazdar, A.F. (2003). Smoke exposure, histologic type and geography-related differences in the methylation profiles of non-small cell lung cancer. *Int J Cancer*, 103, 153-160.

Table 1: Patient profiles and diagnoses

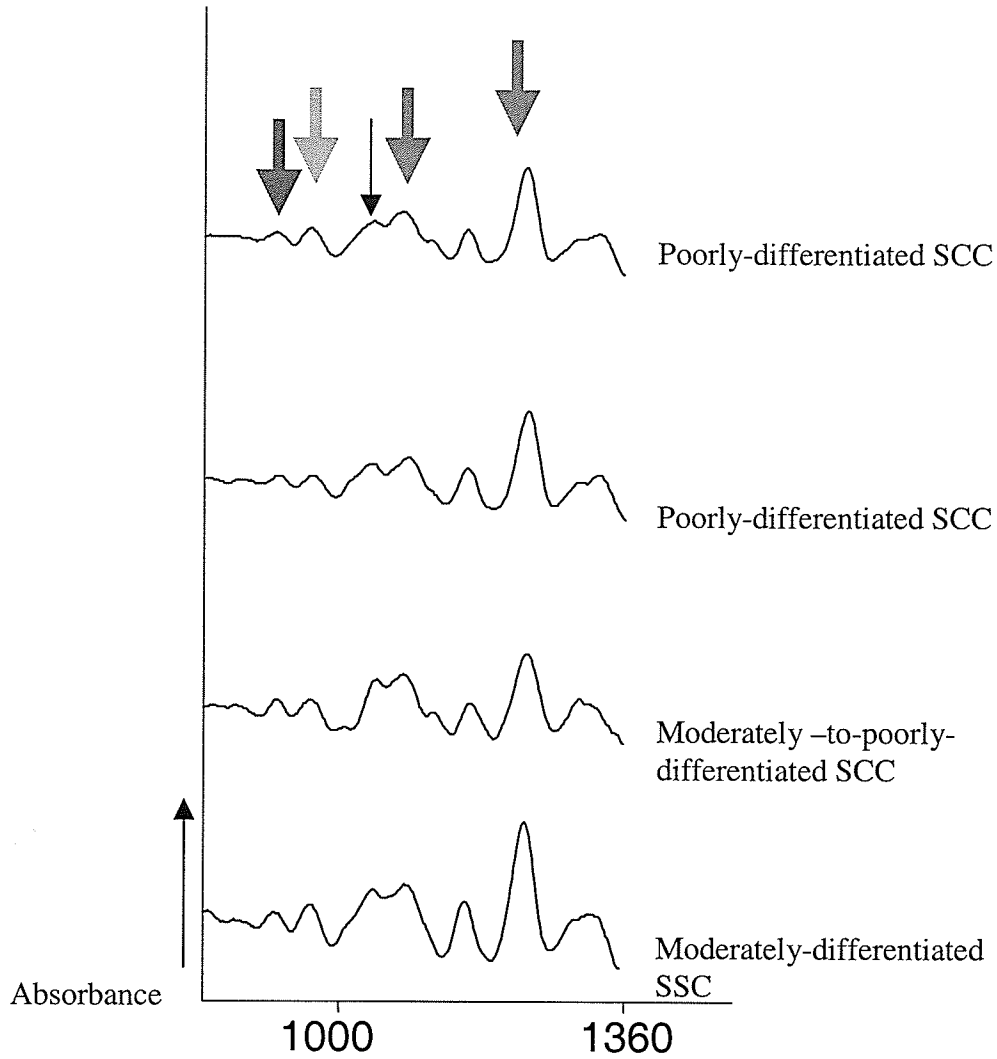
Gender	Age	Diagnosis
Male	65	Adenocarcinoma (poorly differentiated)
Male	71	Adenocarcinoma (well differentiated mucinous)
Male	80	Adenocarcinoma
Female	63	Adenocarcinoma
Female	69	Adenocarcinoma
Male	74	Squamous cell carcinoma (poorly differentiated)
Female	67	Squamous cell carcinoma (poorly differentiated)
Male	73	Squamous cell carcinoma (moderate-poorly differentiated)
Male	66	Squamous cell carcinoma (moderately differentiated)
Female	74	Undifferentiated large cell carcinoma
Male	74	Pleomorphic carcinoma
Male	59	Organizing pneumonia

Figure 1: Absorption spectra of adenocarcinomas



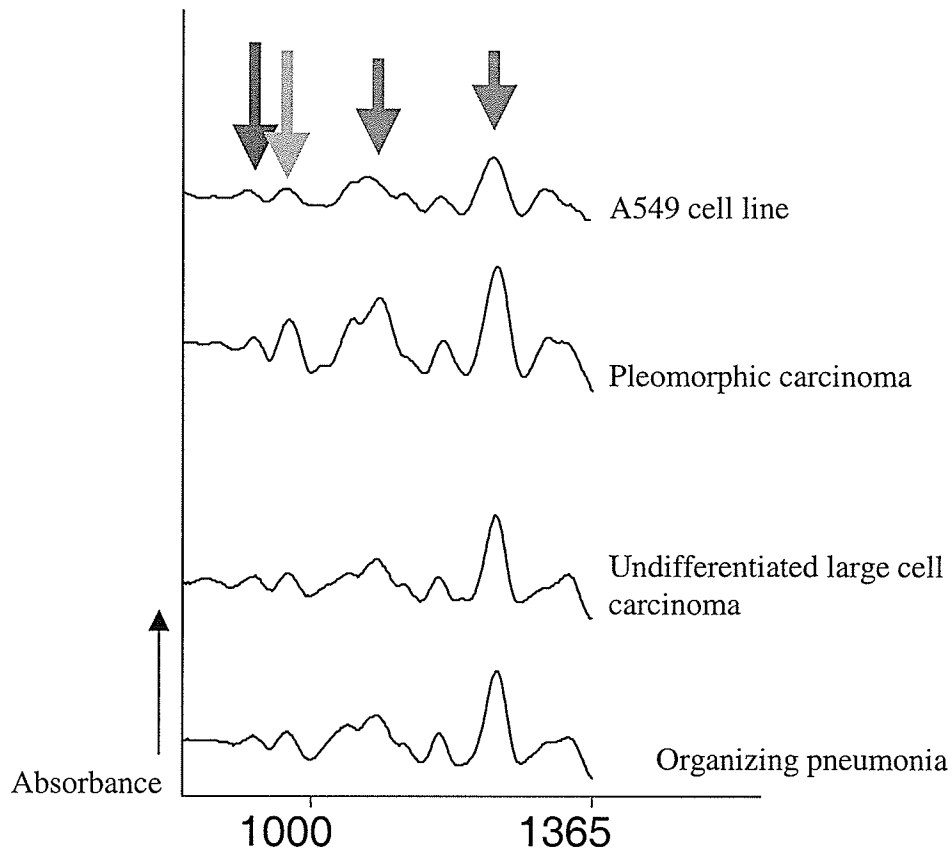
Partial spectra from adenocarcinoma specimens. Frequencies corresponding to molecular components of DNA are highlighted, B-DNA (red), Z-DNA (blue), DNA Marker (green), and A-DNA (purple). Note the differences in the 1036 and 1120 cm^{-1} regions of the well-differentiated mucinous adenocarcinoma spectra compared to the other adenocarcinoma tissue spectra.

Figure 2: Absorption spectra of SSC



Partial spectra (second derivatives) reflecting the biochemistry of squamous cell carcinoma lesions. Arrows point to DNA marker bands: B-DNA (red), Z-DNA (blue), DNA Marker (green). Note the relative intensity of the PO_2^- asymmetric band is stronger in the moderately-differentiated SCC. Note the presence of glycogen (black arrow).

Figure 3: Absorption spectra of lung lesions and A549 cells



Partial spectra comparison of a non-neoplastic lung lesion (organizing pneumonia) and neoplastic lung lesions (excised and cell line). Arrows indicate prominent DNA conformation markers: B-DNA (red), Z-DNA (blue), and DNA Marker (green).

Section 2: Pulmonary surfactant

The following section includes two studies involving analyses of pulmonary surfactant using capillary surfactometry. Chapter 4 describes the role of cholesterol in PS and the effect of excess cholesterol on PS composition and function in conducting airways. The next chapter (Chapter 5) describes also the influence of excess cholesterol on airway PS composition and function obtained from both healthy and tumor-bearing hypercholesterolemic mice. The role of PS cholesterol is not clearly established however, it plays a significant part in fluidizing the SAF.

Chapter 4

The effect of hypercholesterolemia on pulmonary surfactant function*

K.C. McCrae,¹ B. Weltman,¹ S. Alyward,¹ R.A. Shaw,⁴ M.G. Sowa,⁴ H.W. Unruh,³ T.G. Rand,⁵ J.A. Thliveris,² J.E. Scott,^{1,2*} Departments of Oral Biology,¹ Human Anatomy & Cell Science,² and Surgery,³ Faculties of Dentistry and Medicine, University of Manitoba, the National Research Council, Institute for Biodiagnostics,⁴ Winnipeg, Manitoba, and St. Mary's University, Halifax, NS⁵

*(2004) The effect of hypercholesterolemia on pulmonary surfactant function. *Chem Phys Lipids* (submitted).

Abstract

It has been established that phospholipids and cholesterol interact in films of pulmonary surfactant (PS). Generally it is thought that phospholipids increase film stability while cholesterol increases film fluidity. Research has shown altered cholesterol concentrations influence PS stability. We modified PS cholesterol in mice through diet; high cholesterol (hc) vs. standard diet (sd), and investigated PS stability using a capillary surfactometer (CS), which measures airflow resistance and patency. PS was collected by bronchoalveolar lavage and centrifuged to obtain the surface-active film (SAF). The hc-SAF had significantly more cholesterol than sd-SAF. CS analyses at 37°C showed no significant differences in airflow resistance between hc-SAF and sd-SAF. At 37°C, sd-SAF showed greater ability to maintain patency compared to hc-SAF, whereas at 42°C hc-SAF showed patency ability similar to sd-SAF. Results suggest that increased cholesterol in hc-SAF induced less stability in the SAF at physiological temperatures possibly due to cholesterol's fluidizing effect on phospholipids at physiological temperatures.

Introduction

The interactions between phospholipids and cholesterol have been studied extensively for decades. Phospholipids exist in either solid-ordered or liquid-disordered states depending upon their characteristic phase transition temperatures (T_m), e.g. the T_m for dipalmitoylphosphatidylcholine (DPPC 16:0/16:0) is $\sim 41^\circ\text{C}$ [3]. Solid-ordered phospholipids can be fluidized in water either by raising the temperature above phase transition or by the addition of cholesterol [25]. Cholesterol interacts with phospholipids, particularly saturated species, by intercalating between the fatty acid chains. As such, at temperatures above T_m , cholesterol rigidifies phospholipids, whereas below T_m , it liquefies phospholipids [3,25]. Therefore the stability and fluidity of biological films may be controlled tightly by the phospholipid:cholesterol system.

Pulmonary surfactant (PS) is a biological film that lines the air/water interface within the lungs. PS, synthesized and secreted by alveolar type II (AT II) cells, reduces the surface tension created by a thin aqueous layer coating the inner surfaces of alveoli and conducting airways [43,45]. The PS film is composed of proteins (~ 10 wt%) and lipids (~ 90 wt%). According to most reports, ~ 80 wt% of surfactant lipids are phospholipids, primarily phosphatidylcholine (75-85 wt%) and ~ 8 -10 wt% are neutral lipids, mainly free cholesterol (80-90 wt% or 1-20 mol%) [reviewed in 42].

PS lipid molecules orientate naturally with hydrophobic tails along the air surface and hydrophilic heads suspended in the water phase, forming a surface-active film (SAF) [20]. Saturated phospholipids, specifically DPPC, can withstand very high compression forces before collapse [21] and therefore serve to stabilize the SAF at high surface tensions [42]. However at physiological temperatures (37°C) DPPC exists in a gel state

and hence lacks the fluidity required for diffusing quickly through the lung liquid lining and re-spreading to the air/water interface after collapse [44]. Cholesterol, on the other hand, functions as a fluidizing agent in PS films [30,42] where the molecules act as spacers between DPPC molecules [4].

The phospholipid:cholesterol interaction appears to be important for influencing the stability and fluidity—and perhaps organization [9-11]—of pulmonary surfactant films. To demonstrate the effect of excess cholesterol on PS film stability within small conducting airways, we altered PS cholesterol levels through diet and investigated PS function using a capillary surfactometer (CS). The CS, designed to simulate small airways, measures film stability in terms of the pressure (cm H₂O) needed to rupture the meniscus formed by a liquid within the capillary to allow airflow and the length of time (%) the capillary remains patent to airflow. The current experiment in its entirety was conducted three times.

Experimental Procedures

Animals and diet treatment

Female CD-1 mice (aged 4-6 weeks) were selected randomly (n=24 per group) to receive *ad libitum* either a standard rodent diet without cholesterol (ProlabRMH 3000, LabDiet, PMI Nutrition International LLC, MO), which served as the control group, or a cholesterol-supplemented rodent diet (2% cholesterol, Complete Rat, ICN Biomedical, OH) for one month. Mice were kept on a 12hour light/dark cycle in plastic cages with aspen-chip bedding and received regular tap water for drinking. Weight and food consumption were monitored weekly. All procedures involving the animals were approved by the Canadian Council on Laboratory Animals.

Mice were euthanized by an intraperitoneal injection of sodium pentobarbital (Euthanyl, BiModa-MTC Animal Health, Inc, ON Canada). One ml of blood was collected immediately from each mouse into microtainer capillary blood collection vials with EDTA (K₂) (Fisher Scientific, Canada) and spun at 200xg before total serum cholesterol was determined using a Kodak Ektachem DT60 Analyzer (Eastman Kodak Company, NY).

Lung lavage

Bronchoalveolar lavage fluid (BALF) was collected immediately after exsanguinations as previously described by our laboratory [28]. Briefly the trachea was exposed and a blunt-end butterfly needle was inserted through a slit made in the trachea. One ml sterile saline (0.9%, Braun Medical, CA) was instilled and collected with a syringe (4x, total = 4 ml BALF per mouse). The volume of aspirated BALF was measured and recovery rate was approximately 85% per mouse.

BALF fractionation

To obtain the surface-active film (SAF) at the air/water interface, BALF was fractionated by differential centrifugation as described previously by our laboratory [28] and Oulton et al. [32]. Briefly cellular debris was removed via low-speed spin (140xg, 5 min) and the supernatant (whole surfactant) was then centrifuged (Beckman fixed rotor 80Ti) at 10,000xg/30 min to pellet large aggregates (e.g. lamellar bodies, tubular myelin) [32]. Supernatant recovered from this spin was centrifuged at 60,000xg/60 min to pellet intermediate aggregates, which represent the SAF at the air/water interface. The aggregates were resuspended in 500 µl sterile saline and kept at 4°C until analyzed. SAF

from standard diet fed mice and high cholesterol diet fed mice were designated as sd-SAF and hc-SAF, respectively.

Biochemical analyses

Phospholipid concentration within SAF was quantified according to the method of Rouser et al. [36]. Cholesterol concentration was analyzed using a cholesterol enzyme assay (Cholesterol CII, Wako Pure Chemical Industries, Ltd, VA) and micro-plate reader (Micro Manager, Bio-Rad Laboratories, Inc, CA).

Capillary Surfactometer

Film stability of the SAF was analyzed using a capillary surfactometer (Calmia Medical, Inc, Canada) as described by Enhorning [12]. Briefly 0.5 μ l of sample was pipetted into a small capillary tube forming a meniscus at the narrowest diameter (0.25 mm). Pressure from air injected through the tube ruptures the meniscus allowing continuous airflow for 120 seconds. Data were recorded as initial pressure (cm H₂O) required for meniscus rupture and percent of time the capillary tube remained patent. Analyses were conducted at 37 and 42°C.

Statistical analyses

Statistical significance was tested using Duncan's Multiple Range Test (Statistica, 1999 edition, Statsoft, Inc, OK) and data were checked for homogeneity of variance between groups using Levene's Test (Statistica, 1999 edition, Statsoft, Inc, OK).

Results

Animal data

The final weights and daily food consumption for both groups of mice did not differ significantly (Table 1). Total serum cholesterol (TSC) levels for cholesterol-

supplemented-mice were significantly higher than TSC for mice receiving a standard rodent diet (Table 1).

SAF biochemical data

The results of biochemical analyses of phospholipid and cholesterol in SAF were converted to mol% using average molecular weights (phospholipids = 760 & cholesterol = 387) [41] (see Table 2). Comparing the amount of individual components within BALF retrieved in the current study to results obtained by other research groups is made difficult due to variability in fluid recovery [2]. However following careful lavage procedures, demonstrated by an excellent recovery rate, and subfractionation methods used previously by our laboratory, we found consistency of results that are comparable with others [32].

Surface-active film stability

Results from the CS were interpreted as the ability of an amphipathic film, suspended in saline, to allow unrestricted airflow through a capillary tube thus simulating small conducting airways [12]. Figure 1 shows a typical tracing obtained from the CS of saline (0.9%) without surfactant. The strong attractive forces of water molecules create high surface tension, as evidenced by multiple collapses of the liquid within the capillary tube. Consequently, saline alone could not maintain unobstructed airflow.

Figures 2 and 3 show typical tracings obtained from CS analyses of SAF recovered from the mice. Initial pressures to rupture the menisci (or resistance to airflow) did not differ significantly between the groups (Table 3). At 37°C the sd-SAF demonstrated the ability to ensure continuous airflow through the capillary tube (about 96% patency). However at physiological temperatures, hc-SAF ability to maintain

patency of the capillary tube was inhibited initially, as shown by the multiple collapses (meniscus formation) of the fluid sample before securing airflow. At higher temperatures, the SAF of both groups had similar initial pressures although the resistance to airflow was significantly less compared to pressures at physiological temperatures. The hc-SAF demonstrated greater ability to maintain continuous airflow at 42°C (about 91%) compared to 37°C while the sd-SAF stability was not changed significantly.

Discussion

An aqueous liquid coats the inner surfaces of conducting airways within the lungs [45]. The surface tension generated by strong attractive forces of water molecules may cause the formation of menisci, or liquid occlusions, within narrow portions of small airways [16,31]. In the current study, the surface tension instabilities of saline were demonstrated by repetitive closure of the capillary tube (Figure 1). We observed a dramatic difference with the presence of a SAF suspended in saline, as evidenced by the ability to lower resistance to airflow, maintain patency, and prevent menisci reformation (Figure 2A). This finding is in good agreement with other reports [16,26,31] that show PS's ability to ensure unobstructed airflow through a narrow tube. The surface tension-reducing properties of PS are due in large part to amphipathic molecules like phospholipid and cholesterol [42].

It is widely accepted that saturated phospholipids, specifically DPPC, stabilize the PS film, and as such are the major constituents of surfactant lipids [42]. The long saturated acyl chains of DPPC are aligned parallel with each other and, due to conformational compatibility, compact easily at a slight tilt due to the large methylated heads. This energetically favorable orientation gives DPPC films the compressibility at

high surface pressures because upon compression, the phospholipid molecules decrease the tilt angle without decreasing intermolecular distance [21]. Fluorescence microscopy (FM) and Brewster angle microscopy (BAM) of purified surfactant phospholipids, demonstrated non-random partitioning of phospholipid molecules into liquid-condensed (LC) phases, composed of saturated phospholipids—specifically DPPC—and liquid-expanded (LE) phases composed of unsaturated phospholipids [9]. The LC phase has been shown to collapse at higher surface pressures compared to the LE phase [47]. Characteristic temperature-dependent phase transitions may influence the surface tension-reducing properties of SAF. DPPC films above $T_m \sim 41^\circ\text{C}$ exist in a liquid-disordered state (liquid refers to the bulk phase state and disordered refers to the orientation of the acyl chains [35]), whereas at physiological temperatures, DPPC exists in a solid-ordered state, which is necessary to maintain the stability of the SAF.

However DPPC alone does not make an adequate surfactant [42]. Earlier studies of DPPC films demonstrated that upon over-compression, DPPC could not adsorb into the monolayer rapidly after collapse, which resulted in the inability of film to obtain minimal surface tensions over subsequent cycles [reviewed in 42]. Fluidity of the SAF is critical for diffusing through the aqueous liquid to the air/water interface and re-spreading rapidly after collapse of the film [47]. Cholesterol plays a significant role in liquefying the phospholipid film, and such represents a major component of pulmonary surfactant lipids [30].

Amphiphilic in nature, the cholesterol molecule has a planar tetracyclic ring system, a short hydrophobic tail, and a hydrophilic 3β -hydroxyl group [3,29]. Cholesterol orients itself with the hydroxyl group in close proximity to the phospholipid chain-

backbone linkage region at the air/water interface and the rigid steroid ring parallel to the hydrocarbon chains of phospholipids [3,4,29]. When cholesterol intercalates between the acyl chains, the effect on phospholipids is an increased degree of chain order (or orientation) [3], reduced chain tilt angle [39], and increased fluidity of phospholipid dispersions [13]. The effect of cholesterol is strongest on saturated phospholipids due to the streamlined nature of both molecules, which creates a better fit [29]. Due to conformity mismatch, cholesterol is not strongly associated with phospholipid molecules of varying degrees of unsaturation [5,33].

The stereospecific phospholipid:cholesterol interaction may form an intermediate phase in co-existence with solid-ordered or liquid-disordered phases, depending upon the concentration of cholesterol. The intermediate phase, called liquid-ordered (LO) in which the bulk phase is fluid but the acyl chains are ordered, has characteristics of both solid-ordered phase (tightly packed acyl chains) and liquid-disordered phase (fast lateral motion) [3,29]. Non-uniform regions of phospholipid and cholesterol molecules may serve to organize individual constituents within lipid films [9], and these regions appear to have different physical properties that may influence the stability of the film [47].

At low cholesterol concentrations (<10 mol%) a LO phase may not be evident, so that phospholipids remain in a gel phase [24] with random distribution of two-molecule complexes composed of cholesterol bonded preferentially to saturated phospholipids [6]. In the present study, there was a small amount of cholesterol (~8 mol%) compared to a large amount of phospholipid (~92 mol%) within the sd-SAF. We envisaged one cholesterol molecule to approximately 12 phospholipid molecules, which probably would not cause significant perturbation of the phospholipid film. For this reason stability of the

sd-SAF was maintained (Figure 2A). However at low concentrations, cholesterol maintains some fluidizing effect on phospholipids, which is necessary for a well functioning PS, because even a small amount of cholesterol (4-10 mol%) has been shown to influence phospholipid molecules within their vicinity [3,24,34].

At moderate concentrations (~10-20 mol%), a LO phase co-exists within phospholipid gel or liquid states [29]. In the current study, the amount of cholesterol (~12 mol%) may have been sufficient to induce micro-immiscibility of the hc-SAF. The behavior of micro-immiscible surfactant films during compression has been documented using FM and BAM. Discher et al., [9] demonstrated domain formation patterns over a broad range of surface pressures. Initially upon compression surfactant components separated into LC and LE phases, with cholesterol partitioning predominantly into the LC phases and an abrupt remixing of phases occurred at a critical point during compression. Schief et al. [38] showed that cholesterol-rich condensed domains tended to collapse at lower surface pressures.

In the present study, we made two assumptions, (1) cholesterol associates selectively with saturated phospholipids in the LC phase and (2) cholesterol fluidizes saturated phospholipids, at physiological temperatures, by intercalating between the acyl chains. Based on these facts, we believe that the increased amount cholesterol in the hc-SAF (compared to sd-SAF) may have facilitated repeated collapse of the film (Figure 2B). However, above melting temperatures the effect of cholesterol intercalation is rather interesting in that by imparting order to the acyl chains, it actually reduces the disorder of phospholipids in the liquid-disordered state [1,19], in other words cholesterol stabilizes the film. This effect was observed in the present study as the stability of hc-SAF

improved significantly at higher temperatures (Figure 3) as evidenced by improved patency (91%), which was nearly equivalent to sd-SAF patency (94%).

While cholesterol enhances fluidity of PS films at physiological temperatures, it facilitates the tendency for film collapse. For this reason we believe that the increased concentration of cholesterol in the hc-SAF, due to its fluidizing effect, decreased the ability of the film to secure stable and continuous airflow through the capillary tube at 37°C (Figure 2). The improved capability of hc-SAF to ensure patent airflow at 42°C (Figure 3) provided additional evidence for the ordering or stabilizing effect cholesterol on phospholipid films.

Pulmonary surfactant obtained by bronchoalveolar lavage contains other components such as surfactant proteins and anionic phospholipids. As such this cannot be ignored as a contributing factor to the fluidity of the PS film. We believe that the slight initial instability of sd-SAF (Figure 2) may be attributed to other surfactant constituents, along with cholesterol, which contribute to re-spreading of the surface-active film *in vivo*. Studies using whole surfactant preparations demonstrated that surfactant proteins and/or anionic phospholipids increase adsorption to the air/water interface [44]. However, most reports suggest that cholesterol plays a profound role in lipid fluidity [30]. For this reason, the altered stability of the hc-SAF may have been due mostly to the effects of the phospholipid:cholesterol interaction.

The present study describes a relatively simple *in vivo* model for altering PS cholesterol levels and demonstrates the effects of hypercholesterolemia on pulmonary surfactant composition. It is widely accepted that most (99%) of surfactant-bound cholesterol comes from serum lipoproteins [18], particularly VLDL [15]. Davidson et al.

[8] found that lowering serum cholesterol, by inhibiting the release of hepatic lipoproteins, did not affect the amount of cholesterol in surfactant because the lung cells were able to synthesize cholesterol whereas inhibiting endogenous synthesis by lung cells resulted in decreased surfactant cholesterol.

Furthermore, the destination of the cholesterol taken up by lung cells as well as which of the 40 plus cell types making up lung tissue [23] participates in the production of surfactant cholesterol, is not fully understood. Hass & Longmore [17] demonstrated that at least 20% of the cholesterol taken up by AT II cells is destined for release into the lung liquid lining for incorporation into extracellular surfactant. Darrah et al. [7] showed that cholesterol was distributed throughout many lung cells but concentrated mostly within lipid vacuoles of septal cells. While the issue related specifically to surfactant cholesterol uptake, storage, and release certainly intriguing, it is clearly beyond the scope of the present study and must await future examination.

Conclusions

We modified the amount of cholesterol in the SAF successfully using a relatively simple *in vivo* mouse model. The fluidizing effect of cholesterol was demonstrated by the CS, in terms of decreased ability to stabilize the film at the air/water interface within the capillary tube to ensure continuous airflow at physiological temperatures. We are currently pursuing studies using captive bubble surfactometry analyses, which will detail the surface tension-reducing properties of our surface-active films.

Acknowledgements

This work was supported by operating and equipment grants from Natural Sciences and Engineering Council of Canada and the Manitoba Institute of Child Health (MICH). KCM was generously supported by a Biology of Breathing group fellowship provided through MICH. The authors wish to thank Mr. R. Summers, Statistical Services Officer, National Research Council, Institute for Biodiagnostics, Winnipeg, Manitoba, Canada.

References

1. Almeida, P.F.F., Vas, W.L.C., & Thompson, T.E. 1992. Lateral diffusion in the liquid phases of dimyristoylphosphatidylcholine/cholesterol lipid bilayers: a free volume analysis. *Biochemistry*, 31, 6739-6747.
2. Baughman, R.P. 1997. The uncertainties of bronchoalveolar lavage. *Eur Respir J*, 10, 1940-1942.
3. Bernsdorff, A., Winter, R. 2003. Differential properties of the sterols cholesterol, ergosterol, β -sitosterol, *trans*-7-dehydroscholesterol, stigmasterol, and lanosterol on DPPC bilayer order. *J Phys Chem*, 107, 10658-10664.
4. Bhattacharya, S., & Haldar, S. 2000. Interactions between cholesterol and lipids in bilayer membranes. Role of lipid headgroup and hydrocarbon chain-backbone linkage. *Biochem Biophys Acta*, 1467, 39-53.
5. Brzustowicz, M.R., Cherezov, V., Caffrey, M., Stillwell, W., & Wassall, S.R. 2002. Molecular organization of cholesterol in polyunsaturated membranes: microdomain formation. *Biophys J*, 82, 285-298.
6. Chui, S.W., Jakobsson, E., Mashl, R.J., & Scott, H.L. 2002. Cholesterol-induced modifications in lipid bilayers: a simulation study. *Biophys J*, 83, 1842-1853.
7. Darrah, H.K., & Hedley-Whyte, J. 1971. Distribution of cholesterol in lung. *J Appl Physiol*, 30, 78-90.
8. Davidson, K.G., Acton, S.M., Barr, H.A., & Nicholas, T.E. 1997. Effect of lowering serum cholesterol on the composition of surfactant in adult rat lung. *Am J Physiol Lung Cell Mol Physiol*, 272, L106-L114.
9. Discher, B.M., Maloney, K.M., Grainger, D.E., & Hall, S.B. 2002. Effect of neutral lipids on coexisting phases in monolayers of pulmonary surfactant. *Biophys Chem*, 101-102, 333-345.
10. Discher, B.M., Maloney, K.M., Grainger, D.W., Sousa, C.A., & Hall, S.B. 1999a. Neutral lipids induce critical behavior in interfacial monolayers of pulmonary surfactant. *Biochem*, 38, 374-383.
11. Discher, B.M., Schief, W.R., Vogel, V., & Hall, S.B. 1999b. Phase separation in monolayers of pulmonary surfactant phospholipids at the air-water interface: composition and structure. *Biophys J*, 77, 2051-2061.
12. Enhorning, G. 2001. Pulmonary surfactant function studied with the pulsating bubble surfactometer (PBS) and the capillary surfactometer (CS). *Comp Biochem Physiol A Mol Integr Physiol*, 129, 221-226.

13. Evans, R.E., Willaims, M.A., & Tinoco, J. 1980. Surface viscosities of phospholipids along and with cholesterol in monolayers at the air-water interface. *Lipids*, 15, 524-533.
14. Fleming, B.D., & Keough, K.M.W. 1988. Surface respreading after collapse of monolayers containing major lipids of pulmonary surfactant. *Chem Phys Lipids*, 49, 81-86.
15. Guthmann, F., Harrachruprecht, B., Looman, A.C., Stevens, P.A., Robenek, H., & Rustow, B. 1997. Interaction of lipoproteins with type II pneumocytes in vitro: morphological studies, uptake kinetics and secretion rate of cholesterol. *Eur J Cell Biol*, 74, 197-207.
16. Halpern, D., & Grotberg, J.B. 1993. Surfactant effects on fluid-elastic instabilities of liquid-lined flexible tubes: a model of airway closure. *J of Biomech Eng*, 115, 271-277.
17. Hass, M.A., & Longmore, W.J. 1979. Surfactant cholesterol metabolism of the isolated perfused rat lung. *Biochim Biophys Acta*, 573, 166-174.
18. Hass, M.A., & Longmore, W.J. 1980. Regulation of lung surfactant cholesterol metabolism by serum lipoproteins. *Lipids*, 15, 401-406.
19. Hemminga, M.A. 1975. An ESR spin label study of structural and dynamical properties of oriented lecithin-cholesterol multibilayers. *Chem Phys Lipid*, 14, 151-173.
20. Hills, B.A. 2002. Surface-active phospholipid: a Pandora's box of clinical applications. Part 1. The lung and air spaces. *Internal Medicine J*, 32, 170-178.
21. Kaganer, V.M., Möhwald, H., & Dutta, P. 1999. Structure and phase transitions in Langmuir monolayers. *Rev Mod Phys*, 71, 779-819.
22. Keough, K.M. 1990. Influence of chain unsaturation and chain position on thermotropism and intermolecular interactions in membranes. *Biochem Soc Trans*, 18, 835-837.
23. Kuhn, C. 1982. The cytology of the lung: ultra-structure of the respiratory epithelium and extracellular lining layers. In *Lung Development: Biological and Clinical Perspectives*, Vol I. Ferrel, P.M. (Ed). Academic Press:NY NY, 27-55.
24. Kurad, D., Jeschke, G., & Marsh, D. 2004. Lateral ordering of lipid chains in cholesterol-containing membranes: high-field spin-labeled EPR. *Biophys J*, 86, 264-271.
25. Ladbrooke, B.D., Williams, R.M., & Chapman, D. 1968. Studies on lecithin-cholesterol-water interactions by differential scanning calorimetry and x-ray diffraction. *Biochim Biophys Acta*, 150, 333-340.

26. Liu, M., Wang, L., Li, E., & Enhorning, G. 1991. Pulmonary surfactant will secure free airflow through a narrow tube. *J Appl Physiol*, 71, 742-748.
27. McConnell, H.M., & Vrljic, M. 2003. Liquid-liquid immiscibility in membranes. *Annu Rev Biophys Biomol Struct*, 32, 469-492.
28. McCrae, K.C., Rand, T., Mason, C., Oulton, M.R., Hastings, C., Cherlat, T., Thliveris, J.A., Shaw, R.A., Mantsch, H.H., MacDonald, J., & Scott, J.E. 2001. Analysis of *Stachybotrys chartarum* (atra) spores and pulmonary surfactant from spore-exposed mice by Fourier-transform infrared spectroscopy. *Chem Physics of Lipids*, 110, 1-10.
29. Miao, L.M., Nielsen, M., Thewalt, J., Ipsen, J.H., Bloom, M., Zuckermann, M.J., & Mouritsen, O.G. 2002. From lanosterol to cholesterol: structural evolution and differential effects on lipid bilayers. *Biophys J*, 82, 1492-1444.
30. Orgeig, S., & Daniels, C.B. 2001. The roles of cholesterol in pulmonary surfactant: insights from comparative and evolutionary studies. *Comp Biochem Physiol*, 129A, 75-89.
31. Otis, D.R., Johnson, J.M., Pedley, T.J., & Kamm, R.D. 1993. Role of pulmonary surfactant in airway closure: a computational study. *J Appl Physiol*, 75, 1323-1333.
32. Oulton, M., MacDonald, J., Janigan, D.T., & Faulkner, G.T. 1993. Mouse alveolar surfactant: characterization of subtypes prepared by differential centrifugation. *Lipids*, 28, 715-720.
33. Pasenkiewicz-Gierula, M., Subczynski, W.K., & Kusumi, A. 1990. Rotational diffusion of a steroid molecule in phosphatidylcholine-cholesterol membranes: fluid-phase microimmiscibility in unsaturated phosphatidylcholine-cholesterol membranes. *Biochem*, 29, 4059-4069.
34. Presti, F.T., Pace, R.J., & Chan, S.I. 1982. Cholesterol-phospholipid interaction in membranes. 2. Stoichiometry and molecular packing of cholesterol-rich domains. *Biochem*, 21, 3831-3835.
35. Rappolt, M., Vidal, M., Kriechbaum, M., Steinhart, M., Amenitsch, H., Bernstorff, S., & Laggner, P. 2003. Structural, dynamic and mechanical properties of POPC at low cholesterol concentration studied in pressure/temperature space. *Eur Biophys J*, 31, 575-585.
36. Rouser, G., Fleischer, S., & Yamamoto, A. 1970. Two dimensional thin layer chromatographic separation of polar lipids and determination of phospholipids by phosphorus analysis of spots. *Lipids*, 5, 494-496.

37. Scheidt, H.A., Müller, P., Herrmann, A., & Huster, D. 2003. The potential of fluorescent and spin-labeled steroid analogs to mimic natural cholesterol. *JBC*, 278, 45563-45569.
38. Schief, W.R., Anita, M., Discher, B.M., Hall, S.B., & Vogel, V. 2003. Liquid-crystalline collapse of pulmonary surfactant monolayers. *Biophys J*, 84, 3792-3806.
39. Smondyrev, A.M., & Berkowitz, M.L. 1999. Structure of dipalmitoylphosphatidylcholine/cholesterol bilayer at low and high cholesterol concentrations: molecular dynamics simulation. *Biophys J*, 77, 2075-2089.
40. Sugahara, M., Uragami, M., & Regen, S.L. 2003. Selective association of cholesterol with long-chain phospholipids in liquid-ordered bilayers: support for existence of lipid rafts. *J Am Chem Soc*, 125, 13040-13041.
41. Träuble, H, Eibl, H., & Sawada, H. 1974. Respiration—a critical phenomenon? *Naturwissenschaften*, 61, 344-354.
42. Veldhuizen, R., Nag, K., Orgeig, S., & Possmayer, F. 1998. The role of lipids in pulmonary surfactant. *Biochim Biophys Acta Molecular Basis of Disease*, 1408, 90-108.
43. Walters, D.V. 2002. Lung liquid lining—the hidden depths. *Biol-Neonate*, 81, 2-5.
44. Wang, Z., Hall, S.B., & Notter, R.H. 1996. Roles of different hydrophobic constituents in the adsorption of pulmonary surfactant. *J Lipid Res*, 37, 790-798.
45. Widdicombe, J.H., & Widdicombe, J.G. 1995. Regulation of human airway surface liquid. *Respiration Physiol*, 99, 3-12.
46. Worthman, L.A., Nag, K., Davis, P.J., & Keough, K.M. 1997. Cholesterol in condensed and fluid phosphatidylcholine monolayers studied by epifluorescence microscopy. *Biophys J*, 72, 2569-2580.
47. Zasadzinski, J.A., Ding, J., Warriner, H.E., Bringezu, F., & Waring, A.J. 2001. The physics and physiology of lung surfactants. *Current Opinion in Colloid and Interface Science*, 6, 506-513.

Table 1: Final weights, daily food consumption, and total serum cholesterol levels

	sd-mice	hc-mice
Final weights (gm)	38.7 (\pm 7.87)	36.74 (\pm 6.03)
Daily food consumption (gm/day)	3.76 (\pm 0.13)	3.81 (\pm 0.22)
Total serum cholesterol (MMOL/L)	2.65 (\pm 0.15)	3.24 (\pm 0.11)*

Results expressed as averages with standard deviation; * $p < 0.001$

Table 2: Mol% of phospholipids and cholesterol in SAF

	sd-SAF	hc-SAF
Mol% cholesterol	7.84 ± 1.44	12.26 ± 2.83*
Mol % phospholipids	92.15 ± 1.40	87.74 ± 2.80**

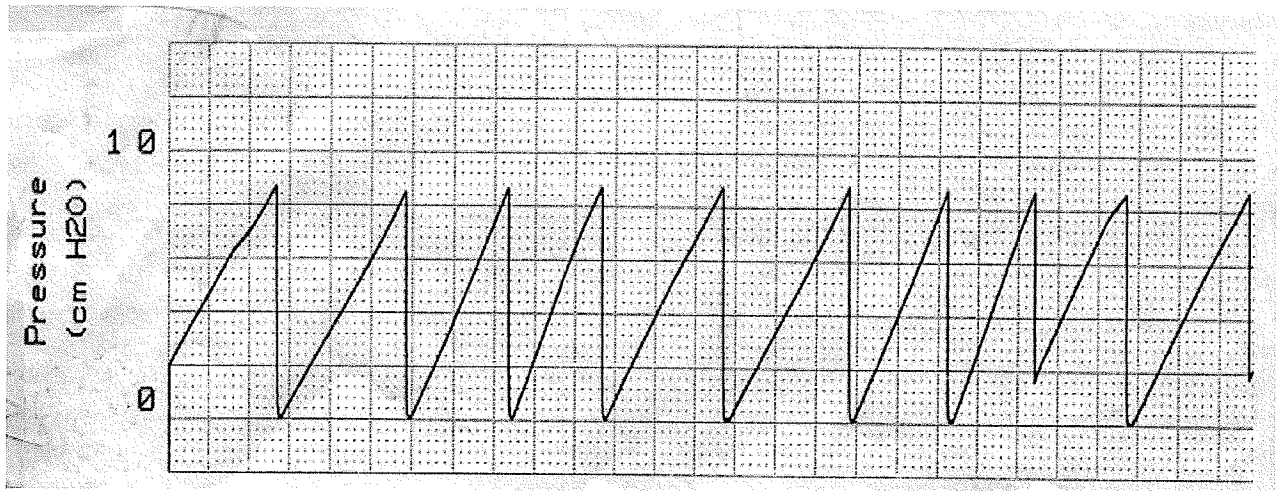
Results expressed as averages with standard deviation; * $p < 0.001$; ** $p < 0.001$

Table 3: Fluid dynamics of SAF at 37 and 42°C

	37°C	42°C
sd-SAF: initial pressure (cm H ₂ O)	9.04 ± 0.38	7.4 ± 0.31 [†]
sd-SAF: patency (%)	95.52 ± 3.4	93.5 ± 4.76
hc-SAF: initial pressure (cm H ₂ O)	9.18 ± 0.56	7.95 ± 0.31 [†]
hc-SAF: patency (%)	83.66 ± 5.08 [*]	90.81 ± 4.7 ^{††}

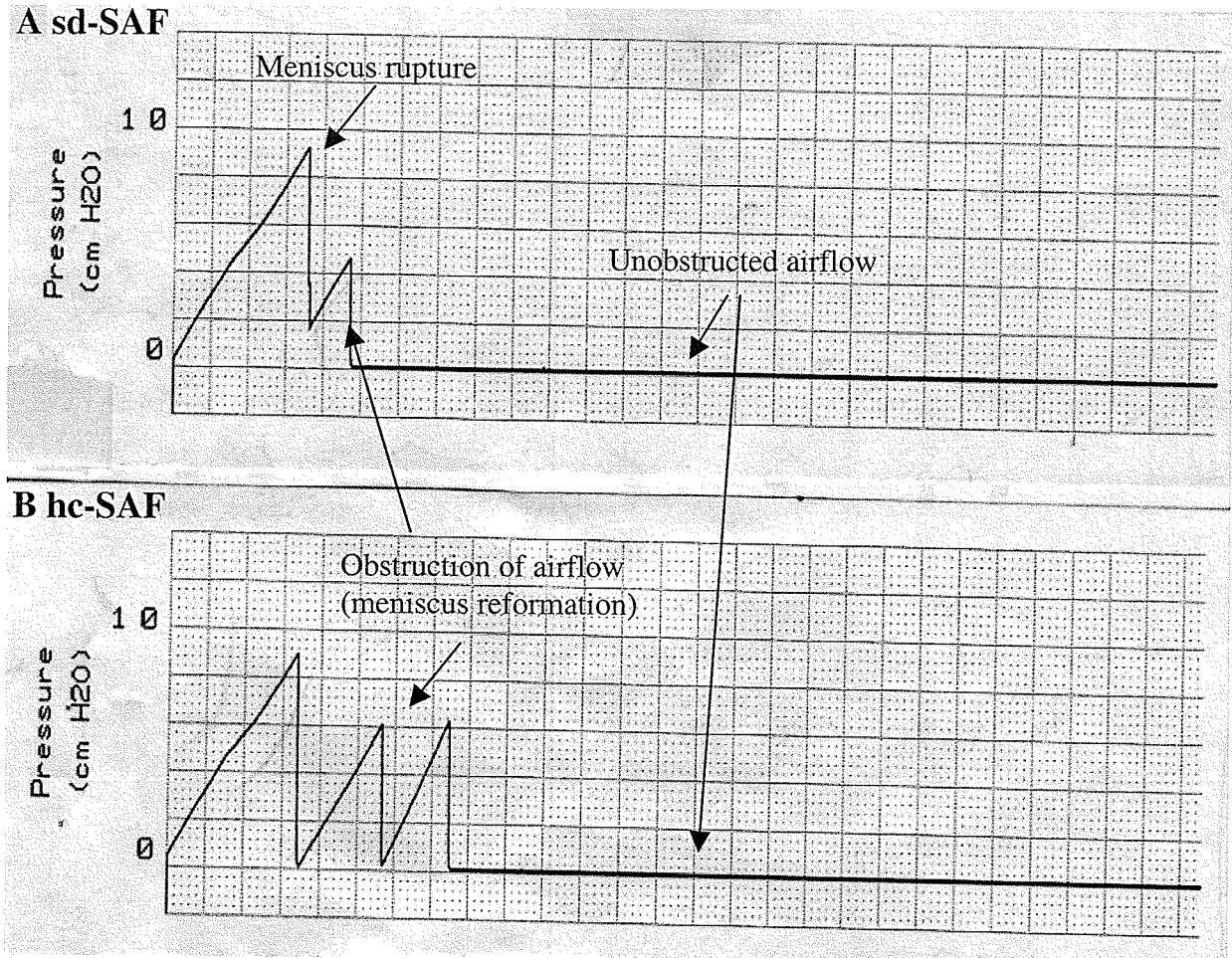
Results expressed as averages with standard deviation; *hc-SAF significantly different from sd-SAF $p < 0.001$; [†]sd-SAF significantly different at 42°C $p < 0.001$; ^{††}hc-SAF significantly different from hc-SAF at 42°C $p < 0.01$

Figure 1: Typical tracing of normal saline obtained from the CS



Normal saline (0.9%) was analyzed at 37°C. Airflow through the capillary tube is blocked repeatedly.

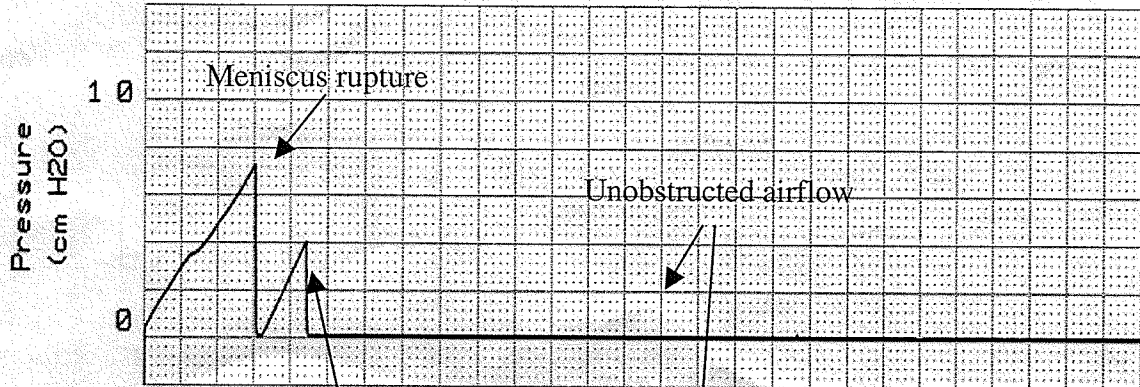
Figure 2: Typical tracings of SAF obtained from the CS at 37°C



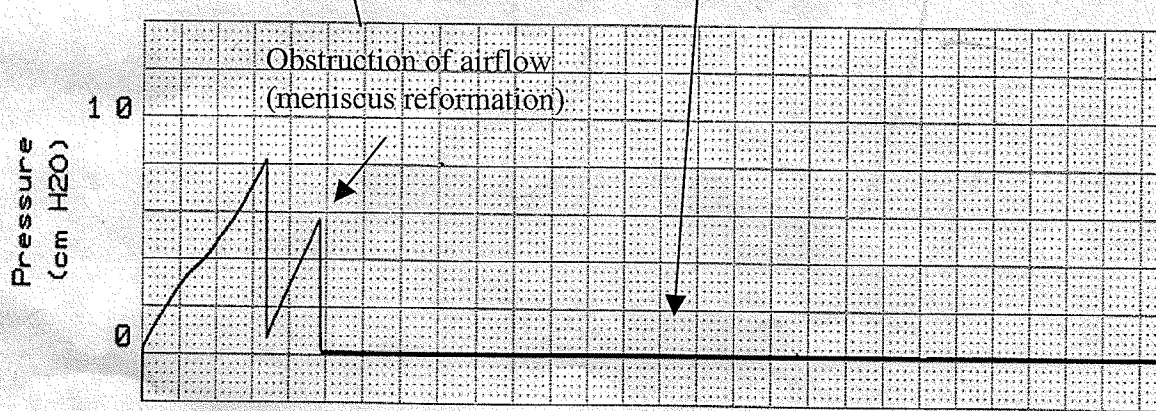
Tracings obtained from the CS show the effect of an amphipatic material (SAF). The tracings showed the typical initial pressures to rupture the meniscus were similar for both SAF (sd-SAF=9.0 cm H₂O & hc-SAF=9.1 cm H₂O). The tracing from the hc-SAF (B) showed capillary tube occlusion by reformation of meniscus before maintaining patency for 84% of the time whereas sd-SAF (A) maintained an open capillary tube for 96% of the time.

Figure 3: Typical tracings of SAF obtained from the CS at 42°C

A sd-SAF



B hc-SAF



Tracings obtained from the CS at phospholipid phase transition temperature. The tracings showed the typical initial pressures to rupture the meniscus were similar for both SAF (sd-SAF=7.4 cm H₂O & hc-SAF=7.9 cm H₂O). The tracing from the hc-SAF (B) showed capillary patency time was similar to sd-SAF (91 & 94%, respectively).

Chapter 5

Altered airway surfactant composition and function in hypercholesterolemic mice with pre-existing lung adenocarcinoma*

K.C. McCrae,¹ J.A. Thliveris,² B. Weltman,¹ S. Alyward,¹ R.A. Shaw,⁴ M.G. Sowa,⁴ H.W. Unruh,³ T.G. Rand,⁵ J.E. Scott,^{1,2*} Departments of Oral Biology,¹ Human Anatomy & Cell Science,² and Surgery,³ Faculties of Dentistry and Medicine, University of Manitoba, the National Research Council, Institute for Biodiagnostics,⁴ Winnipeg, Manitoba, and St. Mary's University, Halifax, NS⁵

*(2004) Altered airway surfactant composition and function in hypercholesterolemic mice with pre-existing lung adenocarcinoma. (In manuscript).

Abstract

The inner surfaces of the airways in lungs are coated with a liquid film. The liquid lining may form liquid occlusions within very small airways. Pulmonary surfactant (PS) minimizes the tendency for liquid obstruction. PS at the air/water interface (or surface-active film, SAF) is made of mostly saturated phospholipids and small amounts of cholesterol. Our previous work showed that PS from healthy hypercholesterolemic mice had diminished capacity to maintain unobstructed airflow. Although cholesterol is generally associated with heart disease or cancer, the effect of hypercholesterolemia in lung disease is not well established. We obtained PS from hypercholesterolemic mice with pre-existing urethane-induced adenocarcinoma and compared its function with PS from healthy mice, healthy hypercholesterolemic mice, and tumor-bearing mice. We analyzed the SAF with a capillary surfactometer, which simulates the small airways by analyzing the ability of a liquid to ensure free airflow, expressed as percentage of time. Results indicated that PS from healthy and tumor-bearing mice maintained unobstructed airflow (95 & 96%, respectively) whereas both healthy and tumor-bearing hypercholesterolemic mice had decreased ability to ensure airflow (about 83% for both). A poorly functioning airway surfactant may lead to airway closure from liquid occlusions, which may decrease ventilation to the affected alveoli.

Introduction

Within the lungs is an irregular branching system, called the tracheobronchial tree, which conducts air to the alveolar sacs. The caliber of conducting airways becomes increasingly smaller from the trachea to the terminal airways (roughly 2.0 cm to 0.2 mm diameter, respectively) [1]. The inner surfaces of small airways are coated with a thin liquid film [2,3] that has a thickness of approximately 10% of the airway radius and viscosity similar to water [4]. The liquid lining may form bridges or occlusions within very small airways, most notably in bronchioles 0.5 mm or less in diameter [1,5]. Liquid occlusions occur frequently at low lung volumes, particularly at end expiration, creating trapped air spaces within the alveolar sacs [6-8].

Pulmonary surfactant (PS), an amphipathic material, minimizes the tendency for liquid obstruction within terminal airways by decreasing the surface tension created by water molecules [9,10]. PS is made of approximately 90% lipids (~80% phosphatidylcholine and 10% neutral lipid) and 10% surfactant-associated proteins (surfactant proteins-A, B, C, & D). Saturated dipalmitoylphosphatidylcholine (DPPC) is the most abundant phospholipid (~50%) and free cholesterol is the major neutral lipid (~90%) [11].

PS lipids are synthesized and secreted by alveolar type II (AT II) cells in membrane-bound lamellar bodies (LB), which are subsequently rearranged into lattice-like structure called tubular myelin (TM) [12,13]. TM is reorganized into smaller aggregates that diffuse throughout the lungs including the airways. Aggregates of surfactant material collect beneath the air/water interface in the surfactant reservoir (SR) [14]. At the air/water interface, phospholipid and cholesterol molecules orientate

naturally and rapidly, forming the surface-active film (SAF), with hydrophobic heads in the air phase and the hydrophilic tails in the water phase [15]. PS components may be re-incorporated into the SR for re-adsorption into the SAF or recycled by primarily AT II cells (80%) [16] and degraded by alveolar macrophages (AM) (20%) [12,13].

The SAF lining the airways is generally thought to consist of mostly DPPC molecules that exist in the gel state at physiological temperatures. This gives the SAF stability, to withstand high compression forces within the lungs [reviewed in 10]. However the gel state prohibits rapid re-spreading of the phospholipid film, which is necessary during respiration to maintain minimal surface tension over subsequent cycles [10,11]. SAF contains also a small amount of cholesterol molecules that serve to fluidize the phospholipid film at physiological temperatures [reviewed in 17]. Cholesterol molecules interact preferentially with saturated DPPC [18] in the SAF to give the film critical stability and fluidity to maintain unobstructed airflow through the small airways.

The SAF may be disrupted by infiltration of non-surfactant-related proteins, such as plasma protein albumin, due to complications from inflammation [19], or destabilized due to abnormal proportions of surfactant constituents [20]. Respiratory conditions, such as asthma [22], and nutritional status [22-24] are known to influence PS composition and function. In a previous study we reported that the lipid composition SAF recovered from otherwise healthy hypercholesterolemic mice was altered, and we used capillary surfactometry (CS) to demonstrate that increased SAF cholesterol levels in the SAF contributed to decreased ability of the film to maintain patent airways [25].

The CS is a novel instrument developed to test the ability of a fluid to maintain patent airflow through narrow capillary tubes [26]. This technique has been used

extensively to evaluate the function of surfactant recovered from subjects with a variety of conditions, e.g. asthma [21], and to study the impact of non-surfactant related proteins, e.g. albumin on the stability of surfactant preparations [19].

The current study was an extension to our previous investigation on the effects of hypercholesterolemia on pulmonary surfactant from healthy mice [25]. Although cholesterol is most notably associated with heart disease (high serum cholesterol) or cancer (low serum cholesterol) [27], the effect of hypercholesterolemia in lung disease is not well established. Currently we report on the effects of high cholesterol in mice with pre-existing lung adenocarcinoma in terms of PS profile and stability.

Materials and Methods

Animals

Outbred female CD-1 mice (aged 4-6 weeks) were selected randomly (n=56 per group) to receive urethane treatment or serve as healthy controls. Mice were fed a standard rodent diet (ProlabRMH 3000, LabDiet, PMI Nutrition International LLC, MO) and kept on a 12 h light/dark cycle in plastic cages with aspen-chip bedding. Weight and water and food consumption were monitored weekly. All procedures involving the animals were approved by the Canadian Council on Laboratory Animals.

Urethane treatment: lung adenocarcinoma induction

Lung adenocarcinomas (LA) were induced as previously described by our laboratory [28]. Briefly urethane (ethyl carbamate) was dissolved in sterile saline (0.9%, Braun Medical, CA) at a concentration of 0.1g/ml. At the beginning of the study, mice were treated with a single intraperitoneal injection (1 mg/g body weight). The control group received an equal volume of sterile saline by the same route. Urethane was

dissolved in drinking water to make a 1% solution and given to treated mice for four months; control mice received regular tap water.

Diet treatment: cholesterol-supplemented rodent diet

Urethane treatment was stopped after four months and half the mice from each group (n = 28 per group) were randomly selected to continue the standard rodent diet (without cholesterol) or receive a cholesterol-supplemented diet (2% cholesterol, Complete Rat, ICN Biomedical, OH) *ad libitum* for one month until day of sacrifice. On the day of sacrifice, mice were euthanized by one intraperitoneal injection of sodium pentobarbital (Euthanyl, BiMeda-MTC Animal Health, Inc, ON Canada). One ml of blood was collected immediately from each mouse into microtainer capillary blood collection vials with EDTA (K2) (Fisher Scientific, Canada) and spun at 200xg before total serum cholesterol (TSC) was determined using a Kodak Ektachem DT60 Analyzer (Eastman Kodak Company, NY).

Bronchoalveolar lavage collection

Extracellular surfactant was obtained via bronchoalveolar lavage fluid (BALF) immediately after exsanguination as previously described [29]. Briefly the trachea was exposed and a blunt-end butterfly needle was inserted through a slit in the trachea. One ml sterile saline (Ca²⁺-free, 0.9%, Braun Medical, CA) was instilled and aspirated with a syringe (4x, total = 4 ml BALF per mouse). The volume of aspirate was measured and recovery rate was approximately 85% per mouse.

Electron microscopy

After lavage, lungs were removed, snap-frozen and stored at -85°C . a portion of lung was fixed in 2% buffered gluteraldehyde followed by post-fixation in 1% osmium tetroxide for examination by electron microscopy as described previously [28].

BALF differential centrifugation

To isolate PS subfractions, BALF was fractionated by differential centrifugation as described previously by our laboratory [29] and Oulton et al. [30]. Briefly cellular debris was removed via low-speed spin (140xg, 5 min) and the supernatant (representing whole surfactant) was centrifuged (Beckman fixed rotor 80Ti) at 10,000xg/30 min to pellet large—or ultraheavy [31]—aggregates, consisting of newly secreted LB and TM [30]. Recovered supernatant was centrifuged at 60,000xg/60 min to pellet intermediate—or heavy [31]—aggregates, representing the SAF [30]. Recovered supernatant was spun at 100,000xg/18 h to pellet small—light [31]—aggregates, which correspond to spent surfactant or metabolic products of SR for re-adsorption and/or recycling [31]. The aggregates were resuspended in 500 μl sterile saline and kept at 4°C until analyzed. Each fraction was labeled according to group and subfractionated pellet: C = control; U = urethane-treated; CH = cholesterol-supplemented; UCH = urethane & cholesterol-supplemented; and P10 = 10,000xg; SAF = 60,000xg; P100 = 100,000xg.

Biochemical analyses

The concentration of phospholipid was quantified according to the method of Rouser et al. [32]. Cholesterol was determined using a cholesterol enzyme assay (Cholesterol CII, Wako Pure Chemical Industries, Ltd, VA) and micro-plate reader (Micro Manager, Bio-Rad Laboratories, Inc, CA).

Capillary surfactometer

SAF stability was analyzed using a capillary surfactometer (Calmia Medical, Inc, Canada) as described previously by our laboratory [25] and Enhorning [20]. Briefly 0.5 μ l of sample was pipitted into a small glass capillary obstructing the narrowest diameter (0.25 mm). Pressure from air injected through the tube pushes the fluid occlusion out, coating the sides of the tube and allowing airflow for 120 seconds. Data were recorded as initial pressure (cm H₂O) to open the capillary and percentage of time capillary tube remained patent. Analyses were conducted at 37°C to simulate physiological temperatures and at 42°C to verify the dualistic nature of cholesterol.

Statistical analyses

Statistical significance, set at $p < 0.05$, was tested using Duncan's Multiple Range Test (Statistica Software, place) and data were checked for homogeneity of variance between groups using Lavene's Test (Statistica). For the Duncan's test, an analysis of variance was performed before each test.

Results

The weights and daily food and water consumption were unaffected by urethane or diet treatment and TSC was significantly higher in the diet-treated groups [Table 1]. Upon visual inspection, lungs from control and cholesterol-supplemented groups appeared normal whereas lungs from both urethane-treated groups displayed multiple slightly bulging small pearly white nodules (approximately 1-2 mm diameter). Electron microscopy revealed that the nodules were composed of AT II cells that were indistinguishable from control AT II cells [Figure 1]. Morphologically, lung tissue from healthy cholesterol-supplemented mice was similar to healthy control lung tissue (data

not shown) and non-neoplastic lung tissue from cholesterol-supplemented/urethane-treated mice was comparable to urethane-treated mice. The number of LB contained within AT II cells from normal lungs and non-neoplastic portions of lungs from all four groups were comparable, however AT II cells comprising neoplasms removed from both urethane-treated groups had significantly more LB [Table 2, Figure 1D]. Features characteristic of idiopathic cholesterol pneumonitis or cholesterol granulomas were not observed microscopically, e.g. foamy macrophages, multinucleated giant cells, or cholesterol-associated lesions [33-35].

Pulmonary surfactant subfraction lipid profile

Comparing the amount of individual components within BAL surfactant recovered in the present study to results obtained by other research groups is made difficult due to the lack of standardized BAL isolation methods and fractionation techniques [31,36]. However following careful lavage procedures, demonstrated by an excellent recovery rate, and subfractionation methods used previously by our laboratory, we found consistency of results that were comparable with others [30,31]. The yields of phospholipids and cholesterol were converted to mol based on molecular weights (phospholipid=760 & cholesterol=386 [37]) and expressed as phospholipid and cholesterol mol% [Table 3].

Roughly three quarters of the newly secreted lipids were phospholipid molecules and approximately one quarter was cholesterol molecules. Although the amount of cholesterol was increased in the newly secreted fraction recovered from the cholesterol-supplemented mice, the differences in recovered lipids from all four groups were not significant. Similarly the proportion of lipids destined for recycling or re-adsorption was

comparable between all four groups with a slight increase in cholesterol within the spent surfactant from the cholesterol-supplemented groups. The amount of cholesterol retained within the SAF fraction was significantly higher ($p < 0.05$) for the cholesterol-supplemented groups than the standard rodent diet groups.

Capillary surfactometry: SAF stability

Results from the CS were interpreted as the ability of an amphipathic film, suspended in saline, to allow unrestricted airflow through a capillary tube thus simulating the role of PS within small conducting airways [20]. Figure 2A shows a typical tracing obtained from the CS of saline without an amphipathic material like surfactant. Surface tension is created by water molecules, which continually pull the fluid into the column thus obstructing the flow of air through the narrow portion of the capillary tube. A stable surfactant lowers the surface tension created by the water molecules thereby decreasing the resistance to airflow (initial pressure), which pushes the fluid out of the narrow tube and allows free airflow (% patency) [Figure 2B]. Initial pressure corresponds to the resistance to airflow and simulates the workload of breathing whereas patency represents continuous unobstructed airflow [20].

Figures 3 and 4 show typical tracings obtained from CS analyses of SAF at 37 and 42°C. The resistance to airflow (initial pressures) of the SAF recovered from all four groups was comparable [Table 4]. The stability, in terms of the ability to maintain continuous airflow, of the C-SAF and U-SAF were not significantly different [Table 4 & Figure A-B]. However the stability was significantly lower for both groups receiving cholesterol-supplemented diets, as evidenced by the initial instability demonstrated by the CS [Table 4 & Figure 3 C-D]. Figure 4 shows typical tracings obtained from CS analyses

of SAF at 42°C. The initial resistance to airflow of the SAF from all four groups did not differ significantly [Table 4]. The stability of the SAF from the four groups was comparable at the higher temperatures, as evidenced by the abilities of all four SAF to maintain continuous airflow [Table 4 & Figure 4 A-D].

Discussion

CS simulates the small airways of the lungs and has been used extensively to study the ability of PS to maintain unobstructed airflow [20]. Smaller airways (0.25 mm diameter) may be occluded by the formation of a liquid bridge created by the surface tension of water molecules within the liquid lining inner surfaces of the narrow airways [38]. In the current study the ability saline to resist and inhibit free airflow was evident. In contrast the stability of PS was demonstrated by the SAF recovered from healthy control mice, evidenced by the decreased pressure to open the capillary tube and maintain patent airflow. For adequate ventilation to the alveolar sacs, air must flow unobstructed through the conducting airways. An important factor in the development of liquid obstruction is accumulation of liquid within the airway [38] and the most important factor in delaying the formation of liquid bridges is a well-functioning PS [6,8].

PS is synthesized and secreted by AT II cells in the form of membrane-bound LB, which are reorganized into TM [12]. The fact that phospholipid was increased in new PS recovered from both urethane-treated groups was not surprising considering that the number of LB contained within the AT II cells comprising the neoplasms was nearly double that of normal AT II cells taken from both the tumor-bearing lungs and healthy lungs. Previous investigations have demonstrated the ability of urethane-transformed AT II cells to synthesize surfactant components, at higher rates than healthy control cells [41-

43]. Furthermore, Bocking et al. [44] analyzed lung tissue from urethane-treated mice and found increased activity of esterase-7, an enzyme associated with extrusion of LB into the alveolar space. Taken together, this suggests that at least some of the AT II cells comprising the neoplasm in the current study were capable of secreting excess LB into the lung liquid lining.

The fact that the amount cholesterol was increased in the surfactant subfractions recovered from both cholesterol-supplemented groups was not unexpected. In a previous study we demonstrated an increase in cholesterol levels within the SAF fraction recovered from healthy hypercholesterolemic mice [25]. Although it is generally thought that approximately 99% of the cholesterol destined for surfactant is derived from the blood [45], it is not certain which of the 40 plus types of lung cell(s) [46] secrete surfactant cholesterol. Darrah et al. [47] found cholesterol accumulated throughout the lung tissue, mostly within septal cells, whereas Hass and Longmore [48] demonstrated at least 20% of serum cholesterol taken up by AT II cells is subsequently secreted in LB. Although the difference was not significant, the amount of cholesterol in the newly secreted fraction recovered from the cholesterol-supplemented/urethane-treated mice was slightly lower compared to the cholesterol-supplemented healthy mice. This was interesting considering that cholesterol is a key substrate in cell membrane formation [49, 50] and perhaps, in the present study, some excess cholesterol was diverted to constructing membranes of rapidly dividing lung neoplasms.

PS components may be metabolized by AM (20%) [13], or recycled into LB by AT II cells (80%) [51]. The up-take of surfactant components may be determined by a feedback system [12], e.g. Dobbs et al. [52] demonstrated that surfactant components

inhibited surfactant secretion by normal AT II cells *in vitro*. The current study found increased amounts of lipid constituents within the spent subfraction recovered from both urethane-treated groups. This may be an accumulation of surfactant components due to altered (or lost) feedback systems in neoplastic AT II cells and the inability of the surrounding normal AT II cells to recycle the excess surfactant products. Concomitantly AM may have diminished capacity to internalize efficiently the accumulating PS constituents [13].

Furthermore, case reports have documented non-cancerous cholesterol-associated lesions within lung tissue called cholesterol granulomas or cholesterol pneumonitis [33, 35]. Although rare, case studies document accumulation of lesions consisting of cholesterol deposits surrounded by foamy macrophages containing fat and cholesterol, giant multinucleated cells, and fibrosis [33-35]. The etiology remains uncertain, however it has been suggested that cholesterol accumulations may be due to hyperplastic AT II cells and/or dysfunctional AM [34]. In the current study, despite the buildup of PS material (phospholipids and/or cholesterol) in spent fractions recovered from the three treated groups, no microscopic features consistent with cholesterol-associated lesions were observed.

It is generally thought that SAF at the air/water interface is composed of mostly DPPC [53] and some cholesterol [17], as evidenced by the proportions of phospholipid to cholesterol for both the healthy controls and the urethane-treated group in the present study. More cholesterol was retained within the CH-SAF and UCH-SAF compared to C-SAF and U-SAF. This may be due in part to excess cholesterol within the surfactant material and to cholesterol's affinity for saturated phospholipids. Cholesterol molecules

intercalate preferentially between saturated phospholipid acyl chains [18]. Due to conformity mismatch, other phospholipids (which typically have bends in the acyl chains) tend to be excluded from the film upon compression [54]. A well-functioning SAF requires a large amount of DPPC for stability and a small amount of cholesterol for fluidity [55].

Abnormal proportions of PS constituents may influence SAF function [20]. This effect was demonstrated in our previous study [25] in which elevated levels of cholesterol were retained within the SAF recovered from healthy hypercholesterolemic mice. We used CS to analyze the stability of the SAF, in terms of ability to decrease resistance to airflow and maintain patency. The previous study demonstrated that elevated levels of cholesterol within the SAF significantly reduced the ability to maintain patent airways compared to SAF from control mice, which was consistent with what is known about the phospholipid:cholesterol interaction.

The phospholipid:cholesterol interaction has two affects depending upon the temperature of the phospholipid film since phospholipids have specific phase transition temperatures, e.g. DPPC $T_m=41^{\circ}\text{C}$ [56]. Firstly, below T_m the phospholipid film is solidified thus at physiological temperatures the SAF exists in a solid state. The long saturated acyl chains of DPPC molecules align parallel with each other, which gives DPPC films compressibility at high surface pressures [57]. Surface tension within the airways is reduced, which decreases the resistance to airflow and maintains patency [9].

The stability of well-functioning SAF was demonstrated in the current study by the SAF from the healthy controls, and interestingly, the urethane-treated group, which ensured free airflow for about 95 and 96 % of the time, respectively, at physiological

temperatures. The fact that the U-SAF stability was comparable to the healthy SAF was somewhat surprising considering that excess production or reduced metabolism of surfactant components may be associated with a condition that affects some cancer patients known as secondary alveolar proteinosis, an abnormal accumulation of PS material within the alveoli that may impair gas-exchange [58]. Possibly the excess surfactant material recovered from the urethane-treated mice in the current study was not enough to disrupt the functioning of the SAF within the airways. The SAF from both cholesterol-supplemented groups were significantly less able to secure free airflow at physiological temperatures (~83% patency for both groups). Considering the proportion of phospholipid to cholesterol in the CH-SAF and UCH-SAF, this was not surprising since many studies have demonstrated the tendency for cholesterol to facilitate collapse of PS films at physiological temperatures [53,55,59-60]. Cholesterol in the phospholipid film acts much like a spacer molecule between the phospholipid molecules, which then reduces the compressibility of the film [61].

Secondly, the phospholipid film is liquefied at temperatures above phase transition [62]. At melting temperatures, phospholipid molecules exist in a liquid-like form and the dualistic nature of cholesterol is evident in the ability to rigidify the fatty acyl chains (reducing the degree of freedom) thereby stabilizing the film [62]. In the current study, this stabilizing feature was confirmed by analysis of the SAF from the cholesterol-supplemented groups. At the higher temperature (42°C), the phospholipid films with a greater proportion of cholesterol, CH-SAF and UCH-SAF, showed significantly greater stability as evidenced by higher percentage of time the capillary

remained patent (~91% for both groups), which was comparable to the C-SAF and U-SAF.

Conclusions

In summary, the present study demonstrated that PS composition in hypercholesterolemic mice with or without pre-existing lung adenocarcinoma was modified and the SAF function was subsequently altered, as measured by the CS. A well-functioning airway SAF recovered from healthy control mice, composed of large amounts of phospholipid and small amounts of cholesterol, decreased the resistance to airflow and maintained unobstructed airflow through the capillary tube. The SAF from urethane-treated mice, composed of roughly similar proportions of lipids (compared to control mice) functioned as well as the SAF from healthy control mice. However SAF obtained from cholesterol-supplemented healthy mice and urethane-treated mice had retained disproportionately large amounts of cholesterol, which contributed to the SAF initial instability and inability to ensure free airflow through the capillary tube at physiological temperatures. Altered surfactant composition may modify surfactant function within the airways. Consequently, a poorly functioning airway surfactant may lead to airway closure due to liquid occlusions, which may decrease ventilation to the affected alveoli [6].

References

1. Macklem, P.T. Airway obstruction and collateral ventilation. *Physiological Reviews* 51 (1971) 368-436.
2. Walters, D.V. Lung liquid lining—the hidden depths. The 5th Nils W. Svenningsen memorial Lecture. *Biol Neonate* 81 Suppl 1 (2002) 2-5.
3. Widdicombe, J.H., & Widdicombe, J.G. Regulation of human airway surface liquid. *Respiration Physiol* 99 (1995) 3-12.
4. Howell, P.D., Waters, S.L., & Grotberg, J.B. The propagation of a liquid bolus along a liquid-lined flexible tube. *J. Fluid Mechanics* 406 (2000) 309-335.
5. Frazer, D.G., Stangel, P.W., & Weber, K.C. Meniscus formation in airways of excised rat lungs. *Respiration Physiology* 36 (1979) 121-129.
6. Gaver, D.P., Samsel, R.W., & Solway, J. Effects of surface tension and viscosity on airway reopening. *Am Physiol Soc* 69 (1990) 74-85.
7. Ghadiali, S.N., & Gaver, D.P. An investigation of pulmonary surfactant physicochemical behavior under airway reopening conditions. *J Appl Physiol* 88 (2000) 493-506.
8. Otis, D.R., Johnson, M., Pedley, T.J., & Kamm, R.D. Role of pulmonary surfactant in airway closure: a computational study. *J Appl Physiol*, 75 (1993) 1323-1333.
9. Halpern, D., & Grotberg, J.B. Surfactant effects on fluid-elastic instabilities of liquid-lined flexible tubes. *J Biomech Eng* 244 (1993) 271-277.
10. Zasadzinski, J.A., Ding, J., Warriner, H.E., Bringezu, F., & Waring, A.J. The physics and physiology of lung surfactants. *Current Opinions in Colloid and Interface Science* 6 (2001) 506-513.
11. Veldhuizen, R., Nag, K., Orgeig, S., & Possmayer, F. The role of lipids in pulmonary surfactant. *Biochim. Biophys. Acta* 1408 (1998) 90-118.
12. Rooney, S.A., Young, S.L., & Mendelson, C.R. Molecular and cellular processing of lung surfactant. *FASEB J* 8 (1994) 957-967.
13. Wright, J.R., & Hawgood, S. Pulmonary surfactant metabolism. *Clin Chest Med* 10 (1989) 83-93.
14. Schurch, S., Qanbar, R., Bachofen, H., & Possmayer, F. The surface-associated surfactant reservoir in the alveolar lining. *Biol Neonate* 67 Suppl 1 (1995) 61-76.

15. Hills, B.A. Surface-active phospholipid: a Pandora's box of clinical applications. Part I. The lung and air spaces. *Internal Medical Journal* 32 (2002) 170-178.
16. Poelma, D.L.H., Zimmermann, L.J.I., Scholten, H.H., Lachmann, B., & van Iwaarden, J.F. In vivo and in vitro uptake of surfactant lipids by alveolar type II cells and macrophages. *Am J Physiol Lung Cell Mol Physiol* 283 (2002) L648-L654.
17. Orgeig, S., & Daniels, C.B. The roles of cholesterol in pulmonary surfactant: insights from comparative and evolutionary studies. *Comp Biochem Physiol* 129A (2001) 75-89.
18. Miao, L.M., Nielsen, M., Thewalt, J., Ipsen, J.H., Bloom, M., Zuckermann, M.J., & Mouritsen, O.G. From lanosterol to cholesterol: structural evolution and differential effects on lipid bilayers. *Biophys J* 82 (2002) 1492-1444.
19. Enhorning, G., & Holm, B.A. Disruption of pulmonary surfactant's ability to maintain openness of a narrow tube. *J Appl Physiol* 74 (1993) 2922-2927.
20. Enhorning, G. Pulmonary surfactant function studied with the pulsating bubble surfactometer (PBS) and the capillary surfactometer (CS). *Comp Biochem Physiol A Mol Integr Physiol* 129 (2001) 221-226.
21. Wright, S.M., Hockey, P.M., Enhorning, G., Strong, P., Reid, K.B.M., Holgate, S.T., Djukanovic, R., & Postle, A.D. Altered airway surfactant phospholipid composition and reduced lung function in asthma. *J Appl Physiol* 89 (2000) 1283-1292.
22. Brown, L.S., Bliss, A.S., & Longmore, W.J. Effect of nutritional status on the lung surfactant system: food deprivation and caloric restriction. *Exp Lung Res* 6 (1984) 133-147.
23. Faridy, E.E. Effect of food and water deprivation on surface activity of lung of rats. *J Appl Physiol* 29 (1970) 493-498.
24. Weiss, H.A., & Jurrus, E. Starvation on compliance and surfactant of the rat lung. *Respiration Physiology* 12 (1971) 123-129.
25. McCrae, K.C., Weltman, B., Alyward, S., Shaw, R.A., Sowa, M.G., Unruh, H.W., Rand, T.G., Thiveris, J.A., Scott, J.E. The effect of hypercholesterolemia on pulmonary surfactant function. *Chem Phys Lipids* (submitted).
26. Lema, G., Enhorning, G. Surface properties after a simulated PLA2 hydrolysis of pulmonary surfactant's main component, DPPC. *Biochim Biophys Acta* 1345 (1997) 86-92.
27. Cirillo, D.J., Agrawal, Y., & Cassano, P.A. Lipids and pulmonary function in the Third National Health and Nutrition Examination Survey. *Am J Epidemiol* 155 (2002) 842-848.

28. McCrae, K.C., Mantsch, H.H., Thliveris, J.A., Scott, J.E., & Shaw, R.A. Analysis of neoplastic changes in mouse lung using Fourier-transform infrared microspectroscopy. *Vibrational Spectroscopy* 28 (2002) 189-197.
29. McCrae, K.C., Rand, T.G., Shaw, R.A., Mason, C., Oulton, M.R., Hastings, C., Cherlet, T., Thliveris, J.A., Mantsch, H.H., MacDonald, J., Scott, J.E. Analysis of pulmonary surfactant by Fourier-transform infrared spectroscopy following exposure to *Stachybotrys chartarum* (atra) spores. *Chem Phys Lipids* 110 (2001) 1-10.
30. Oulton, M., MacDonald, J., Janigan, D.T., & Faulkner, G.T. Mouse alveolar surfactant: characterization of subtypes prepared by differential centrifugation. *Lipids* 28 (1993) 715-720.
31. Gross, N.J., & Narine, K.R. (1989). Surfactant subtypes in mice: characterization and quantitation. *J Appl Physiol* 66 (1989) 342-349.
32. Rouser, G., Fleischer, S., & Yamamoto, A. Two dimensional thin layer chromatographic separation of polar lipids and determination of phospholipids by phosphorus analysis of spots. *Lipids* 5 (1970) 494-496.
33. Fischer, E.G., Marek, J.M., Morris, A., & Nashelksy, M.B. Cholesterol granulomas of the lungs associated with microangiopathic hemolytic anemia and thrombocytopenia in pulmonary hypertension. *Arch Pathol Lab Med* 124 (2000) 1813-1815.
34. Kay, J.M., Heath, D., Hasleton, P.S., & Littler, W.A. Aetiology of pulmonary cholesterol-ester granulomas. *Brit J Dis Chest* 64 (1970) 55-57.
35. Lawler, W. Idiopathic cholesterol pneumonitis. *Histopathology* 1 (1977) 385-395.
36. Baugham, R.P. The uncertainties of bronchoalveolar lavage. *Eur Respir J* 10 (1997) 1940-1942.
37. Trauble, H., Eibl, H., & Sawada, H. Respiration—a critical phenomenon? *Naturwissenschaften* 61 (1974) 344-354.
38. Halpern, D., & Grotberg, J.B. Fluid-elastic instabilities of liquid-lined flexible tubes. *J Fluid Mech* 244 (1992) 615-632.
39. Enhorning, G., Duffy, L.C., & Welliver, R.C. Pulmonary surfactant maintains patency of conducting airways in the rat. *Am J Respir Crit Care Med* 151 (1995) 554-556.
40. Liu, M., Wang, L., Li, E., & Enhorning, G. Pulmonary surfactant will secure free airflow through a narrow tube. *J Appl Physiol* 71 (1991) 742-748.

41. Snyder, C., Malone, B., Nettesheim, P., & Snyder, F. Urethan-induced pulmonary adenoma as a tool for the study of surfactant biosynthesis. *Cancer Res* 33 (1973) 2437-2443.
42. Snyder, F., & Malone, B. (1975). Acyltransferase and the biosynthesis of pulmonary surfactant lipid in adenoma alveolar type II cells. *Biochem Biophys Res Commun* 66, 914-919.
43. Stoner, G.D., Hallman, M., & Troxell, M.C. Lethithin biosynthesis in a clonal line of lung adenoma cells with type II alveolar cell properties. *Exp Mol Pathol* 29 (1978) 102-114.
44. Bocking, B., Mittermayer, C., & von Deimling, O. Urethane-induced lung hyperplasia: carboxylesterase isozymes as markers in lung pathology. *Lab Invest* 44 (1981) 138-143.
45. Hass, M.A., & Longmore, W.J. Regulation of lung surfactant cholesterol metabolism by serum lipoproteins. *Lipids* 15 (1980) 401-406.
46. Kuhn, C. The cytology of the lung: ultra-structure of the respiratory epithelium and extracellular lining layers. In *Lung Development: Biological and Clinical Perspectives*, Vol I. P.M. Ferrel (Ed). Academic Press: NY NY (1982) 27-55.
47. Darrah, H.K., & Hedley-Whyte, J. Distribution of cholesterol in lung. *J Appl Physiol* 30 (1971) 78-90.
48. Hass, M.A., & Longmore, W.J. Surfactant cholesterol metabolism of the isolated perfused rat lung. *Biochim Biophys Acta* 573 (1979) 166-174.
49. Bennis, F., Favre, G., Le Gaillard, F., & Soula, G. Importance of mevalonate-derived products in the control of HMG-CoA reductase activity and growth of human lung adenocarcinoma cell line A549. *Int J Cancer* 55 (1993) 640-645.
50. Wood, R. Tumor lipids: identification of sterol ester species in Ehrlich ascites cells. *Cancer Research* 30 (1970) 151-154.
51. Dobbs, L.G., Wright, J.R., Hawgood, S., Gonzales, R., Venstrom, K., & Nellenbogen, J. Pulmonary surfactant and its components inhibit secretion of phosphatidylcholine from cultured rat alveolar type II cells. *Proc Natl Acad Sci USA* 84 (1987) 1010-1014.
52. Hildebran, J.N., Goerke, J., & Clements, J.A. Pulmonary surface film stability and composition. *J Appl Physiol*, 47 (1979) 604-61.
53. Brzustowicz, M.R., Cherezov, V., Caffrey, M., Stillwell, W., & Wassall, S.R. Molecular organization of cholesterol in polyunsaturated membranes: microdomain formation. *Biophys J* 82 (2002) 285-298.

54. Schief, W.R., Antia, M., Discher, B.M., Hall, S.B., & Vogel, V. Liquid-crystalline collapse of pulmonary surfactant monolayers. *Biophys J* 84 (2003) 3792-3806.
55. Bernsdorff, A., & Winter, R. Differential properties of the sterols cholesterol, ergosterol, β -sitosterol, *trans*-7-dehydroscholesterol, stigmaterol, and lanosterol on DPPC bilayer order. *J Phys Chem*, 107 (2003) 10658-10664.
56. Kaganer, V.M., Möhwald, H., & Dutta, P. Structure and phase transitions in Langmuir monolayers. *Rev Mod Phys*, 71 (1999) 779-819.
57. Ladeb, S., Fleury-Feith, J., Escudier, E., van Nhieu, J.T., Bernaudin, J., & Cordonnier, C. Secondary alveolar proteinosis in cancer patients. *Support Cancer Care* 4 (1996) 420-426.
58. Discher, B.M., Schief, W.R., Vogel, V., & Hall, S.B. Phase separation in monolayers of pulmonary surfactant phospholipids at the air-water interface: composition and structure. *Biophys J* 77 (1999) 2051-2061.
59. Discher, B.M., Maloney, K.M., Grainger, D.W., Sousa, C.A., & Hall, S.B. Neutral lipids induce critical behavior in interfacial monolayers of pulmonary surfactant. *Biochem* 38 (1999) 374-383.
60. Bhattacharya, S., & Haldar, S. Interactions between cholesterol and lipids in bilayer membranes. Role of lipid headgroup and hydrocarbon chain-backbone linkage. *Biochem Biophys Acta* 1467 (2000) 39-53.
61. Almeida, P.F.F., Vas, W.L.C., & Thompson, T.E. Lateral diffusion in the liquid phases of dimyristoylphosphatidylcholine/cholesterol lipid bilayers: a free volume analysis. *Biochemistry* 31 (1992) 6739-6747.

Table 1: Weight and daily water & food consumption and total serum cholesterol (TSC)

	C-group	U-group	CH-group	UCH-group
Final weight (gm)	53.4 ±3.4	54.5 ±2.9	57.4 ±2.0	59.6 ±1.4
Food (gm/day)	3.76 ± 0.13	3.71 ±0.26	3.81 ± 0.22	3.83 ±0.35
Water (ml/day)	15.4 ±0.49	15.3 ±0.59	16.5 ±1.4	16.1 ±0.3
TSC (mmol/L)	2.65 ± 0.15	2.56 ±0.1	3.24 ± 0.11*	3.41 ±0.12*

Results expressed as mean ±SD; * $p < 0.01$ compared to control and urethane-treated mice

Table 2: Number of LB contained within AT II cells

	C-group	U-group	CH-group	UCH-group
Healthy AT II cells	7.46 \pm 4.1	----	6.26 \pm 2.3	----
Non-neoplastic AT II	----	7.25 \pm 3.6	----	8.62 \pm 7.3
Neoplastic AT II	----	11.55 \pm 4.5*	----	10.4 \pm 5.7*

Results expressed as mean \pm SD; * p <0.05 compared to non-neoplastic & healthy AT II cells

Table 3: PS subfraction lipid summary

	C-group	U-group	CH-group	UCH-group	
P ₁₀	PL (mol%)	69.7 ±2.8	75.3 ±0.9	68.5 ±14.0	73.6 ±0.6
	CH (mol%)	30.3 ±3.0	24.7 ±0.8	31.5 ±11.0	26.4 ±0.7
SAF	PL (mol%)	92.2 ±0.8	91.4 ±1.5	87.7 ±2.0*	88.0 ±1.5 *
	CH (mol%)	7.8 ±1.2	8.6 ±1.1	12.3 ±2.4*	12.0 ±1.7*
P ₁₀₀	PL (mol%)	68.3 ±6.3	75.8 ±6.4	60.8 ±9.2	70.4 ±9.7
	CH (mol%)	31.7 ±6.0	24.2 ±6.0	39.2 ±9.0	29.6 ±9.6

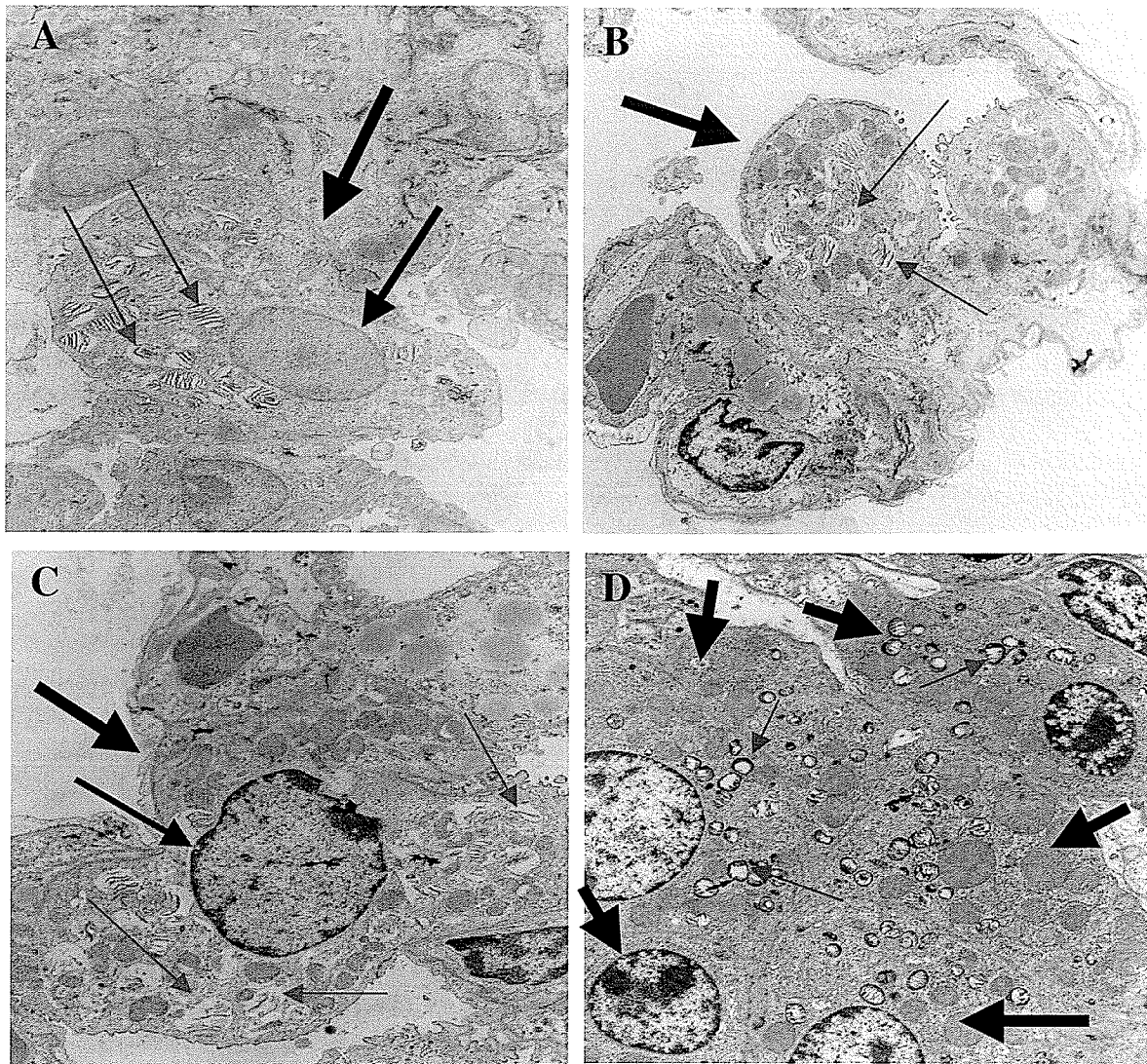
Results expressed as mean ±SD; * $p < 0.05$ compared to groups receiving the standard rodent diet (without cholesterol)

Table 4: Initial pressure and percentage patency of SAF at 37 and 42°C

	C-SAF	U-SAF	CH-SAF	UCH-SAF
37°C				
Pressure (cm H ₂ O)	9.0 ±0.4	8.9 ±0.4	9.2 ±0.6	9.4 ±0.3
% patency	95.5 ±3	96.8 ±3	83.7 ±5*	83.2 ±5*
42°C				
Pressure (cm H ₂ O)	7.4 ±0.3	7.7 ±0.2	7.8 ±0.3	7.5 ±0.3
% patency	93.5 ±5	94.1 ±2	90.8 ±5	91.0 ±4

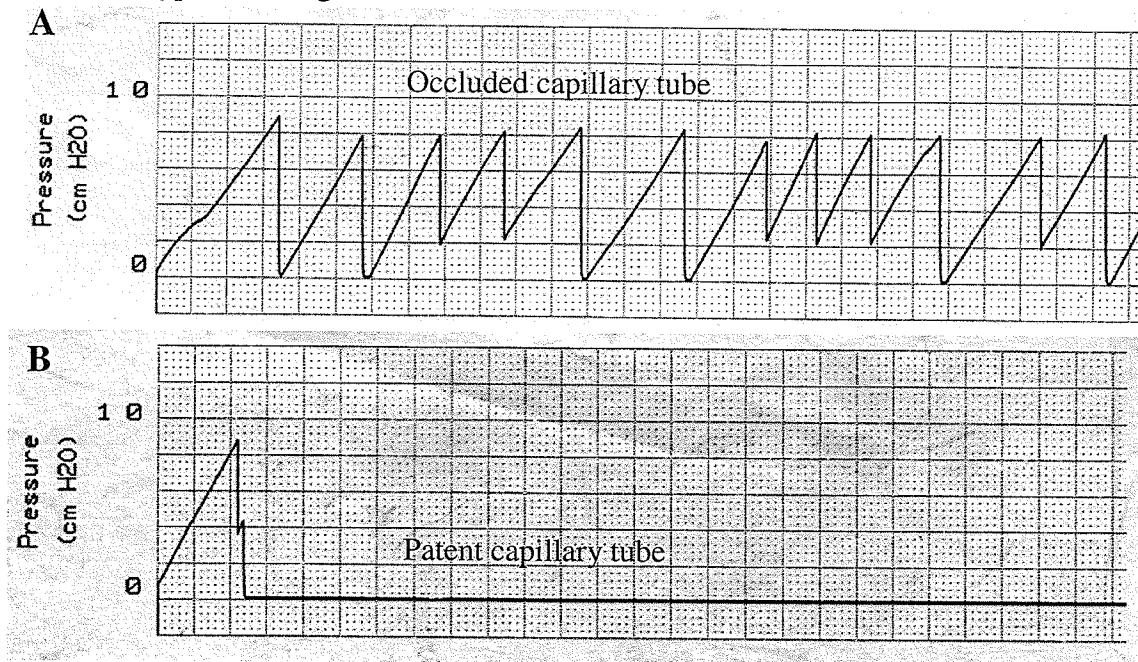
Results expressed as mean ±SD; * $p < 0.01$ compared to C-SAF and U-SAF

Figure 1: Electron micrographs of mouse lung tissue



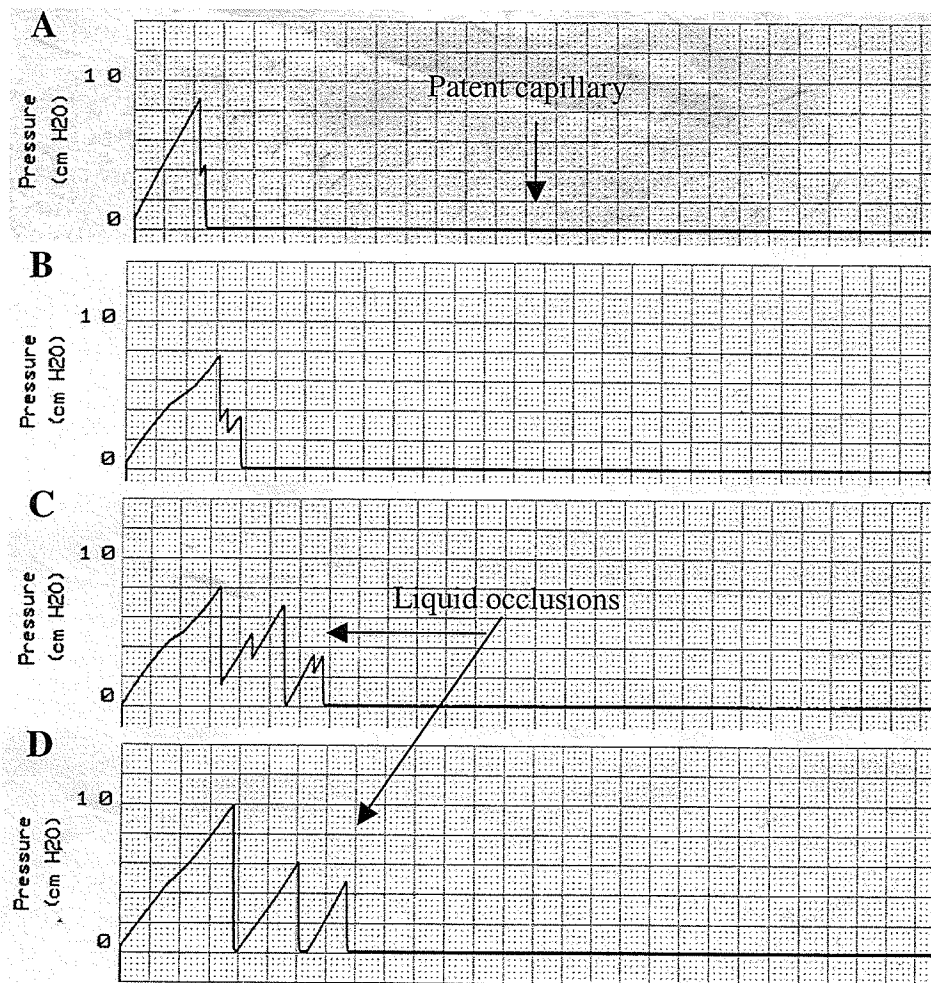
Electron micrographs of lung tissue. Panel A: electron micrograph of lung from a healthy control mouse. Thick arrow points to an AT II cell with a distinct nucleus (thin arrow) and several LB are present in the cytoplasm (blue arrows). Panel B: electron micrograph of a non-neoplastic AT II cell from a control tumor-bearing mouse (thick arrow). AT II cytoplasm contains distinct LB (blue arrows) and is indistinguishable from healthy control mice. Panel C: electron micrograph of non-neoplastic AT II cell from a urethane-treated hypercholesterolemic mouse with a distinct nucleus (thin arrow) and many LB in the cytoplasm (blue arrows). Panel D: electron micrograph of at least five membrane-bordered AT II cells (thick arrows) within a lung neoplasm from a urethane-treated mouse. Note numerous LB in the cytoplasm (blue arrows) (magnification x4700).

Figure 2: Typical tracings of saline and SAF



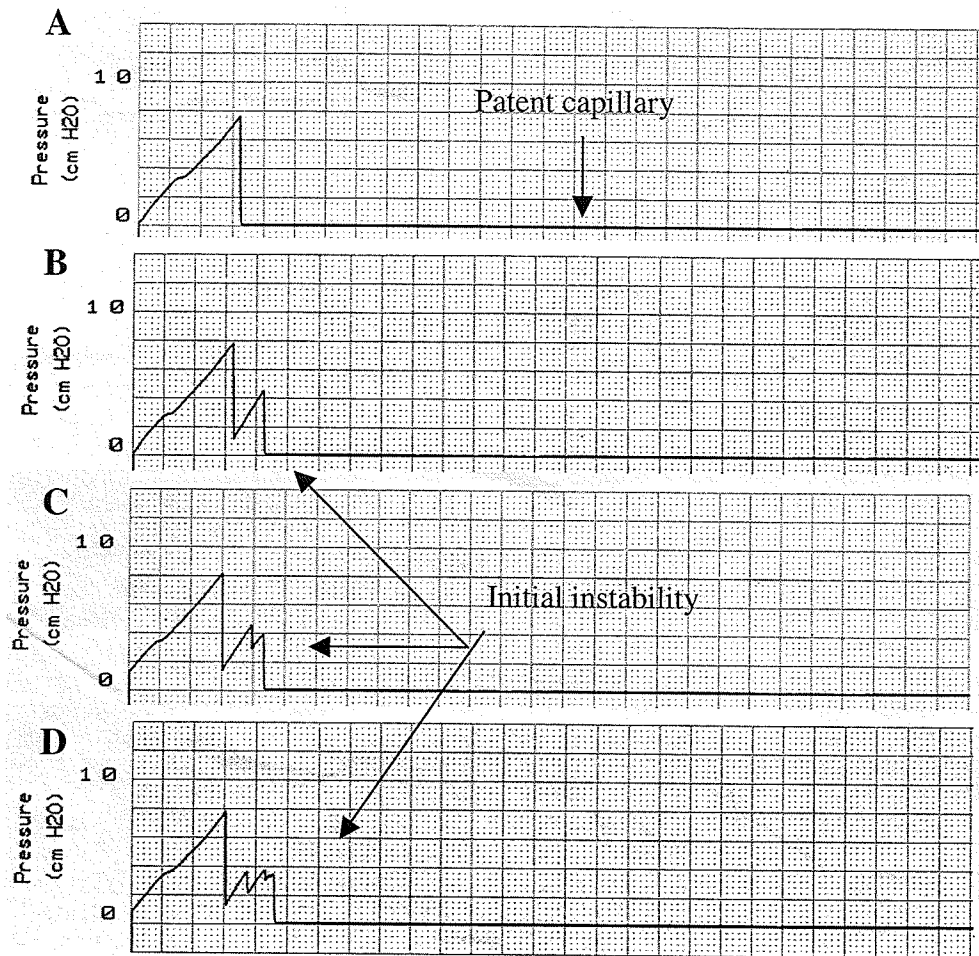
[A] Normal saline (0.9%) was analyzed at 37°C. Airflow through the capillary tube is blocked repeatedly. [B] Typical tracing from normal SAF recovered from healthy control mice shows the effect of the presence of an amphipathic material suspended in saline. The capillary tube remained patent for ~95% of the time.

Figure 3: Typical tracings of SAF at 37°C



Tracings obtained from the CS show the effect of SAF with excess cholesterol. Initial pressures to extrude the liquid occlusions were comparable. A & B show typical tracings from the C-SAF and U-SAF, both ensured patent airflow. C & D show tracings obtained from cholesterol-supplemented groups, CH-SAF and UCH-SAF. Liquid occlusions reformed within the narrow capillary tube, which obstructed initially the flow of air initially.

Figure 4: Typical tracings of SAF at 42°C



Tracings obtained from the CS at phospholipid phase transition temperature. The tracings from all four groups were comparable. SAF from the treated groups (B-D) showed initial instability however patency was maintained for most of the time.

Section 3: *Stachybotrys chartarum*

Thus far the current studies have focused on the influence of non-inhalation substances (urethane and cholesterol) on the pulmonary system. However, lungs are vulnerable to particulates, toxic or otherwise, that may be inhaled and deposited deep within the lungs. One especially harmful substance is *S. chartarum*—a mold that produces highly toxic spores. The following chapters describe the effect of exposure to the pulmonary system. Chapter 6 demonstrates altered PS composition from mice after *in vivo* exposure to toxic spores. Chapter 7 documents the epigenetic capabilities of *S. chartarum* spores through analysis of DNA damage in developing lung fibroblasts.

Chapter 6

Analysis of pulmonary surfactant by Fourier-transform infrared spectroscopy following exposure to *Stachybotrys chartarum* (atra) spores*

K.C. McCrae¹, T. Rand³, R.A. Shaw⁴, C. Mason³, M.R. Oulton⁵, C. Hastings¹, T. Cherlet², J.A. Thliveris², H.H. Mantsch⁴, J. MacDonald⁵ and J.E. Scott^{1,2,*}
Departments of Oral Biology¹ and Anatomy², Faculties of Dentistry and Medicine, University of Manitoba, Winnipeg, Manitoba, the Department of Biology³, St. Mary's University, Halifax, Nova Scotia, the National Research Council Institute for Biodiagnostics⁴, Winnipeg, Manitoba and the Department of Obstetrics and Gynecology⁵, Faculty of Medicine, Dalhousie University, Halifax, Nova Scotia

*(2001). Analysis of *Stachybotrys chartarum* (atra) spores and pulmonary surfactant from spore-exposed mice by Fourier transform infrared spectroscopy. *Chem. Physics of Lipids* 110, 1 – 10.

Abstract

Lung cells are among the first tissues of the body to be exposed to air-borne environmental contaminants. Consequently the function of these cells may be altered before other cells are affected. As gas exchange takes place in the lungs, changes in cellular function may have serious implications for the processes of oxygen uptake and carbon dioxide elimination. In order for these processes to occur, the lung must maintain a high degree of expandability. This latter function is accomplished in part by the pulmonary surfactant, which is synthesized and released by alveolar type II cells. Previous studies have shown that exposure to gas phase materials such as smoke or organic solvents can alter the composition and function of the surfactant. The present study examines the ability of highly toxigenic mold spores to alter surfactant composition. *Stachybotrys chartarum* spores suspended in saline were instilled into mouse trachea as described previously. After 24 hours the lungs were lavaged and the different processing stages of surfactant isolated by repeat centrifugation. Intracellular surfactant was isolated from the homogenized lung tissue by centrifugation on a discontinuous sucrose gradient. Samples were extracted into chloroform:methanol, dried and analyzed by Fourier Transform infrared spectroscopy (FTIR). Exposure to *S. chartarum* induced an overall reduction of phospholipid among the three surfactant subfractions. The intermediate and spent surfactant fractions in particular were reduced to about half of the values observed in the saline-treated group. The relative distribution of phospholipid was also altered by spore exposure. Within the intracellular surfactant pool, higher levels of phospholipid were detected after spore exposure. In addition changes were observed in the nature of the phospholipids. In particular strong

intramolecular hydrogen bonding, together with other changes, suggested that spore exposure was associated with absence of an acyl chain esterified on the glycerol backbone, resulting in elevated levels of lysophospholipid in the samples. This study shows that mold spores and their products induce changes in regulation of both secretion and synthesis of surfactant as well as alterations in the pattern of phospholipid targeting the pulmonary surfactant pools.

Introduction

Stachybotrys chartarum (atra) is an important environmental mold, which is commonly recovered from chronically wet building materials such as gypsum, drywall and ceiling tiles [1,2,3] in water damaged building environments [1,4]. This species produces an array of potent toxins including macrocyclic trichothecenes [5], which are potent protein synthesis inhibitors [6]. Due to its ubiquitous worldwide distribution and high toxicity [3,4], there is considerable interest in the health effects of inhalation exposure to *S. chartarum* spores and/or dust and mycelial fragments, all containing toxins [5,7,8], on humans and animals. While it is clear that exposure to materials heavily contaminated with this species can lead to stachybotryotoxicosis and even death in humans and animals [9,10,11], what is less clear is the impact of sub-acute exposures on health outcome.

Toxin exposure may occur in a variety of ways. For mold spores, the most common pathway is through the respiratory tract [12], which provides an area of at least 70 – 80m², several-fold larger than that of any other body surface [13]. This is in fact the major site of body exposure to the environment and thus to any air-borne toxic contaminants [14]. Furthermore the extremely attenuated nature of the blood-air barrier within the lung [15] means that, in contrast to the skin, toxicants may readily reach the blood, providing rapid and complete exposure of the entire body. Previous work from our laboratories has shown that instillation of *S. chartarum* spores into mouse trachea induces changes in pulmonary surfactant properties resulting in redistribution of phospholipids among the different processing stages [16,17]. Furthermore in intact isolated fetal type II cells, the spores depress precursor incorporation into disaturated

phosphatidylcholine (DSPC), the major surfactant phospholipid. Taken together, these results suggest *in vivo* *S. chartarum* may reduce pulmonary surfactant phospholipid levels and concurrently induce changes in extracellular surfactant processing.

To determine if these changes are reflected as molecular alterations of the phospholipid components of pulmonary surfactant, Fourier transform infrared spectroscopy [18,19] was used to examine lung surfactant subfractions isolated from animals exposed to *S. chartarum* conidial spores.

Materials and Methods

Random-bred pathogen free Carworth Farms white male mice of 21 – 28g were used in this study. All animals were housed and treated according to protocols approved through the Canadian Council of Animal Care and their local representative agencies. *S. chartarum* isolate from mold-contaminated drywall material from Hawaii, USA as described previously [16] was used. Isolates were grown on 2% malt extract agar at 25°C over several weeks. For spore isolation, cultures were flooded with sterile physiological saline and gently agitated using a heat sterilized Pasteur pipette. Spores were collected and placed into Eppendorf centrifuge tubes and washed by centrifuging three times for 2 min each at 750 g. After washing, the pelleted spores were resuspended in sterile saline, and prepared to a final concentration of 1×10^6 spores/ml saline using a haematocytometer.

Prior to intratracheal instillation, mice were anesthetized using a mixture of ketamine and xylazine administered intramuscularly. Intratracheal instillation was done after the method described by Brain et al. [12] as we have described earlier [16]. Each mouse was placed on a board, dorsal side down with the board inclined at 20° such that

the animal's head was higher. The animal was supported by an elastic band under the upper incisors and the mouth was held open. Tracheal access was obtained, and a blunt #22 gauge needle used to deliver the conidial suspension into the trachea. Each sample was supplied in a total volume of 50 μ l of 1×10^7 conidia/ml. Mice were maintained on the board for a one minute period to ensure the deposition did not leave the trachea. Control mice received an identical volume of saline.

Mice were euthanized 24 hours after instillation by an intraperitoneal injection of sodium pentobarbital. Lungs were lavaged with 0.9% NaCl in 4 x 0.8 aliquots as described previously [20]. Lavage from each group of animals was pooled, a portion removed for phospholipid measurement, and the remaining fluid fractionated as described originally by Gross et al. [21,22] and modified by Oulton et al. [23] and Knells et al. [19]. Briefly, lung lavage was centrifuged at 140g for 8 minutes to obtain a cellular debris pellet, which was discarded. The resulting supernate was centrifuged three times: at 10,000g (30 minutes; pellet P₁₀), at 60,000g (60 minutes; pellet P₆₀) and at 100,000g (18 hours; pellet P₁₀₀) to separate lung surfactant components [21]. The final supernate was identified as S₁₀₀. Approximately six ml of high purity distilled water (Milli-Q Water System, Millipore Corporation, Ontario) was used to resuspend each pellet.

The intracellular pool of stored surfactant was isolated as described previously [23,24]. Fresh homogenate from mouse lungs was prepared in 0.010M Tris/0.145M NaCl buffer (pH 7.4) using a Polytron (Kinematica, Luzern). Samples were centrifuged for five min at 140g yielding a crude nuclear pellet, which was discarded. A mitochondrial pellet was prepared by centrifuging for 30 min at 10,000g. This pellet was resuspended in 2.0 ml of Tris buffer and layered on a discontinuous sucrose gradient consisting of 5.0 ml of 0.68M

under 5.0 ml of 0.25M sucrose. The gradient was centrifuged at 65,000g for 60 min, producing a lamellar body fraction, the stored intracellular surfactant, which collected at the interface of the gradient.

Infrared spectroscopy

Prior to the spectroscopic measurements, the phospholipid concentrations were estimated from aliquots of each subfraction after extraction into chloroform:methanol:1% KCl (final ratio, 2:2:1.8) [25]. The lower phase was dried under N₂ and assayed for inorganic phosphorus [24]. Phosphorus concentrations were multiplied by 25 to give an estimate of phospholipid concentration.

Aliquots of each subfraction were separated into lipid (organic-soluble material) and protein phases (water-soluble material) by extraction into chloroform:methanol using the method described above. Infrared absorption spectra were acquired only from the organic-soluble phase. This phase was concentrated under N₂. In addition, infrared spectra were acquired for standard samples of sodium palmitate (Sigma), dipalmitoyl phosphatidylcholine (DPPC) (Sigma), sodium caproate (Sigma), lysophosphatidylcholine (Sigma) and isolated *Stachybotrys chartarum*.

The spectra were recorded with a resolution of 4 cm⁻¹ using a Bio-Rad FTS 40 spectrometer equipped with a mercury cadmium telluride (MCT) nitrogen-cooled detector and purged continuously with clean dry air to minimize atmospheric absorptions (water vapour, CO₂). The spectra for palmitate and *S. chartarum* standards were acquired using the Split-PeaTM horizontal reflection accessory (Harrick Scientific Corporation, Ossining, NY). The Split-PeaTM accessory was configured for internal reflectance with a three mm diameter hemispherical silicon crystal and included a calibrated pressure

applicator, which was set at 2.5 kg to provide good contact between the sample and the crystal.

The organic-soluble components were prepared for spectroscopy by first spreading an aliquot over an infrared-transparent (barium fluoride) window, and evaporating the solvent. Absorption spectra were acquired for the resulting films, by first averaging 256 scans, ratioing against a background spectrum (a clean barium fluoride window), and converting to absorbance units. WIN-IR software (Bio-Rad Laboratories) was used to collect and process the spectral data. Minor deviations in the spectral baselines were corrected using this software.

Results

The infrared spectra of the lavage subfractions reflect both the nature and relative concentrations of the constituents [26]. Figures 1 and 2 show spectra of subfractions isolated from saline-treated or *S. chartarum*-treated mice, respectively. All of the spectra display an absorption at 1738-1739 cm^{-1} that is emblematic of a large phospholipid component (see Table 1). Both control and spore-treated animals showed the lowest concentration of surfactant phospholipid in the P₆₀ subfractions (Table 2). For the control animals, the phospholipid concentrations increased in the order P₆₀<P₁₀≅P₁₀₀, while the order of the *S. chartarum*-treated animals was P₆₀<P₁₀₀<P₁₀. In all instances, the lipid concentration of a given subfraction was lower in the *S. chartarum*-treated animals compared to the corresponding fraction from control animals. The difference was most pronounced for the P₆₀ and P₁₀₀ subfractions where the lipid levels of the spore-treated group were about half that of the control group (Table 2). The lipid levels within the P₁₀ subfractions were similar in control and spore-treated samples.

In addition to spectral components attributable to phospholipids, Figures 1 and 2 show certain strong absorptions not generally associated with this class of molecules. For example the prominent bands at 1500-1650 cm^{-1} were observed in surfactant subfraction spectra from both control and *S. chartarum*-exposed animals. The constituent(s) responsible for these absorptions occurred in approximately equal concentrations in all three subfractions of control animals (Figure 1). However the P₆₀ and P₁₀₀ fractions isolated from surfactants of *S. chartarum*-treated animals showed markedly higher concentrations (Figure 2). Since the species responsible for bands in the 1500-1650 cm^{-1} region are not phospholipids, and the spectra could be viewed as a superposition of phospholipid and 'other' contributions, an attempt was made to separate the spectral features of phospholipid components from other spectral features. This was accomplished by interactive subtraction of one spectrum (the P₆₀ subfraction of the control group) from another (the P₁₀₀ fraction of the same group), adjusting the subtraction factor to minimize the residual intensity in the 1500-1650 cm^{-1} spectral region. The same process was carried out using the corresponding subfraction spectra for the *S. chartarum*-treated group.

Figure 3 shows the spectra obtained by iteratively subtracting the spectra of P₆₀ subfraction from that of P₁₀₀ until the common absorption from non-lipid components was minimized (the same difference spectrum was obtained for all three possible subtraction pairs, viz. P₁₀₀-P₆₀, P₁₀₀-P₁₀, or P₁₀-P₆₀). Comparison with the spectrum of DPPC confirms that the difference spectra of both the control and *S. chartarum*-treated animals are very similar to that of the pure lipid component (Figure 3).

Having isolated the spectra of the subfraction lipid constituents of control and spore-treated animals, these spectra were subtracted from the original spectra to reveal the absorption profiles for the non-lipid constituents (Figure 4). As was the case for the phospholipid components, spectra for the non-lipid surfactant constituents of control and *S. chartarum* exposed animals were similar. The very strong absorptions in the region 1500-1650 cm^{-1} suggested these non-lipid constituents might include fatty acid salts, since the terminal COO^- group typically shows a strong feature in this region. The spectrum of sodium palmitate is included for comparison in Figure 4 and shows a strong absorbance peak at 1556 cm^{-1} . While the profile of this absorption suggests fatty acids as possible constituents of the organic-soluble subfractions, the overall profile rules out palmitate as the component.

Figure 5 shows the infrared spectra of the organic-soluble fraction of intracellular stored surfactant from control and *S. chartarum*-treated mice. The spectrum of the control P₆₀ extracellular surfactant subfraction is included for comparison. Much higher phospholipid levels were detected in the intracellular surfactant pool of spore-exposed mice compared to control mice. In particular the intensity of peaks at 1250 and 1738 cm^{-1} were markedly increased in the intracellular surfactant pool in *S. chartarum*-treated mice (the PO_2^- and C=O stretching vibrations respectively).

Processing similar to that previously applied to remove non-lipid components was used with spectra from the intracellular surfactant. The results are shown in Figure 6. The spectrum of the control P₁₀ and P₆₀ phospholipids is included for reference. The most obvious feature of this comparison is that the spectrum of the control group intracellular

phospholipid fraction is virtually identical to the spectrum of the P₆₀ fraction. However exposure to *S. chartarum* induced substantial changes in lipid constituents of the intracellular stored surfactant fraction. Furthermore, the intratracheal spore instillation not only raised the absolute lipid levels but also altered the nature of the lipids relative to the control group. In addition a weak absorption occurred at $\sim 3465\text{ cm}^{-1}$ only in the spectrum of the intracellular surfactant of the *S. chartarum*-treated animals.

Further differences were clearly illustrated by detailed comparison of the deconvolved spectra (Figure 7). A shift in position of the ester C=O absorption, from 1738 cm^{-1} in the intracellular stored surfactant of the saline-treated group to 1731 cm^{-1} in the spore-exposed animals was observed. In addition, in the region $1260 - 1290\text{ cm}^{-1}$, two new absorptions ascribed to the PO₂⁻ stretching region (1269 cm^{-1} and 1286 cm^{-1}) were present in spectrum of the *S. chartarum*-exposed group. Finally clear differences in intensities of the CH₂ stretching absorptions at $\sim 2852\text{ cm}^{-1}$ and $\sim 2920\text{ cm}^{-1}$ occurred as the spore-treated animals showed a marked reduction in band intensities compared to those from the saline-treated animals.

Discussion

Pulmonary surfactant is an extremely complex mixture of several major lipids and proteins. Many minor constituents are also present [27]. Surfactant is synthesized within type II alveolar cells in the most distal regions of the lung and secreted onto the surface epithelium of the alveolus. As a result it is present both as an intracellular fraction representing stored surfactant that acts as a pool for stimulated release, and as an extracellular fraction. This latter fraction may be collected by lung lavage. This material

may be separated by centrifugation into three distinct subfractions [22,23], which differ biochemically, morphologically and in their ability to reduce surface tension. It is largely on the basis of this latter attribute that it has been suggested the subfractions represent progressive stages of the surfactant cycle within the alveolus, from newly secreted surfactant existing mainly as lamellar bodies (P_{10}) to an intermediate form of active surfactant (P_{60}) and finally spent surfactant prior to being recycled or degraded (P_{100}).

The present study has revealed several features of surfactant subfractions from mice exposed to *S. chartarum* spores. Firstly, the lipid concentration is lower in all three extracellular surfactant subfractions compared to fractions from the control animals, but no substantial differences were detected in the nature of the lipids. This finding is consistent with previous work that *Salmonella minnesota* lipopolysaccharide exposure in rats promotes a decrease in phospholipid recoverable by bronchoalveolar lavage [28]. In contrast, studies involving experimental exposure to a variety of injurious agents (diesel fuel particles, silica dust, ozone, radiation, and smoke from burning polyethylene foam) revealed an increase in alveolar surfactant phospholipids [20,29].

Surprisingly, the spectra of all subfractions revealed large amounts of a second class of constituents that appear not to be phospholipids. The most obvious spectroscopic feature was a strong absorption or set of absorptions in the region $1500\text{-}1650\text{ cm}^{-1}$. The list of compounds whose strongest absorptions lie in this range is not a long one. Proteins invariably show two distinct absorptions at $\sim 1540\text{ cm}^{-1}$ and $\sim 1650\text{ cm}^{-1}$ corresponding to the amide II (N-H bending vibration) and amide I (C=O stretching vibration) as well as a strong band (N-H stretching vibration, or 'amide A' band) at $\sim 3300\text{ cm}^{-1}$. The observed profile is therefore incompatible with high protein levels. The surfactant-associated

hydrophobic proteins may contribute to the overall absorption profile, but only very minor bands are expected for these low-concentration proteins in any case.

The only class of biological molecules that seems compatible with the absorption profile shown in Figure 4 is the fatty acid salts, with strong absorptions typically at ~ 1550 cm^{-1} corresponding to the asymmetric COO^- stretching mode. The possibility exists that these may be the products of phospholipid hydrolysis however the absorption profile is incompatible with long methylene chains. Comparing the spectrum of sodium palmitate to that of the unknown species in Figure 4 showed that the ratio of band intensities at 2920 cm^{-1} (CH_2 stretch) and 2955 cm^{-1} (CH_3 stretch), provides an estimated chain length of 7:1 for sodium palmitate but only 2:1 for the difference spectra. This suggests an average chain length of C6 (caproate), but does not rule out the possibility that several carboxylates of various lengths contribute to the spectra. The observation of two major COO^- stretching modes (at 1560 and 1596 cm^{-1}) suggests at least two species contribute to this absorption profile.

S. chartarum spore exposure had a dramatic influence on the pulmonary intracellular stored surfactant. The elevated lipid levels (Figures 5 and 6), and the differences in the nature of the recovered lipids (Figures 6 and 7), suggest that the spores altered both the rate and character of lipid synthesis in type II alveolar cells. In particular, the spectroscopic differences cited earlier are consistent with strong intramolecular hydrogen bonding to both the $\text{C}=\text{O}$ and PO_2^- groups, promoting the observed frequency shifts and a substantially lower CH_2/CH_3 ratio than observed in samples from the control animals. The latter observation is intriguing, particularly since the diminished intensity in the CH_2 stretching absorptions (2820 and 2950 cm^{-1}) is

approximately halved relative to the control group with no corresponding drop of intensity of the C=O stretching absorption. This observation is consistent with the loss of one of the acyl chains in the predominant lipid making up the intracellular stored surfactant. The fact that the intensity of the C=O stretching mode is largely unaffected (relative to e.g. the PO_2^- asymmetric stretching mode and the CH_3 stretching modes) further suggests that the ester moiety is preserved in the major new lipid constituent. In addition, the appearance of an absorption at 3465 cm^{-1} suggests the presence of intramolecularly hydrogen-bonded OH [31] for at least one of the new lipid components that emerge upon exposure to *S. chartarum*.

DSPC, predominantly dipalmitoyl in configuration, is the major surface-active phospholipid within the pulmonary surfactant [27]. Approximately 50% of the DPPC is synthesized by a deacylation-reacylation mechanism in type II alveolar cells [30]. The presence of a strong hydrogen bonding donor implied by the spectra of the intracellular stored surfactant fraction may suggest that this deacylation-reacylation mechanism has been depressed by spore exposure. This suggestion is further supported by considering possible structures that are consistent with all of the spectroscopic observations. Since the acyl chain at the sn-2 position of the glycerol lipid backbone is most susceptible to deacylation-reacylation, the spectroscopic evidence may be interpreted to suggest that this chain has been replaced by a much shorter one; the presumption that is most consistent with the spectra is that the 2-position is occupied by an acetoxy group rather than palmitoyl or other long chain fatty acid. This postulate is not sufficient to explain the OH stretching absorption in the *S. chartarum*-treated surfactant. The OH may reflect the presence of lipid oxidation products (the same mechanism may also be partially

responsible for the reduced chain length). An alternative suggestion, and one which seems more likely if the normal deacylation-reacylation mechanism is disrupted, is that the OH reflects the presence of lysophospholipids in addition to the acetoxy-substituted species.

Generally lysophospholipids are maintained at very low levels due to their detergent-like action [32]. However previous work has shown elevated lysophospholipid levels in cells under stress [33]. Furthermore the lipopolysaccharide (LPS) capsule that surrounds the spores may have detrimental effects on the pulmonary surfactant. Following infusion of LPS into rat lungs, surfactant phospholipids were reduced, pulmonary compliance and resistance altered and the numbers of lamellar bodies within the type II cells affected [28]. Similarly in guinea pig, LPS induced release of a secretory phospholipase A₂ which interacted with surfactant protein A and preferentially produced lysophosphatidylcholine [34]. These latter observations are particularly interesting as they suggest changes occur in both the stored intracellular surfactant pool and secreted surfactant after exposure to LPS, such as observed in the present study. In addition the reduced compliance observed by Fehrenbach et al. [28] supports the present contention that elevated levels of lysophospholipids may be the end result of exposure to *S. chartarum* spores since lysophosphatidylcholine effectively inhibits the ability of surfactant to reduce surface tension [35].

In summary, exposure to *S. chartarum* promotes a decrease in the concentration of extracellular phospholipids and an increase in the intracellular surfactant levels. Of the three alveolar surfactant fractions isolated here, P₆₀, and P₁₀₀, which represent the intermediate and the spent surfactant respectively, are most strongly affected by spore

exposure. The mechanism of spore-induced changes appears to involve generation of lysophospholipid species.

Acknowledgements

Supported by the Natural Sciences and Engineering Research Council of Canada. KM is supported by a fellowship through the University of Manitoba.

References

1. S. Gravesen, P.A. Nielsen, R. Iversen, and K. Fog-Nielsen (1999). Microfungal contamination of damp buildings—examples of risk constructions and risk materials. *Environ. Health Persp.*, 107(3), 505-508.
2. E. Johanning, R. Biagnini, D. Hull, P. Morey, B. Jarvis and P. Landsbergis (1996a). Health and immunology study following exposure to toxigenic fungi (*Stachybotrys chartarum*) in a water-damaged office environment. *Int. Arch. Occup. Environ. Health*, 68(4), 207-218.
3. S.C. Jong and E.E. Davis, (1976). Contribution to the knowledge of *Stachybotrys* and *memnoniella* in culture. *Mycotaxon*, III(3), 409-485.
4. E. Johanning, M. Gareis, C.S. Yang, E.-L. Hintikka, M. Nikulin, B. Jarvis and R. Dietrich, (1996b). Toxicity screening of materials from buildings with fungal indoor air quality problems (*Stachybotrys chartarum*). *Mycotoxin Res.*, 14, 60-73.
5. B.B. Jarvis, J. Salemmé and A. Morais, (1995). *Stachybotrys* toxin. *Natural Toxins*, 3, 10-16.
6. M. Lee, S. Li, B. Jarvis and J.J. Pestka, J.J. (1999). Effects of satratoxins and other macrocyclic tricothescenes on IL-2 production and viability of EL-4 thymoma cells. *J. Toxicol. Environ. Health.*, 57(7), 459-474.
7. B. Jarvis, and E.P. Mazzola, (1982). Macrocyclic and other novel tricothescenes: Their structure, synthesis and biological significance. *Acc. Chem. Res.*, 15, 388-395.
8. B. B. Jarvis, Y.-W. Lee, S.N. Comezoglu and C.S. Yatawara, (1986). Tricothescenes produced by *stachybotrys atra* from Eastern Europe. *App. Environ. Micro.*, 915-918.
9. V.G. Drobotko (1945). *Stachybotryotoxicosis*: A new disease of horses and humans. *Am. Rev. Soviet Med.*, 2, 238-242.
10. M.J. Hodgson, P. Morey, W. Leung, L. Morrow, D. Miller, B.B. Jarvis, H. Robbins, J.F. Halsey, and E. Storey, (1998). Building-associated pulmonary disease from exposure to *Stachybotrys Chartarum* and *Aspergillus versicolor*. *JOEM*, 40(3), 241-249.
11. J.V. Rodricks and R.M. Eppley (1974). *Stachybotrys* and *stachybotryotoxicosis*. In: I.F.H. Purchase (Ed.). *Mycotoxins*, Elsevier Scientific Publishing Company, pp. 181-196.
12. J.D. Brain, D.E. Knudson, S.P. Sorokin, and M.A. Davis (1976). Pulmonary distribution of particles given by intratracheal instillation or by aerosol inhalation. *Environ. Res.*, 11, 13-33.

13. E.R. Weibel (1963). In: Morphometry of the human lung. Academic Press Inc., New York, NY.
14. J.L. Mauderly and J.M. Samet (1991). General environment. In: R.G. Crystal and J.B. West (eds.), The Lung Scientific Foundations. pp. 1947 - 60. Raven Press, New York.
15. E.E. Schneeberger (1991). Alveolar type I cells. In: R.G. Crystal and J.B. West (eds.), The Lung Scientific Foundations. Raven Press, New York, pp. 229 - 34.
16. C.D. Mason, T. Rand, M. Oulton, J. MacDonald and J.E. Scott (1998). An evaluation of the effects of *Stachybotrys Chartarum* (atra) conidia and isolated toxin on lung surfactant production and homeostasis in juvenile mice. *Natural Toxins*, 6(1), 27-33.
17. M.W. Sumarah, T.G. Rand, M. Oulton, J.E. Scott, J. MacDonald, and M. Anthes (2000) Effects of *Stachybotrys chartarum* and isosatratoxin F on DSPC/PC ratios in mouse lung surfactant. *Lipids* (submitted)
18. R.M. Das, M.K. Ahmed, H.H. Mantsch and J.E. Scott (1997). FT-IR spectroscopy of methylmercury-exposed mouse lung. *Molec. Cell. Biochemistry*, 145, 75-79.
19. G. Knells, M.K. Ahmed, R.M. Das, M.R. Oulton, H.H. Mantsch and J.E. Scott (1997). Fourier-transform infrared spectroscopic analysis of rabbit lung surfactant: Subraction-associated phospholipid and protein profiles. *Chem. Physics Lipids*, 77, 193-201.
20. J.E. Scott, P.G. Forkert, M. Oulton, M. Dolphin, M. Fraser, M.G. Rasmusson, S. Temple and S. Whitefield (1988). Trichloroethylene-induced changes in intra-and extracellular surfactant profiles and relation to phospholipase A₂ activity in subcellular fractions of adult mouse lung. *Exp. Molec. Path.*, 49, 141-150.
21. N.J. Gross, E. Barnes and K.R. Narine, (1988). Recycling of surfactant in black and beige mice: Pool sizes and kinetics. *J. Appl. Physiol*, 64, 2017-2025.
22. N.J. Gross and K.R. Narine (1989). Surfactant subtypes of mice: Metabolic relationships and conversion *in vitro*. *J. Appl. Physiol*, 67, 414-421.
23. M. Oulton, J. MacDonald, D.T. Janigan and G.T. Faulkner (1993). Mouse alveolar surfactant: Characterization of subtypes prepared by differential centrifugation. *Lipids*, 28, 715-720.
24. M. Oulton, M. Fraser, M. Dolphin, R. Yoon and G.T. Faulkner (1986). Quantification of surfactant pool sizes in rabbit lung during perinatal development. *J. Lipid Res.*, 27, 602-612.

25. J.D. Bligh, and W.J. Dyer (1959). A rapid method of total lipid extraction and purification. *Can. J. Biochem. Physiol.*, 37, 911-917.
26. H.H. Mantsch, H.L. Casal and R.N. Jones (1986). Resolution enhancement of infrared spectra of biological systems. In: R.J.H. Clark and R.E. Hester (eds.) *Spectroscopy of Biological Systems*. *Adv. Spectroscopy*, 13, 1-46.
27. R. Veldhuizen, K. Nag, S. Orgeig and F. Possmayer, (1998). The role of lipids in pulmonary surfactant. *Biochim. Biophys. Acta*, 1408, 90-108.
28. H. Fehrenbach, F. Brasch, S. Uhlig, M. Weisser, C. Stamme, A. Wendel, and J. Richter (1998). Early alterations in intracellular and alveolar surfactant of the rat lung in response to endotoxin. *Am. J. Respir. Crit. Care Med.*, 157, 1630-9.
29. M. Oulton, H.K. Moores, J.E. Scott, D.T. Janigan and R. Hajela (1990). Effects of smoke inhalation on surfactant phospholipids and phospholipase A₂ activity in mouse lung. *Am. J. Pathol.*, 138, 195 - 202.
30. J.J. Batenburg (1992). Surfactant phospholipids: synthesis and storage. *Am. J. Physiol.*, 262, L367 - L385.
31. M. Tichy (1965). In: *Advances in Organic Chemistry*, R.A. Raphael, E.C. Taylor, and H. Wynberg, eds., 5, 115 IR: Review of intramolecular hydrogen bonding.
32. M.I. Gurr, and A. T. James. (1980). In: *Lipid Biochemistry*, Chapman Hall, New York.
33. J.E. Scott, S.-Y. Yang, E. Stanik, and J.E. Anderson, J.E. (1992). Influence of strain on [³H]thymidine incorporation, surfactant-related phospholipid synthesis and cAMP levels in fetal type II alveolar cells. *Am. J. Respir. Cell Molec. Biol.*, 8, 258-65.
34. L. Arbibe, K. Koumanov, D. Vial, C. Rougeot, G. Faure, N. Havet, S. Longacre, B.B. Vargaftig, G. Béréziat, D.R. Voelker, C. Wolf, L. Touqui (1998). Generation of lysophospholipids from surfactant in acute lung injury is mediated by type-II phospholipase A₂ and inhibited by a direct surfactant protein A-phospholipase A₂ protein interaction. *J. Clin. Invest.*, 102, 1152-60.
35. B.A. Holm, Z. Wang, R.H. Notter (1999). Multiple mechanisms of lung surfactant inhibition. *Pediatr. Res.*, 46(1), 85-93.

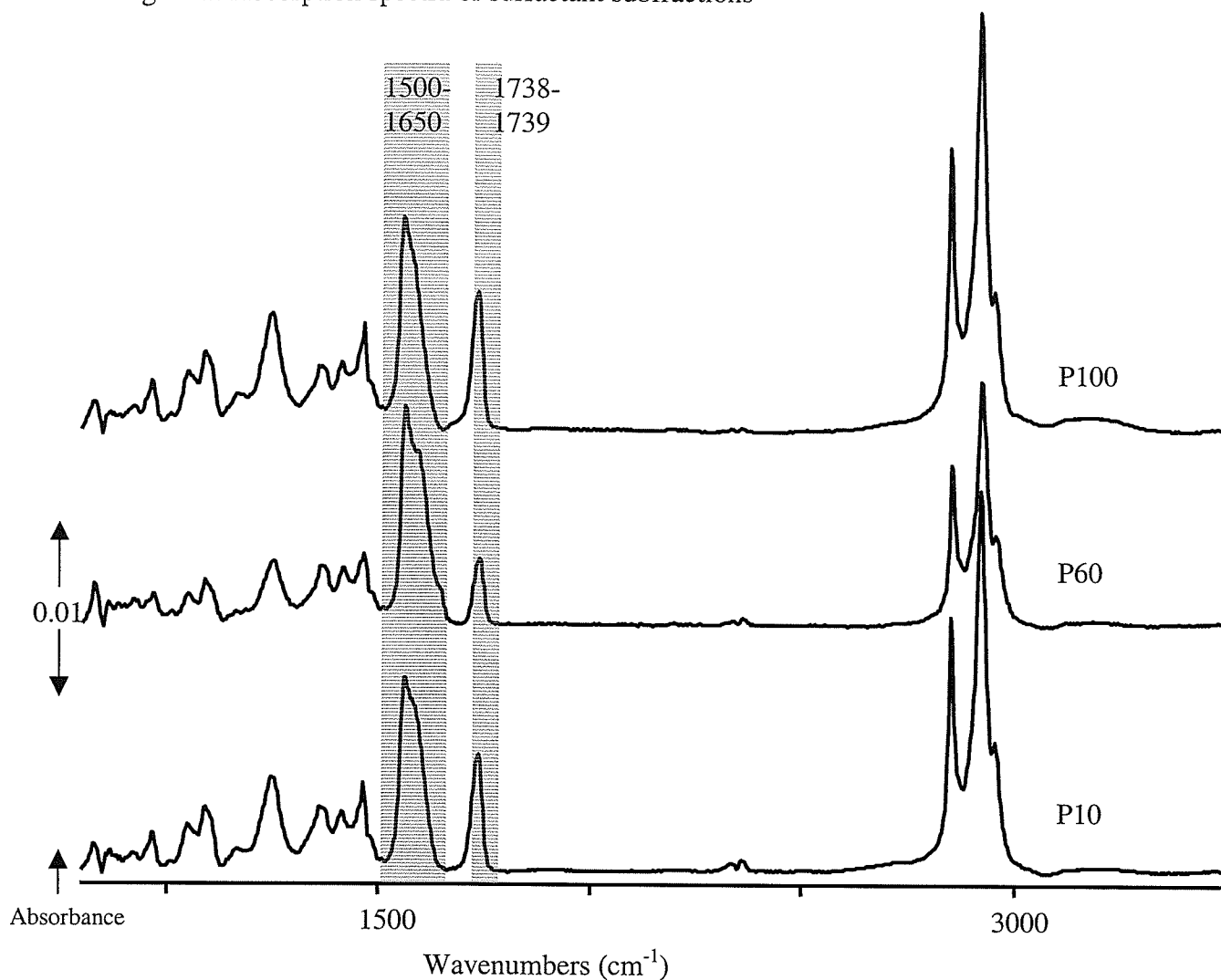
Table 1. Spectral frequency assignments of major peaks observed in the infrared spectra of the organic soluble lipid component of surfactant subfractions isolated from control and *S. chartarum*-treated mouse.

Frequency (cm ⁻¹)	Assignment
2955-2957	CH ₃ asymmetric stretching
2918-2921	CH ₂ asymmetric stretching
2851-2852	CH ₂ symmetric stretching
1738-1739	C=O stretching
1467-1468	CH ₂ scissoring
1250-1256	PO ₂ ⁻ asymmetric stretching
1090-1094	PO ₂ ⁻ symmetric stretching
969-970	(CH ₃) ₃ N ⁺ asymmetric stretching

Table 2. Relative phospholipid ratios in extracellular surfactant subfractions following organic extraction of fractions from control or *S. chartarum*-treated mice. Values are relative to the lowest concentration, set equal to 1 for the experimental P₆₀ subfraction.

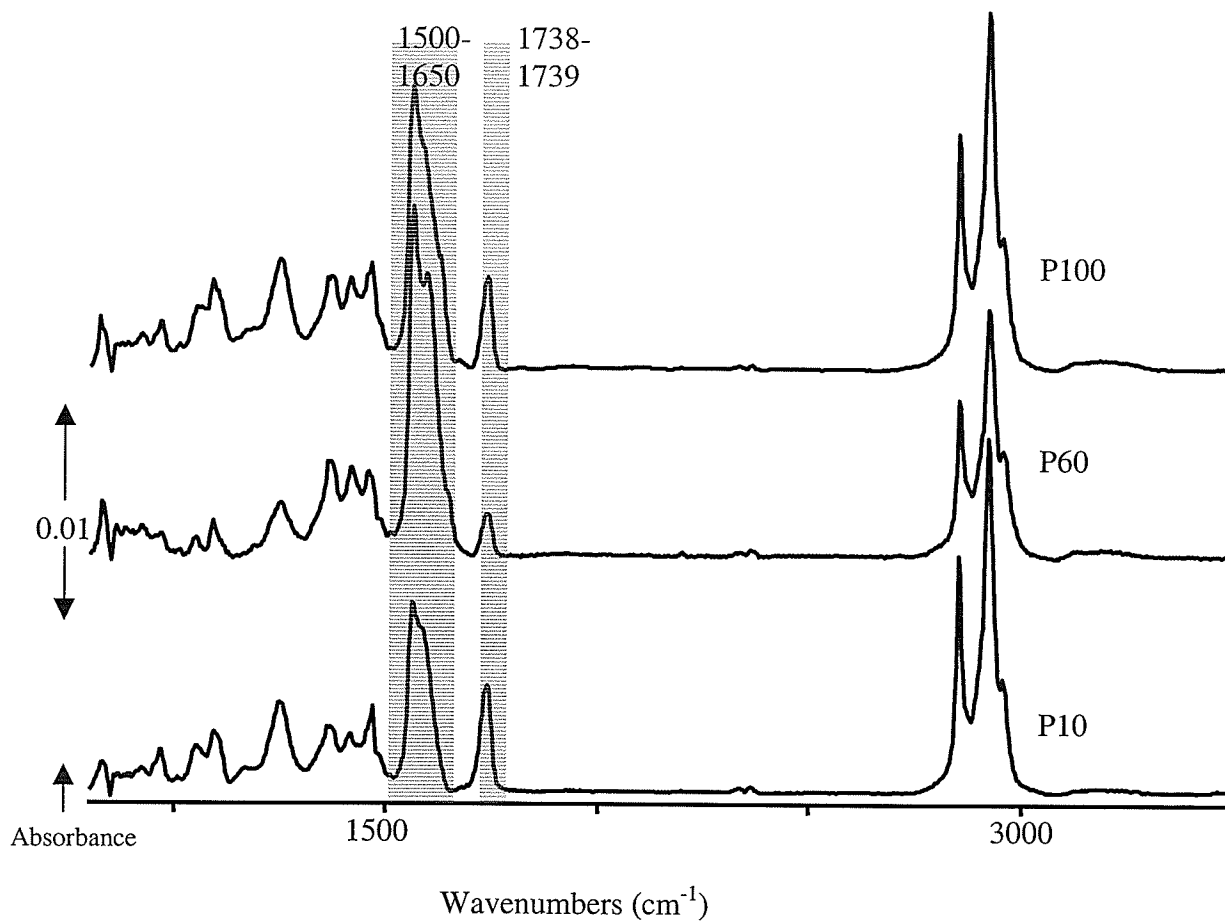
Fraction	Relative phospholipid level		Experimental/Control
	Control Group	Experimental Group	
P ₁₀	4.1	3.5	0.85
P ₆₀	2.3	1.0	0.43
P ₁₀₀	4.8	2.5	0.52

Figure 1: Absorption spectra of surfactant subfractions



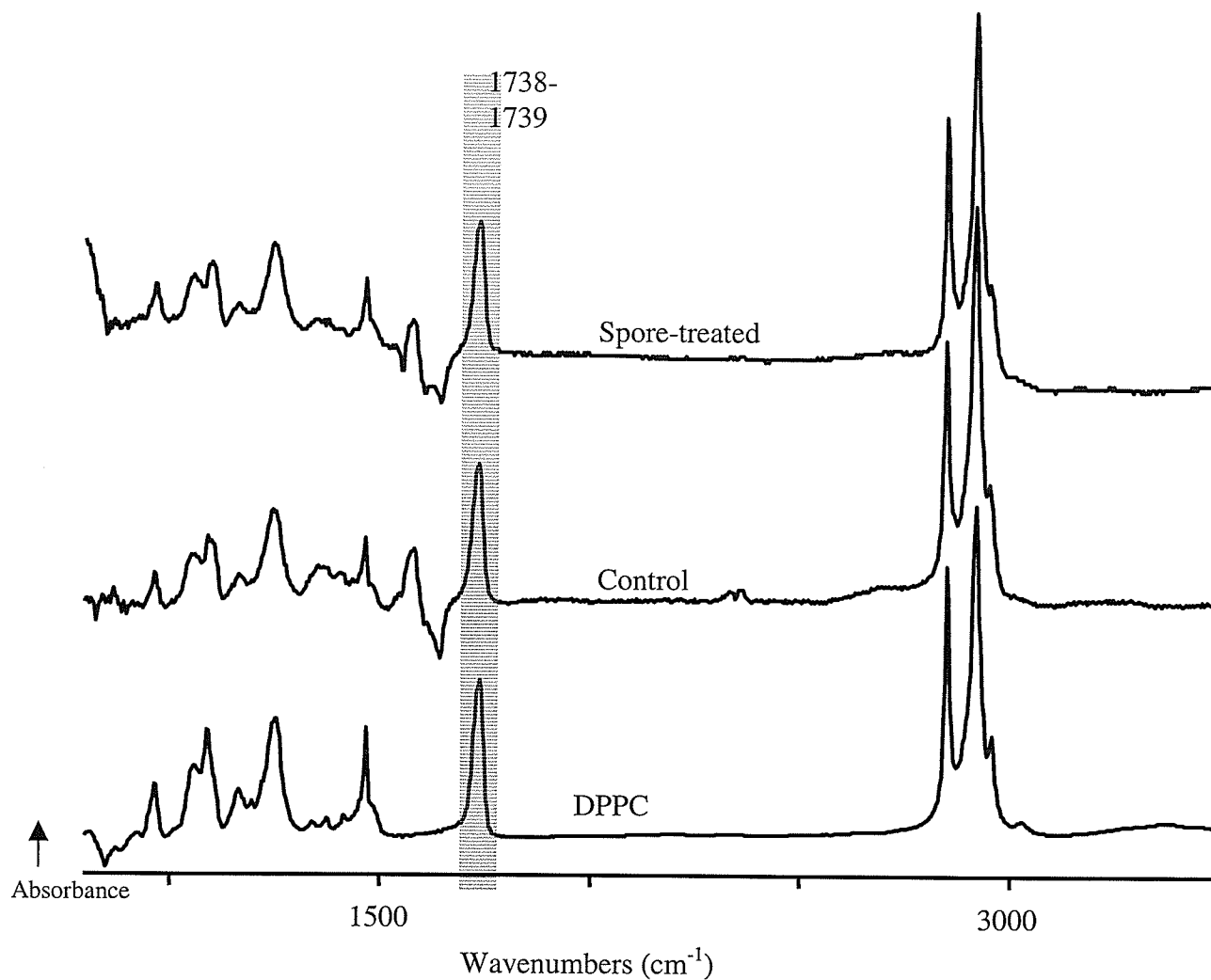
Infrared absorption spectra of surfactant subfractions isolated by repetitive centrifugation at 10,000g (P₁₀), 60,000g (P₆₀) and 100,000g (P₁₀₀) of bronchoalveolar lavage of mouse lung following intratracheal instillation of saline. The spectra have been scaled to a common maximum height and offset for clarity.

Figure 2: Absorption spectra of surfactant subfractions



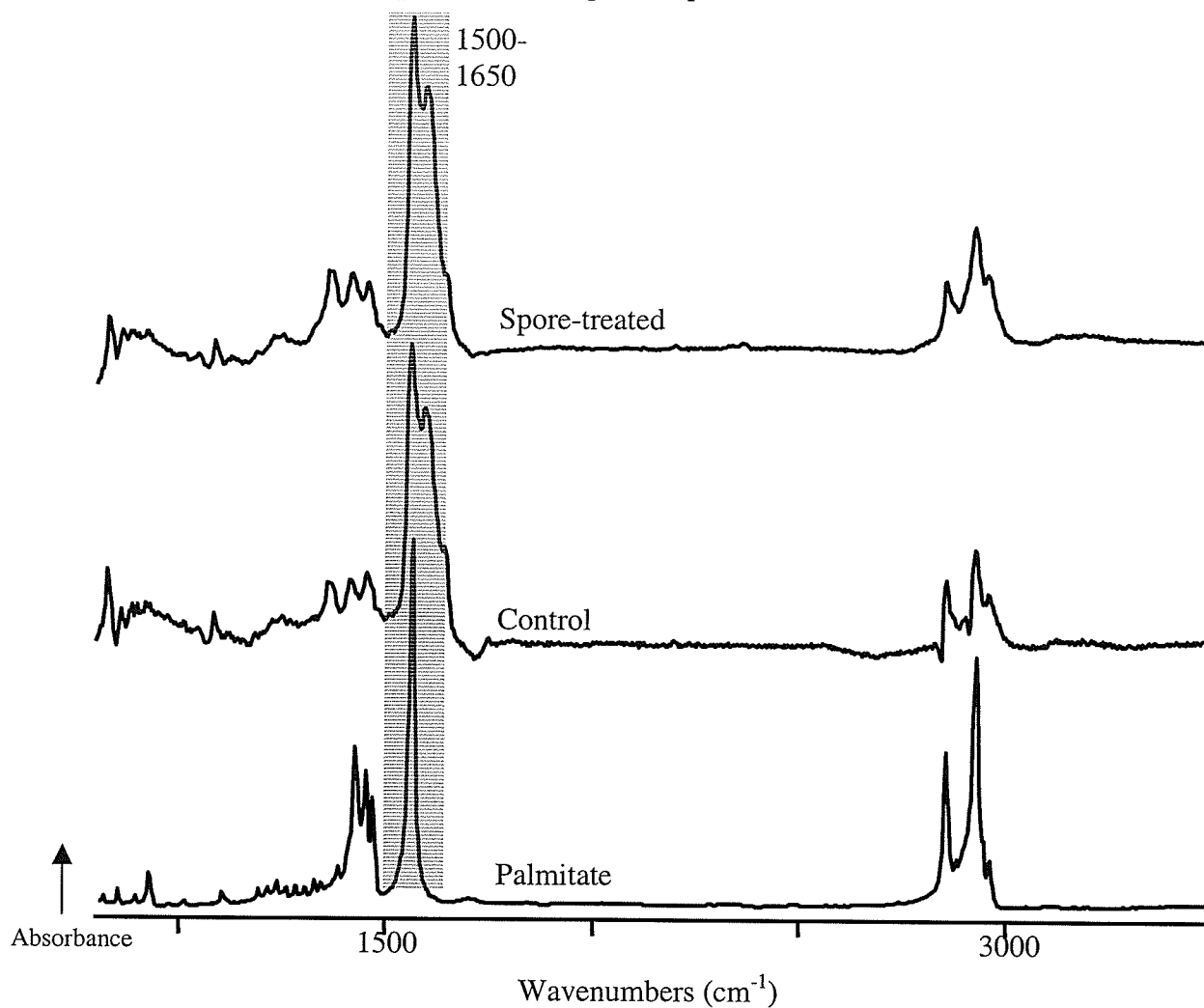
Infrared absorption spectra of surfactant subfractions isolated by repetitive centrifugation of bronchoalveolar lavage of *S. chartarum*-exposed mouse lung. Fractions are labelled as in Figure 1.

Figure 3: Difference spectra of lipid components



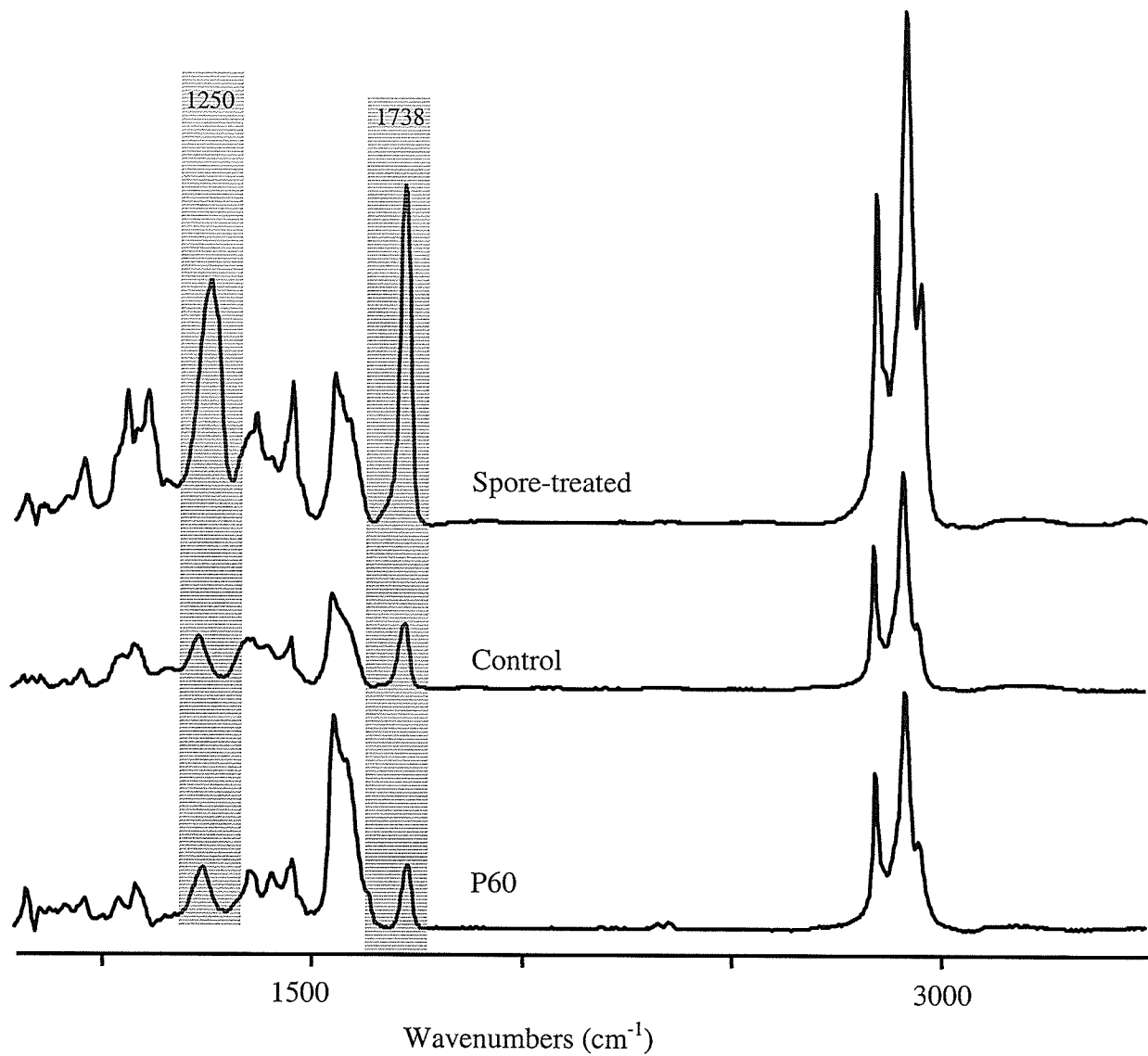
Difference spectra of surfactant lipid components obtained by subtracting the spectrum of P₁₀₀ subfraction from that of P₆₀ subfraction of control and spore-exposed animals. The spectrum of dipalmitoylphosphatidylcholine (DPPC) is shown for comparison.

Figure 4: Difference spectra of non-lipid components



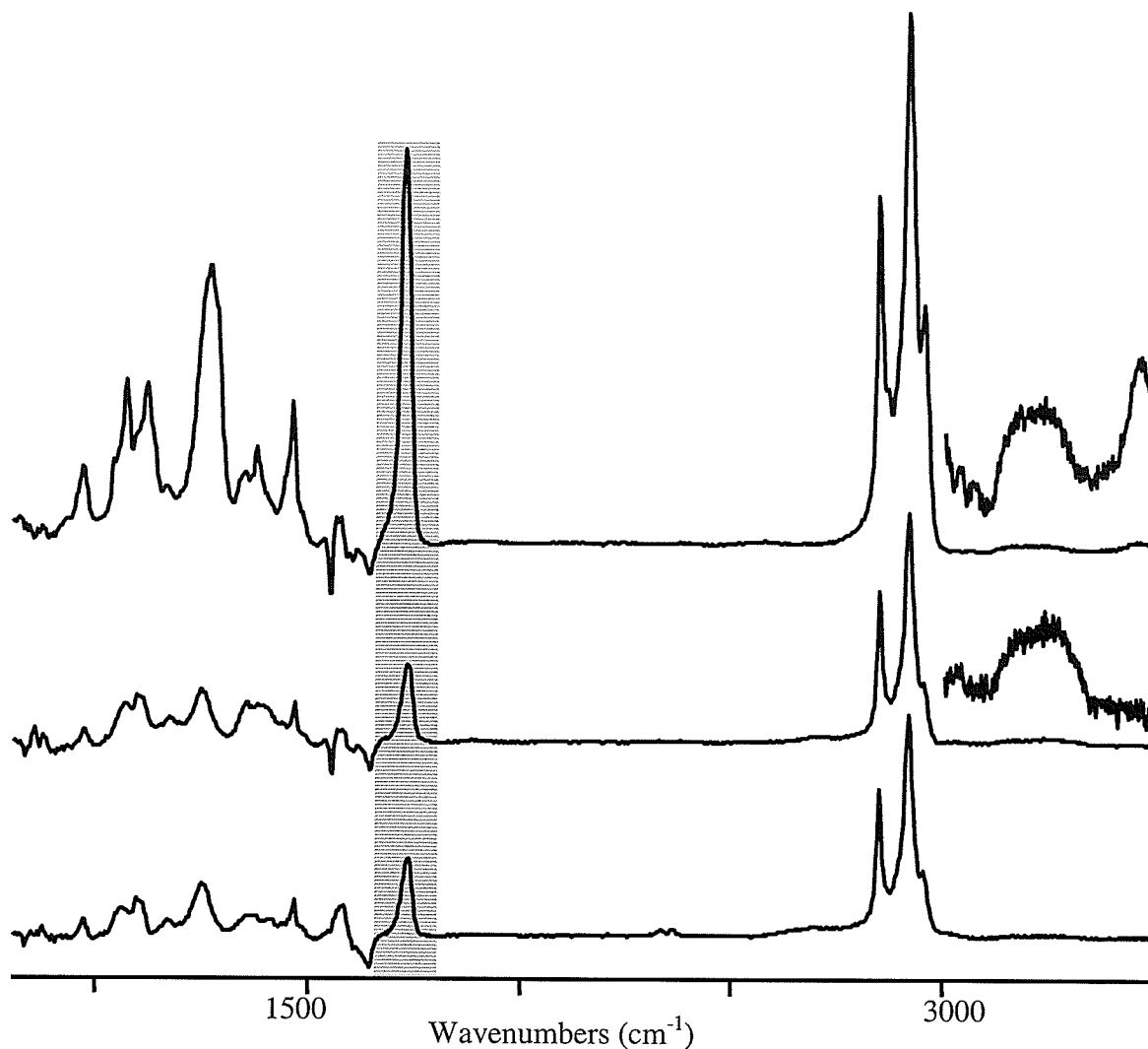
Difference spectra of the non-lipid components obtained by subtracting the spectrum of the lipid components from the spectra of the P₆₀ subfraction of spore-treated and control mice. The spectrum of sodium palmitate is included for comparison.

Figure 5: Absorption spectra of intracellular surfactant



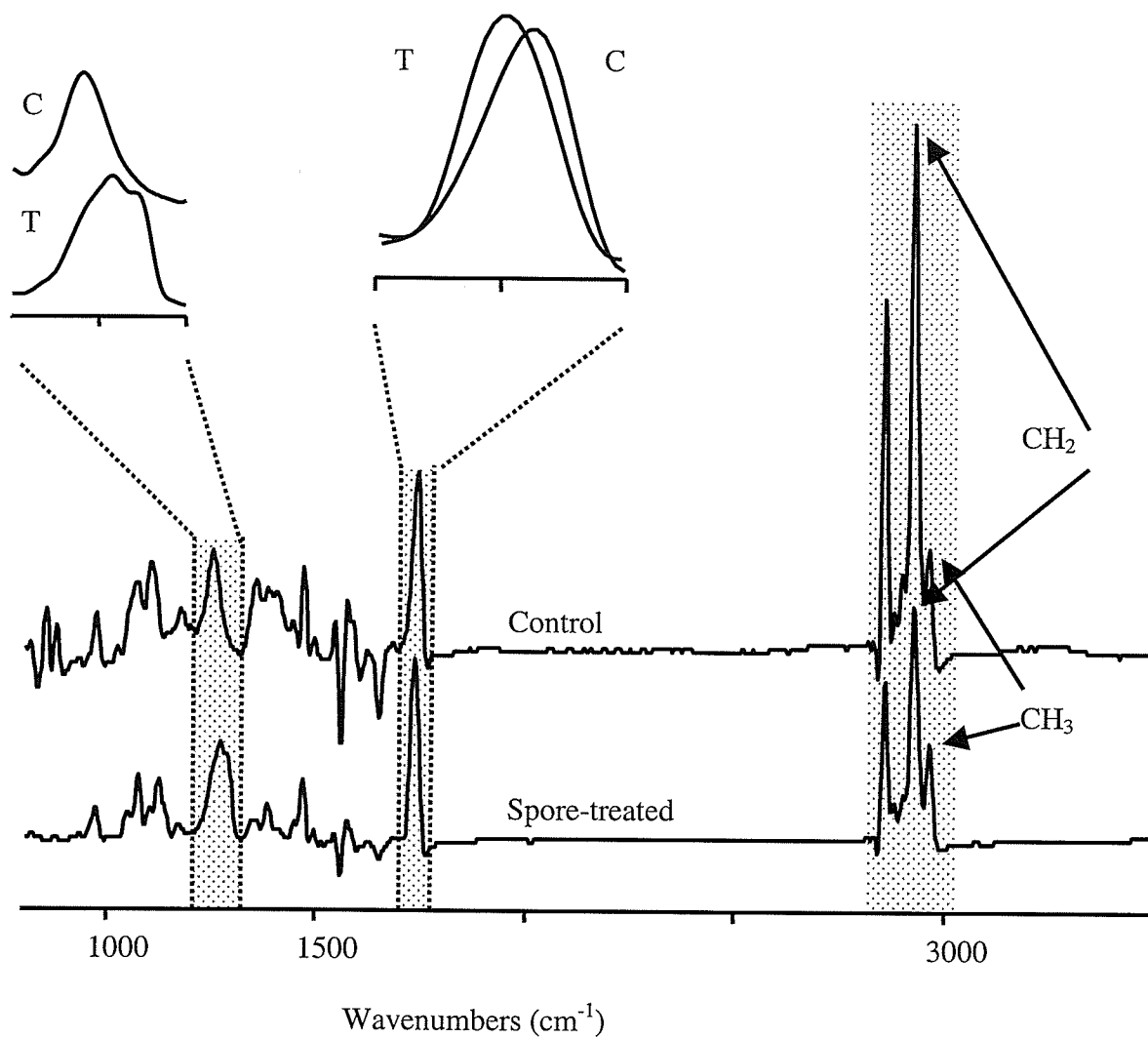
Absorption spectra of intracellular surfactant pool from control and spore-treated mouse lung. The spectra have been scaled to a common maximum height and offset for clarity and a sample spectrum from extracellular surfactant P₆₀ subfraction from control mice is also shown.

Figure 6: Absorption spectra of treated and control intracellular surfactant



Spectra of stored intracellular surfactant pool from mice exposed to saline or *S. chartarum* spores and a sample spectrum from extracellular surfactant P₁₀ and P₆₀ subfractions from control mice. Spectra represent the lipid components obtained by subtracting the spectrum of the non-lipid component from each spectrum.

Figure 7: Absorption spectra



Deconvoluted spectra of intracellular surfactant pool from mice exposed to saline or *S. chartarum*, scaled to a common intensity for the lipid C=O stretching band at 1730-1740 cm^{-1} .

Chapter 7

DNA fragmentation in developing lung fibroblasts exposed to *Stachybotrys chartarum* (atra) spores*

K.C. McCrae^{1,3}, T.G. Rand⁴, R.A. Shaw⁵, H.H. Mantsch⁵, M.G. Sowa⁵, J.A. Thliveris²,
J.E. Scott^{1,2,3}. Departments of Oral Biology¹ and Human Anatomy and Cell Science²,
Faculties of Dentistry and Medicine, University of Manitoba, the Biology of Breathing
Group, Manitoba Institute for Child Health³, Winnipeg Manitoba, and St. Mary's
University⁴, Halifax, Nova Scotia, and National Research Council, Institute for
Biodiagnostics⁵, Winnipeg Manitoba.

*(2004) DNA fragmentation in developing lung fibroblasts exposed to *Stachybotrys chartarum* (atra) spores. Toxicol Lett (submitted).

Abstract

Stachybotrys chartarum (atra) is a toxic mold that grows on water-damaged cellulose-based materials. Research has revealed also that inhalation of *S. chartarum* spores caused marked changes in respiratory epithelium, especially to developing lungs. We analyzed the epigenetic potential of *S. chartarum* spores on developing rat lung fibroblasts using single cell gel electrophoresis (comet assay). Isolated fetal lung fibroblasts were exposed to *S. chartarum* spores for 15 minutes, 3, 14, or 24 hours and control cells were exposed to saline under the same conditions. Cells were embedded in agarose, electrophoresed under alkaline conditions and silver stained. DNA damage was assessed in terms of fragmentation as measured by comet tail length (DNA migration) and intensity (% DNA contained within head & tail). Upon visual inspection, control fibroblasts showed no DNA fragmentation whereas *S. chartarum*-treated cells had definable comets of different degrees depending upon the time-course. Analyses of the comets revealed that exposure to *S. chartarum* spores for at least 15 min to 14 h, induced increased DNA fragmentation in a time-dependent manner. The fact that exposure to toxic spores for 24 h showed less damage suggested that developing lung fibroblasts may have the capability of repairing DNA fragmentation.

Introduction

Fibroblasts are the largest cells, in number and volume, of the mesenchymal cells within the lung parenchyma [1]. These fibroblasts function in several important roles during lung development. One primary role is to maintain the integrity of mechanical scaffolding of lungs through synthesis, secretion, and degradation of extracellular matrix components (e.g. collagen, elastin, fibronectin) [1]. This is especially important during lung development for construction of the fibrous skeleton that attaches alveolar sacs [2]. These structural support cells serve also in response to injury via interaction with inflammatory/immune cells and migration, proliferation, and fibrotic tissue formation [3]. A second role of critical importance relates to fibroblast-epithelial interactions whereby developing AT II cell foot processes penetrate basal lamina discontinuities [4] during critical perinatal periods of lung development. In addition fibroblast-pneumocyte factor [5] originating from mesenchymal fibroblasts has been shown to enhance AT II development of the surfactant system.

Lung tissue growth is a particularly vulnerable process due to the hypersensitivity of cells, high rates of protein and DNA synthesis, and immature defense mechanisms. During this process, exposure to environmental toxicants may impact lung development [6]. A myriad of inhalation toxicants exists; indoor molds, for example, may produce numerous toxic spores [7]. An especially harmful mold, *Stachybotrys chartarum* (*atra*) has been implicated as a factor in the development of infant idiopathic pulmonary hemorrhage and pulmonary fibrosis after exposure to its toxic spores [reviewed in 8].

S. chartarum has been studied extensively for decades. The mold grows well on water-saturated cellulose-based material [9]. Spores produced by *S. chartarum* may

contain an assortment of toxins, e.g. macrocyclic tricothecenes (satratoxins-F, G, & H, roridins, & verrucarins), hemolytic agents (stachylysin), and proteolytic agents (stachyrase) [9]. Pulmonary tissue is particularly vulnerable to spore inhalation due to the large surface area of the lungs exposed to the environment and the small aerodynamic ellipsoidal shape of dry spores (roughly 5 x 8 μm) [10], which can deposit deep within the lungs, especially in infants [11].

The severity and nature of injury from these spores and/or toxins is dependent upon the *S. chartarum* strain (e.g. amount and type of toxins produced), dose, and duration of exposure [Table 1]. Many studies have documented some degree of inflammatory response after spore exposure, regardless of dose or duration [11,12,15,18, 23]. Granulomatous lesions consisting of alveolar macrophages (AM), neutrophils, and fibroblasts were observed frequently surrounding the spores and mycelial fragments [13-15]. Altered immune function was demonstrated by the suppression of protein synthesis [20]. Immediate production of reactive oxygen species (ROS) and increased production of inflammatory mediators by macrophages were documented [23]. Alterations were found also to intracellular and extracellular pulmonary surfactant, which lines the air/water interface within the alveolus [17-19].

The onset of oncosis (accidental cell death) of AT II cells [16] and apoptosis (programmed cell death) in a macrophage cell line [22] has been documented. Both apoptosis and oncosis may result from toxic injury and both pathways of cell death begin with potentially reversible 'prelethal' changes such as DNA fragmentation [24]. A number of toxic agents may fragment DNA, producing primary breaks known as single strand breaks (SSB) [25]. Although SSB, which may be repaired and rejoined, are not

considered major forms of DNA damage, they may reveal (i) a possible cellular target or mode of action of the toxic agent and (ii) a potential cellular response to the toxic injury [24].

The effect of *S. chartarum* on genetic material is not well established. For this reason, we sought to determine if exposure to *S. chartarum* spore toxins induces DNA damage (i.e. fragmentation), and investigate the time-course of damage in developing lung fibroblasts. To measure DNA fragmentation we used single cell gel electrophoresis (SCGE, or comet assay), a technique used to monitor alterations to eukaryotic DNA caused by numerous environmental substances [reviewed in 26 & 27]. An advantage of this assay is its sensitivity to detect DNA fragments from SSB or alkali-labile sites (ALS) caused by low doses of toxic agents [28].

Materials and methods

Animals and fibroblast isolation procedure

Pregnant Sprague-Dawley rats used for the experiments were from the animal care facility at the University of Manitoba, Winnipeg, Canada, and all procedures were approved by the Canadian Council on Laboratory Animals. Lung fibroblasts were isolated aseptically as described previously [19 & 29] with modifications. Briefly, pregnant rats were euthanized by one intraperitoneal injection of Euthanyl (240 mg/ml sodium pentobarbital) on gestational day 22 (term gestation is 23 days in this population). The fetuses were removed by hysterotomy, decapitated, and placed into cold, sterile Hanks Balanced Salt Solution (HBSS, Gibco, ON Canada) (pH 7.1). Fetal lungs were removed and chopped using a Sorval tissue Chopper (Sorval Instrument, Newton, CT) and subsequently dissociated by incubating with trypsin/EDTA (0.05%/0.02%) in HBSS

for 45 min in a water-jacketed trypsinization flask at 37°C. Minimum essential medium (MEM) (Gibco, ON Canada) with 10% newborn calf serum (NCS) (place) and 1% each of antibiotic/antimycotic and Fungizone (AB/AM/F) (Gibco, ON) was added to stop trypsinization and the cell suspension was filtered sequentially through three layers of Nitex gauze before centrifugation for 10 min at 250xg. The pellet was gently resuspended in MEM/NCS/AB/AM/F and cells were plated in 25 cm² flasks for differential adherence, since fibroblasts are the first cells to attach [29], at 37°C in an atmosphere of 95% air/5% CO₂. After one hour the medium was collected from each flask to remove unattached cells and fresh medium was added to enable growth of fibroblast monolayers. The medium was changed at 24 h and 48 h and every 48 h thereafter. Fibroblasts were passaged every fifth day at a ratio of 1 to 3, and after the third passage, cells were allowed to reach confluence, as visualized through a phase contrast microscope, prior to treatment with *S. chartarum* spore toxins. The present experiment was replicated four times in its entirety.

S. chartarum spore toxin isolation

S. chartarum strain 58-17 (Cleveland, OH) is known to produce spores that can contain toxins including macrocyclic tricothecenes (satratoxin-F, G & H) [19] and low levels of stachylysin [14]. *S. chartarum* isolates were grown as previously described [17-19] on 2% malt extract agar at 25°C over several weeks. For spore isolation, cultures were flooded with sterile physiological saline and gently agitated using a heat sterilized Pasteur pipette. Spores were collected and placed into Eppendorf centrifuge tubes and washed and collected by centrifuging three times for 2 min each at 750 g. The pelleted spores were resuspended in sterile saline, and subsequently prepared to a final

concentration of 1×10^6 spores/ml saline. Supernatant containing spore toxins was obtained after spores were incubated for three hours and pelleted [19].

Incubation with *S. chartarum* spores

The method of *S. chartarum* spore toxin incubation was based on previous work [19] with modifications. Spore supernatant was diluted 1:100 in MEM/NCS without AB/AM/F and corresponding controls received sterile saline diluted 1:100 in MEM/NCS without AB/AM/F. Flasks with fibroblast monolayers were selected randomly (3 flasks per treated group; 2 flasks per corresponding controls) for incubation for 15 min, or 3, 14, or 24 h. Incubation was stopped by pouring off the medium and gently washing the cells with cold phosphate buffered saline ($1 \times$ PBS, Ca^{++} & Mg^{++} free, Trevigen, Inc., MD) three times. Cells were harvested immediately by carefully scrapping into cold PBS, and collecting into sterile centrifuge tubes, cell number determined using a Coulter Cell Counter. Cells were collected by centrifugation at low-speed (250xg) to obtain a pellet, which was gently resuspended in PBS (1×10^5 cells/ml) for SCGE. The processing of cells was performed in semi-darkness to avoid UV-light damage to DNA and kept on ice to prevent DNA repair.

Single cell gel electrophoresis (Comet assay): alkaline method

SCGE was carried out according to the alkaline method using a CometAssay™ kit (Trevigen, Inc., MD). All four treated groups and corresponding controls were processed immediately and electrophoresed together in each experimental replication. Briefly, 50 μ l of cell suspension was mixed with 500 μ l of molten low-melt agarose (1% LMA in $1 \times$ PBS) and 75 μ l of this mixture was pipetted onto pretreated microscope slides (Cometslide™, Trevigen, Inc, MD) in duplicate per sample per treated group and

corresponding controls. The agarose solidified for approximately 10 min at 4°C in the dark before slides were immersed in prechilled lysis solution (2.5 M Sodium Chloride, 100 mM EDTA, pH 10, 10 mM Tris Base, 1% Sodium Lauryl Sarcosinate, and 1% Triton X-100) at 4°C for 45 min in darkness. Lysis treatment removes cell membranes, cytoplasm, nucleoplasm, and histones, leaving a nucleoid, embedded within the agarose, composed of nuclear material (DNA, RNA, and proteins) [26]. Slides were removed from the buffer and submerged in freshly prepared alkaline solution (NaOH, 200 mM EDTA, dH₂O, pH 14) at room temperature for 30 min in the dark to allow DNA unwinding [26]. Slides were placed in a horizontal gel apparatus and equilibrated with alkaline running buffer (freshly prepared, 300 mM NaOH, 1 mM EDTA, pH 13) before electrophoresis at 27 V/300 mA for 25 min at 4°C in darkness. Slides were removed and dehydrated in 80% ethanol for five min and air-dried overnight. Nuclear material was fixed and silver stained according to protocol using a CometAssay Silver Staining kit (Trevigen, Inc, MD) for subsequent DNA migration analyses.

Evaluation of DNA migration

100 cells were evaluated per group for each experiment. Comets were captured on slides using a light microscope (x10 objective) coupled to a CCD camera and image analysis system (Quantiscan, Biosoft, UK). Only definable 'nucleoids' or 'comets' (heads & tails) were analyzed. Classification was based on visual inspection. Since nucleoids had little or no measurable tail, they were designated 0. Comets were classified according to overall appearance and assigned a value of 1 (small length tail + gray shade = lowest damage), 2 (medium length tail + dark shade = medium damage), or 3 (long tail + darkest shade = highest damage) [27]. Comets were analyzed further and data were

recorded according to length of comet (total, head, and tail) and intensity (total, head, and tail). Tail length (TL) represents the distance of DNA fragment migration and was measured in μm using a calibrated scale in the ocular micrometer. Relative intensity was expressed as percentage (%DNA) and represents the amount of DNA contained within the head or tail [26]. False color was applied to each comet image to reveal subtle differences in densities that were difficult to distinguish in the silver-stained comet image. Statistical comparisons were done on the %DNA (head and tail) using Duncan's multiple range test and Statistica software (StatSoft, Inc, USA). Results were expressed as overall averages for each treatment and control groups from four experimental replications.

Results

SCGE or comet assay demonstrates the ability of negatively charged DNA fragments to migrate through agarose under an electrical field [26]. The first assumption is that supercoiled intact DNA is too large to migrate and is therefore confined to the nucleoid. In the present study, analysis of control cells revealed the absence of DNA migration (i.e. no measurable tails or $<5\text{-}10\ \mu\text{m}$) [Table 2A], which indicated that typical control fibroblast DNA remained intact within nucleoids. The second assumption is that fragmented DNA is free to travel from the nucleoid toward the anode when a current is applied, generating a comet-like pattern (i.e. head and tail). In principle, small sized pieces of DNA, unattached to the larger molecule, are capable of traveling some distance through the agarose whereas broken ends of the DNA strands still attached to the DNA structure, migrate (or rather stretch) short distances from the nucleoid [26]. The third assumption is that DNA fragmentation represents one form of damage caused by

exposure to a toxic agent; thus measurement of breakage is a way of expressing DNA damage [26]. Upon visual inspection, the majority of *S. chartarum* toxin-treated cells had definable heads with tails of different degrees of migration and intensity depending upon the time-course [Table 2B-D].

Differences in DNA migration and intensity patterns were observed between the treatment groups. Fibroblast DNA from the 15 min toxin exposure extended or stretched only a short distance upon electrophoresis, as evidenced by short comet tails [Table 2B:image]. Comet heads were denser than the corresponding tails, indicating that a larger percentage of DNA remained within the heads [Table 2B:graph]. Applying false color to the comet image provided additional evidence, with the area of highest density, the comet head, colored pink-white and the area of lower density, the comet tail, colored orange-red [Table 2: color bar]. Furthermore, the comet tails were shorter and comet heads were significantly denser compared to comets of the other treated groups [Table 2C-E]. These results suggest that the DNA from fibroblasts exposed to *S. chartarum* toxins for 15 min had low levels of damage hence the fragments may have been too large and/or still attached to the DNA molecule to travel extensively through the agarose upon electrophoresis.

DNA migration increased in those treatment groups exposed to longer spore toxin incubations, as evidenced by longer tails and smaller heads, with the most extensive DNA migration occurring in the 14 h incubation group [Table 2C-E:images]. The images alone did not provide enough visual details to distinguish the comets from each other and expose subtle differences between the groups. Relative intensity measurements revealed that the amount of DNA decreased in the heads and increased within the comet tails of

the 3, 14, and 24 h groups [Table 2C-E:graphs]. However fibroblast DNA from the group exposed to the spore toxin for 14 h had a significantly larger percentage of DNA in the tails, compared to the 3 and 24 h exposure times [Table 2D]. False color confirmed this finding, as evidenced by pink-white areas (highest density) within the tails [Table 2D:image]. Taken together, the results suggested that DNA from the fibroblasts exposed to toxins for 14 h was most likely highly fragmented and therefore the smaller breaks in the DNA were able to migrate efficiently through the agarose upon electrophoresis.

The extent of the migration of DNA from the 24 h toxin-treatment decreased, as evidenced by shorter comet tails (compared to the 14 h group) [Table 2E:image]. A subtle but significant detail was revealed after analysis of relative intensity, in that a smaller percentage of DNA had traveled through the agarose to the tail (76%) and a greater amount was left within the heads (18%) of the 24 h treatment group compared to the 14 h group [Table 2E:graph]. The false color provided additional support for this finding. The results from the 24 h treatment group did not differ significantly from those of the 3 h incubation period [Table 2C:graph]. This suggests that there was most likely less damage to developing lung fibroblast DNA after 24 h incubation compared to 14 h exposure to toxins, which resulted in fewer smaller fragments free to travel through the agarose upon electrophoresis.

Discussion

Over the last decade or so, SCGE (comet assay) has been used extensively to assess the genotoxic potential of a multitude of environmental substances [26-28]. The alkaline version of the assay is highly sensitive in detecting DNA fragmentation, particularly in the form of SSB and/or A-LS [26]. In the current study, SCGE

demonstrated that exposure to *S. chartarum* toxins induced some degree of fragmentation in developing lung fibroblast DNA in a time-dependent manner, beginning within 15 min of exposure, increasing up to 14 h, and decreasing after 24 h.

The fact that DNA was fragmented does not necessarily suggest that the *S. chartarum* toxins damaged the genetic material directly. Neither *S. chartarum* nor its toxins are considered carcinogenic (i.e. DNA-reactive), unlike other molds that produce toxins found to be directly mutagenic, e.g. aflatoxin and ochratoxin, through formation of DNA adducts [30]. However some mold toxins, e.g. Fumonisin B₁ (FB₁) produced by *Fumonisin* species, are considered non-DNA-reactive yet evidently damage DNA indirectly through cellular oxidative stress [31]. Similarly, in the current study DNA may have fragmented due to some cellular reaction(s) to the assault thus *S. chartarum* spores or toxins may have epigenetic capabilities.

Initial DNA breaks, demonstrated within 15 min of exposure, may have formed subsequent to immediate production of ROS, a collective term for oxygen-containing radicals (e.g. O₂⁻, ·OH) and species that can produce oxygen-containing radicals (e.g. H₂O₂, HOCl) [32]. Although ROS are generated in healthy cells through normal cellular metabolism, DNA may be damaged when cells are overwhelmed by an increase in ROS that cannot be removed effectively by normal antioxidant defense mechanisms [32]. SSB are the primary products of DNA damage from oxidative stress, either by damage to the DNA backbone due to oxidation degradation of sugar moieties [25] and/or through A-LS, which happens when bases (purines and/or pyrimidines) are lost, giving rise to SSB in alkaline solutions [32]. Exposure to an exogenous substance may set off a cascade of immune reactions leading to increased production of ROS in activated phagocytes, e.g.

macrophages and neutrophils [32]. Indeed, Ruotsalainen et al., [23] demonstrated that exposure to *S. chartarum* toxins *in vitro* resulted in an immediate increase in ROS in macrophages. Although most research has focused on ROS in phagocytic cells, *in vitro* studies have shown that other cells including fibroblasts increased production of ROS after exposure to exogenous substances, e.g. silica dust [33] or tumor necrosis factor- α (TNF- α), a proinflammatory cytokine [34]. In the current study, exposure to *S. chartarum* toxins may have initiated oxidative stress in developing lung fibroblasts resulting in low-level DNA fragmentation.

Concurrently, DNA fragmentation may have occurred indirectly through the actions of macrocyclic tricothecenes, toxins believed to be responsible for acute toxicity [13]. Tricothecenes are secondary metabolites produced by a number of mold species; they are structurally similar but differ according to the presence or absence of functional groups [35]. *S. chartarum* species generate satratoxins (F, G, & H), roridins, and verrucarins [9]. Macrocyclic tricothecenes produced by *S. chartarum* were shown to incorporate very quickly into lung cells [13]. A well-known cellular target of *S. chartarum* tricothecenes is the protein synthesis machinery (namely ribosomes) involved in initiation, elongation, and/or termination and the mode of action is inhibition of protein synthesis [20]. The *S. chartarum* species used in the current study is known to produce potent protein synthesis inhibitors, specifically satratoxin G and H [13, 19]. Satratoxins may have inhibited initially proteins involved in cellular defense mechanisms thereby contributing to the inability of fibroblasts to effectively remove ROS, resulting in damage to the DNA through oxidative stress.

In the present study DNA fragmentation increased in a time-dependent manner, from 3 h to 14 h exposure to *S. chartarum* toxins. The fact that longer incubations with spores resulted in increased damage was not unexpected since previous studies documented remarkable changes after approximately 3-24 hours of *S. chartarum* exposure, including elevated levels of TNF- α [18] and suppression of protein synthesis [20]. It is evident that tricothecenes target primarily the synthesis of proteins, as opposed to DNA synthesis. FB₁ tricothecene targeted predominantly protein synthesis, which consequently impaired the DNA synthesis cycle and decreased the level of DNA synthesis [36]. During the synthesis phase, DNA is fragmented for the purpose of replication therefore arresting or impairing this process by inhibiting the proteins involved (hence incomplete DNA replication) may have produced the SSB measured by SCGE. It is possible that DNA fragmentation in the current study was produced by alterations in synthesis of DNA in developing lung fibroblasts due to protein synthesis inhibition by tricothecenes.

On the other hand increased DNA fragmentation, after longer exposures, may have occurred due to the onset of apoptosis or oncosis, possibly initiated by oxidative stress. ROS have been demonstrated to induce both pathways of cell death [32]. Apoptosis and oncosis begin with an initial 'prelethal' reversible phase in which cellular and nuclear morphological changes are evident (e.g. DNA fragmentation) [37]. Indeed Yang et al., [22], with extracted macrophage DNA for agarose gel electrophoresis, observed DNA fragmentation—thought to be characteristic of apoptosis—after 4 h exposure to satratoxins *in vitro*, with marked fragmentation after 6 and 12 h incubation. However, Rand et al., [16] reported morphological characteristics, specifically

cytological and mitochondrial changes, consistent with the onset of oncosis in AT II cells. Unfortunately it was not obvious in the current investigation specifically which pathway, apoptosis or oncosis, was induced following exposure to *S. chartarum* toxins. Considering that both pathways may be induced after exposure to toxic agents [32], both pathways may involve similar signaling events (e.g. TNF- α) [34], and both pathways may include DNA fragmentation [37], differentiating between apoptosis and oncosis remains highly complex and requires further analyses beyond the scope of the present investigation. However DNA fragmentation observed in the present study was unmistakably demonstrated in developing lung fibroblasts following exposure to *S. chartarum* spores, and DNA breakage may have resulted from the onset of cell death, either apoptosis or oncosis, after 14 h exposure to *S. chartarum* toxins.

A particularly intriguing result from the present study was the decrease in DNA fragmentation observed after 24 h exposure to *S. chartarum* toxins. As mentioned, the first stage of cell death, the 'prelethal phase,' is thought to be potentially reversible. A common feature of this phase is DNA fragmentation, usually SSB (and/or rarely, double strand breaks) [32, 37]. SSB, whether from oxidative reactions or abasic sites, are not considered major forms of DNA damage mainly because cells developed complex repair mechanisms in order to maintain the integrity of genetic material [6] so that SSB may be repaired and rejoined efficiently by base-excision repair enzymes [25]. With this in mind, developing lung fibroblasts may have had the capability of repairing damaged DNA between 14 and 24 h exposure to the toxic spores thereby preventing complete cell death (necrosis).

In summary, the present study demonstrates clearly the fragmentation of DNA in developing lung fibroblasts in a time-dependent manner following *in vitro* exposure to *S. chartarum* toxins. What may be the impact of this discovery? The method used in the present study, which was *in vitro* exposure of fibroblast monolayers to *S. chartarum* toxins, did not involve other cells such as phagocytic cells. Some studies found satratoxin accumulation primarily within alveolar macrophages but not in fibroblasts [13]. The accumulation of granulomatous lesions composed of phagocytic cells and fibroblasts was also observed [13-15]. While it is possible that fibroblasts themselves are not specific targets of *S. chartarum* spores/toxins *in vivo*, there is an intimate association between macrophages, neutrophils, and fibroblasts in the inflammatory process. Activated phagocytic cells produce proinflammatory cytokines (e.g. TNF- α), which have been shown to induce oxidative stress in fibroblasts. In this way, the epigenetic effects of *S. chartarum* toxins on fibroblasts *in vivo* may be indirect, e.g. through macrophage production of TNF- α following exposure to *S. chartarum* toxins.

Furthermore, the period of rapid growth during development is especially vulnerable to environmental toxicants and the effects of exposure to substances capable of impacting genetic material, directly or indirectly, may not be apparent until adulthood [6]. It is interesting that tricothecenes (FB₁) produced by *Fumonisin* species, which are structurally related to tricothecenes produced by *S. chartarum*, were implicated recently as nongenotoxic (non-DNA-reactive) substances capable of inducing neoplasms through epigenetic properties [31]. Although *S. chartarum* is not considered carcinogenic, it would be worthwhile to elucidate specific mechanisms of DNA fragmentation as well as investigate the effect of chronic exposure to the epigenetic capabilities of this toxic mold.

Conclusions

SCGE is a useful method of measuring DNA damage caused by toxic agents. Damage was assessed in terms of DNA fragmentation, likely due to strand breaks. Analyses of the comets revealed that exposure to *S. chartarum* toxins resulted in increased DNA fragmentation in a time-dependent manner. The lowest level of damage occurred after 15 min while the most damage was found after 14 h. The observation that exposure to toxic spores for 24 h showed less damage suggests that developing lung fibroblasts may have the capability of responding effectively to spore toxin injury. Clearly, epigenetic capabilities of *S. chartarum* require further investigation.

References

1. Weibel, E.R., & Crystal, R.G. 1991. Structural organization of the pulmonary interstitium. In *The Lung*, R.G. Crystal, J.B. West, et al. (Eds). Raven Press, Ltd:New York, 369-380.
2. McGowan, S.E., & Torday, J.S. 1997. The pulmonary lipofibroblast (lipid interstitial cell) and its contributions to alveolar development. *Annu Rev Physiol.*, 59:43-62.
3. Fries, K.M., Blieden, T., Looney, R.J., Sempowski, G.D., Silvera, M.R., Willis, R.A., & Phipps, R.P. 1994. Evidence of fibroblast heterogeneity and the role of fibroblast subpopulations in fibrosis. *Clinical Immunology and Immunopathology*, 72, 283-292.
4. Grant, M.M., Cutts, N. R. & Brody, J. S. 1983. Alterations in lung basement membrane during fetal growth and type 2 cell development. *Dev. Biol.*, 97, 173-83.
5. Smith, B.T., & Post, M. 1989. Fibroblast-Pneumonocyte Factor. *American Journal of Physiology*, 257, L174-L178.
6. Suk, W.A., & Collman, G.W. 1998. Genes and the environment: their impact on children's health. *Environ. Health Perspect.*, 106, 817-820.
7. Fog-Nielsen, K. 2003. Mycotoxin production by indoor molds. *Fungal Genetics and Biology*, 39, 103-117.
8. Hossain, M.A., Ahmed, M.S., & Ghannoum, M.A. 2004. Attributes of *Stachybotrys chartarum* and its association with human disease. *Journal of Allergy and Clinical Immunology.*, 113, 200-208.
9. Miller, J.D., Rand, T.G., & Jarvis, B.B. 2003. *Stachybotrys chartarum*: cause of human disease or media darling? *Medical Mycology*, 41, 271-291.
10. Nikulin, M., Reijula, K., Stjernvall, T., Hintikka, E-L. 1997. Ultrastructure of conidia and hyphae of *Stachybotrys chartarum*. *Karstenia*, 37, 57-64.
11. Yike, I., Miller, M.J., Sorenson, W.G., Walenga, R., Tomashefski, J.F., & Dearborn, D.G. 2001. Infant animal model of pulmonary mycotoxicosis induced by *Stachybotrys chartarum*. *Mycopathologia*. 154, 139-152.
12. Nikulin, M., Reijula, K., Jarvis, B.B., Veijalainen, P., & Hintikka, E-L. 1997. Effects of intranasal exposure to spores of *Stachybotrys atra* in mice. *Fundamental and Applied Toxicology.*, 35, 182-188.
13. Gregory, L., Pestka, J.J., Dearborn, D.G., & Rand, T.G. 2004. Localization of satratoxin-G in *Stachybotrys chartarum* spores and spore-impacted mouse lung using immunocytochemistry. *Toxicol Pathol.*, 32, 26-34.

14. Gregory, L., Rand, T.G., Dearborn, D.G., Yike, I., & Vesper, S. 2002. Immunocytochemical localization of stachylysin in *Stachybotrys chartarum* spores and spore-impacted mouse and rat lung tissue. *Mycophthologia*, 156, 109-117.
15. Rand, T.G., White, K., Logan, A., & Gregory, L. 2002. Histological, immunohistochemical and morphometric changes in lung tissue in juvenile mice experimentally exposed to *Stachybotrys chartarum* spores. *Mycopathologia*, 156, 119-131.
16. Rand, T.G., Mahoney, M., White, K., & Oulton, M. 2002. Microanatomical changes in alveolar type II cells in juvenile mice intratracheally exposed to *Stachybotrys chartarum* spores and toxin. *Toxicol Sciences*, 65, 239-245.
17. McCrae, K.C., Rand, T., Shaw, R.A., Mason, C., Oulton, M.R., Hastings, C., Cherlet, T., Thliveris, J.A., Mantsch, H.H., MacDonald, J., & Scott, J.E. 2001. Analysis of pulmonary surfactant by Fourier-transform infrared spectroscopy following exposure to *Stachybotrys chartarum* (atra) spores. *Chem Phys of Lipids*, 110, 1-10.
18. Flemming, J., Hudson, B., & Rand, T.G. 2004. Comparison of inflammatory and cytotoxic lung responses in mice after intratracheal exposure to spores of two different *Stachybotrys chartarum* strains. *Toxicological Sciences*, 78, 267-275.
19. Hastings, C., Rand, T.G., Bergen, H.T., Thliveris, J.A., Shaw, R.A., Lombaert, G.A., Mantsch, H.H., Giles, B.L., Dakshinamurti, S., & Scott, J.E. 2004. 2002. *Stachybotrys chartarum* alters surfactant-related phospholipids synthesis and CTP:cholinephosphate cytidylyltransferase activity in isolated fetal rat type II cells. *Toxicol. Lett.*, (submitted).
20. Lee, M-G., Jarvis, B.B., & Pestka, J.J. 1999. Effects of satratoxins and other macrocyclic tricothecenes on IL-2 production and viability of EL-4 thymoma cells. *J Toxicol and Environ Health*, 57, 459-474.
21. Vesper, S.J., Magnuson, M.L., Dearborn, D.G., Yike, I., & Haugland, R.A. 2001. Initial characterization of the hemolysin stachylysin from *Stachybotrys chartarum*. *Infection and Immunity*, 69, 912-916.
22. Yang, G-H., Jarvis, B.B., Chung, Y-J., & Pestka, J.J. 2000. Apoptosis induction by the satratoxins and other tricothecene mycotoxins: relationship to ERK, p38 MAPK, and SAPK/JNK activation. *Toxicol and Appl Pharmacol*, 164, 149-160.
23. Ruotsalainen, M., Hirvonen, M-R., Hyvarinen, A., Meklin, T., Savolainen, K., & Nevalainen, A. 1998. Cytotoxicity, production of reactive oxygen species and cytokines induced by different strains of *Stachybotrys* sp. from moldy buildings in RAW264.7 macrophages. *Environ Toxicol and Pharmacol*, 6, 193-199.
24. Trump, B.F., Berezesky, I.K., Chang, S.H., & Phelps, P.C. 1997. The pathways of cell death: oncosis, apoptosis, and necrosis. *Toxicol Pathol*, 25, 82-88.

25. Scharer, O.D. 2003. Chemistry and biology of DNA repair. *Angewandte Chemie International*, 42, 2946-74.
26. Collins, A.R. 2004. The comet assay for DNA damage and repair. *Molecular Biotechnology*, 26, 249-261.
27. Faust, F., Kassie, F., Knasmuller, S., Bodecker, R.H., Mann, M., & Mersch-Sundermann, V. 2004. The use of the alkaline comet assay with lymphocytes in human biomonitoring studies. *Mutat. Res.*, 566, 209-229.
28. Henderson, L., Wolfreys, A., Fedyk, J., Bourner, C., & Windebank, S. 1998. The ability of the comet assay to discriminate between genotoxins and cytotoxins. *Mutagenesis*, 13, 89-94.
29. Batenburg, J.J., Otto-Verberne, S.J.M., Ten Have-Opbroek, A.A.W., & Klazinga, W. 1988. Isolation of alveolar type II cells from fetal rat lung by differential adherence in monolayer culture. *Biochim. Biophys. Acta*, 960, 441-453.
30. Kuhn, D.M., & Ghannoum, M.A. 2003. Indoor mold, toxigenic fungi, and *Stachybotrys chartarum*: infectious disease perspective. *Clinical Microbiology Reviews*, 16, 144-172.
31. Dragan, Y.P., Bidlack, W.R., Cohen, S.M., Goldsworthy, T.L., Hard, G.C., Howard, P.C., Riley, R.T., & Voss, K.A. 2001. Implications of apoptosis for toxicity, carcinogenicity, and risk assessment: Fumonisin B1 as an example. *Toxicol Sci*, 61, 6-17.
32. Halliwell, B., & Arumo, O.I. 1991. DNA damage by oxygen-derived species. *FEBS*, 281, 9-19.
33. Kim, K-A., Kim, Y-H., Seo, M.S., Lee, W.K., Kim, S.W., Kim, H., Lee, K-H., Shin, I-C., Han, J-S., Kim, H.J., & Lim, Y. 2002. Mechanism of silica-induced ROS generation in Rat2 fibroblast cells. *Toxicol Lett*, 135, 185-191.
34. Lin, Y., Choksi, S., Shen, H-M., Yang, Q-F., Mur, G.M., Kim, Y.S., Tran, J.H., Nedospasov, S.A., & Liu, Z-G. 2004. Tumor necrosis factor-induced nonapoptotic cell death requires receptor-interacting protein-mediated cellular reactive onxygen species accumulation. *J Biological Chemistry*, 279, 10822-10828.
35. Sudakin, D.L. 2003. Tricothecenes in the environment: relevance to human health. *Toxicol Lett*, 143, 97-107.
36. Mobio, T.A., Anane, R., Baudrimont, I., Carratu, M-R., Shier, T.W., Dano, S.D., Ueno, Y., & Creppy, E.E. 2000. Epigenetic properties of Fumonisin B1: cell cycle arrest and DNA base modification in C6 glioma cells. *Toxicol and Appl Pharmacol*, 164, 91-96.

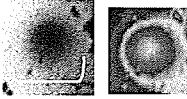
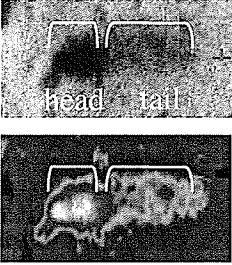
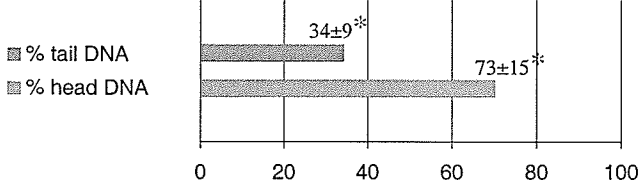
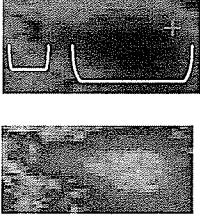
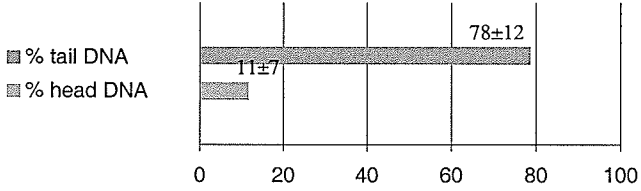
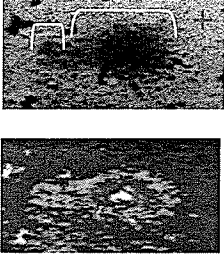
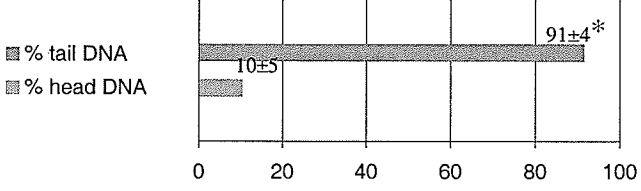
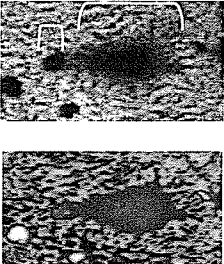
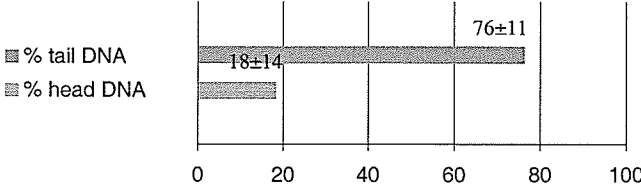
37. Trump, B.F., & Berezesky, I.K. 1994. Cellular and molecular pathobiology of reversible and irreversible injury. In *Methods in Toxicology, Vol 1B, In Vitro Toxicity Indicators*. C.A. Tyson, J.M. Frazier (Eds.). Academic Press:New York, 1-22.

Table 1: Effect of *S. chartarum* exposure

Tissue/cell examined	<i>S. chartarum</i> strains and/or toxins, dose, method & exposure duration		Key consequences of exposure	Ref	
Lung tissue & lung function	s.58-17	1.0-8.0x10 ⁵ spores/gBW	1 IT of 20 µl 3 & 8 days	<ul style="list-style-type: none"> inflammation high dose: pulmonary hemorrhage low dose: altered lung function 	11
Lung tissue	s.72 & s.29	1x10 ³ & 1x10 ⁵ spores/ml	1 IN of 50 µl (total 6 IN) 2x per week over 3 weeks	<ul style="list-style-type: none"> high dose s.72: severe inflammation low dose s.72 & high dose s.29: milder inflammation absence of necrosis 	12
Lung tissue	s.58-17	1.4x10 ⁶ spores/ml	1 IT of 50 µl 48 h	<ul style="list-style-type: none"> granuloma lesions around spores SG accumulation within alveolar macrophages, in lysosomes, in nuclear heterochromatin, & RER 	13
Lung tissue	s.58-17 & s.58-06	1.4x10 ⁶ spores/ml	1 IT of 50 µl 24 & 72 h	<ul style="list-style-type: none"> SL accumulation in granulomas (largest accumulation after 72) SL localization in macrophages 	14
Lung tissue	s.58-17 SF	1.4x10 ⁶ conidia/ml; 35ng/kgBW	1 IT of 50 µl 12, 24, 48, 72, & 96 h	<ul style="list-style-type: none"> granulomatous inflammation ↑ severity with ↑ exposure time depressed collagen synthesis ↓ alveolar air space over time 	15
Lung: AT II cells	s.58-17 SF	1.4x10 ⁶ conidia/ml; 35ng/kgBW	1 IT of 50 µl 24 & 48 h	<ul style="list-style-type: none"> prelethal oncotic changes mitochondrial condensation ↑ LB volume density 	16
Lung: PS	s.002	1x10 ⁷ conidia/ml	1 IT of 50 µl 24 h	<ul style="list-style-type: none"> ↑ lysophospholipid levels ↓ concentration of extracellular PL ↑ intracellular PS levels 	17
Lung: PS	s.58-17 & s.58-06	30, 300, 3000 spores/gBW	1 IT of 50 µl 3, 6, 24, 48, & 96 h	<ul style="list-style-type: none"> dose-dependent inflammatory and cytotoxic responses moderate to high doses: lung response within 24 h 	18
Lungs: PS synthesis by AT II cells	s.58-17 & s.002	varying dilutions	<i>In vitro</i> 15, 30, 60, & 120 min	<ul style="list-style-type: none"> inhibit production of major PS phospholipids, namely dipalmitoyl-phosphatidylcholine (DPPC) 	19
EL-4 thymoma cells	SG, SH, SF, RA, VA	varying doses (ng/ml)	<i>In vitro</i> 24 & 72 h	<ul style="list-style-type: none"> low dose: induce protein production high dose: inhibit protein production 	20
Red blood cells	SL	0.2 µg	<i>In vitro</i> 15, 30 min, 1, 6, 24, 48 h 24 & 72 h	<ul style="list-style-type: none"> slow-acting hemolysis remarkable changes after 15 min lysis begun after 24 h complete lysis after 48 h 	21
Macrophage (RAW 264.7) & leukemic cells (U937)	SF, SG, SH, RA, VA	5 & 10 ng/ml	<i>In vitro</i> 4 & 6 h	<ul style="list-style-type: none"> highly cytotoxic & apoptotic: SG, RA, VA moderately cytotoxic & apoptotic: SF, SH activate signal transduction pathway 	22
Macrophage (RAW 264.7)	>20 strains	10 ³ -10 ⁶ spores/ml	24 h	<ul style="list-style-type: none"> immediate production of ROS produced inflammatory mediators 	23

Satratoxins-F, G, H, roridin A (RA), verrucarin A (VA); stachylysin (SL); intratracheal instillation (IT), intranasal instillation (IN); rough endoplasmic reticulum (RER); lamellar bodies (LB); pulmonary surfactant (PS); phospholipid (PL); reactive oxygen species (ROS)

Table 2: DNA fragmentation analyses

Comet images & false color application**	Comet classification and % DNA in heads and tails						
 <p style="text-align: center;">nucleoid</p>	<p>A. Control fibroblast Classification: 0</p>						
 <p style="text-align: center;">Mean TL: 50.2±21 μm</p>	<p>B. 15 min treatment Classification: 1</p>  <table border="1"> <caption>Data for 15 min treatment</caption> <thead> <tr> <th>Category</th> <th>Value (Mean ± SD)</th> </tr> </thead> <tbody> <tr> <td>% tail DNA</td> <td>34 ± 9*</td> </tr> <tr> <td>% head DNA</td> <td>73 ± 15*</td> </tr> </tbody> </table>	Category	Value (Mean ± SD)	% tail DNA	34 ± 9*	% head DNA	73 ± 15*
Category	Value (Mean ± SD)						
% tail DNA	34 ± 9*						
% head DNA	73 ± 15*						
 <p style="text-align: center;">Mean TL: 71.9±15 μm</p>	<p>C. 3 hr treatment Classification: 2</p>  <table border="1"> <caption>Data for 3 hr treatment</caption> <thead> <tr> <th>Category</th> <th>Value (Mean ± SD)</th> </tr> </thead> <tbody> <tr> <td>% tail DNA</td> <td>11 ± 7</td> </tr> <tr> <td>% head DNA</td> <td>78 ± 12</td> </tr> </tbody> </table>	Category	Value (Mean ± SD)	% tail DNA	11 ± 7	% head DNA	78 ± 12
Category	Value (Mean ± SD)						
% tail DNA	11 ± 7						
% head DNA	78 ± 12						
 <p style="text-align: center;">Mean TL: 102.1±8 μm</p>	<p>D. 14 hr treatment Classification: 3</p>  <table border="1"> <caption>Data for 14 hr treatment</caption> <thead> <tr> <th>Category</th> <th>Value (Mean ± SD)</th> </tr> </thead> <tbody> <tr> <td>% tail DNA</td> <td>10 ± 5</td> </tr> <tr> <td>% head DNA</td> <td>91 ± 4*</td> </tr> </tbody> </table>	Category	Value (Mean ± SD)	% tail DNA	10 ± 5	% head DNA	91 ± 4*
Category	Value (Mean ± SD)						
% tail DNA	10 ± 5						
% head DNA	91 ± 4*						
 <p style="text-align: center;">Mean TL: 83.1±20 μm</p>	<p>E. 24 hr treatment Classification: 2</p>  <table border="1"> <caption>Data for 24 hr treatment</caption> <thead> <tr> <th>Category</th> <th>Value (Mean ± SD)</th> </tr> </thead> <tbody> <tr> <td>% tail DNA</td> <td>18 ± 14</td> </tr> <tr> <td>% head DNA</td> <td>76 ± 11</td> </tr> </tbody> </table>	Category	Value (Mean ± SD)	% tail DNA	18 ± 14	% head DNA	76 ± 11
Category	Value (Mean ± SD)						
% tail DNA	18 ± 14						
% head DNA	76 ± 11						

* $p > 0.001$ compared to other treated groups; * $p > 0.05$ compared to % DNA in tail of 24 hr group;

color density indication: **low  **high**; + indicates direction of DNA migration

General conclusions

Lung cancer

FTIR spectroscopic analyses demonstrated that (1) neoplastic mouse lung tissue has a biochemical composition, or fingerprint, discernible from the biochemical fingerprint of normal tissue, (2) excised human lung lesions have unique biochemical fingerprints, (3) although FTIR spectra reflected the overall biochemical composition of lung tissues, (i.e. absorption bands assigned to molecules associated with lipids, proteins, and DNA), very subtle absorptions signified structural characteristics of DNA of neoplastic lung specimens, and (4) silver-coated glass reflectance slides can be modified to culture neoplastic cells for FTIR microspectroscopy.

So what is the impact of the present studies? Studying changes to the physical and chemical nature of DNA may provide valuable insight into neoplastic transformation of lung cells. Analyzing neoplastic cell populations in culture may be necessary to elucidate unique spectroscopic characteristics, which could be used to differentiate neoplastic lesions. From a clinical perspective, FTIR spectroscopy may be useful as an ancillary technique to light microscopy, for classifying neoplastic tissues based on unique biochemical fingerprints.

Pulmonary surfactant: hypercholesterolemia

The CS studies demonstrated that (1) a relatively simple mouse model was created to study the effects of excess cholesterol on PS, (2) dietary intake of excess cholesterol altered the composition and function of PS, (3) at physiological temperature, SAF obtained from both healthy and tumor-bearing hypercholesterolemic mice, which consisted of an increased amount of cholesterol relative to phospholipid, had diminished

ability to maintain continuous airflow through the narrow capillary tube, compared to SAF from healthy and tumor-bearing control mice, and (4) at phospholipids phase-transition temperatures, the ability of the SAF, with increased cholesterol, to maintain unobstructed airflow was comparable to control SAF.

So what is the impact of the current studies? An animal model may be helpful to understand the influence of excess serum cholesterol on PS *in vivo*. CS is a relatively simple way of studying surface-active material like PS in terms of resistance to airflow and patency, thereby simulating conditions within the smallest conducting airways. From a clinical perspective, altered PS composition (e.g. excess cholesterol) may diminish PS ability to function in the smallest airways leading to the formation of liquid occlusions, which could decrease ventilation to the affected alveolar sacs. Also interesting from a clinical perspective is the influence of temperature on PS function (e.g. 37°C vs. 42°C) and it is intriguing to speculate whether PS composition is altered depending upon body temperature, e.g. increasing the amount of cholesterol in the SAF in response to an increase in body temperature.

Pulmonary toxins: *Stachybotrys chartarum*

Studies involving *in vivo* exposure of mice to *S. chartarum* spores demonstrated (1) changes to intracellular PS (e.g. elevated phospholipid levels), and (2) decreased extracellular PS levels with concomitant increased lysophospholipid levels. Studies involving *in vitro* exposure of developing lung fibroblasts to *S. chartarum* spore toxins revealed that (3) DNA fragmentation occurred in a time-dependent manner (beginning within 15 minutes and increasing significantly after 14 hours), and (4) DNA fragmentation decreased significantly after 24 h exposure.

So what is the impact of these current studies? The *S. chartarum* spore/toxins may have evolved some mechanism to alter the PS-producing function of AT II cells, or some cellular reaction (e.g. inflammation) to the spores may influence the primary function of AT II cells, or perhaps a combination of the two. Spore toxins may have epigenetic properties (e.g. through production of ROS), as evidenced by the time-dependent fragmentation of fibroblast DNA. Developing lung fibroblasts may have sufficient mechanisms to repair fragmented DNA, as evidenced by decreased fragmentation after a period of exposure.

From a clinical perspective, exposure to *S. chartarum* spores appears to have an effect on PS phospholipid composition and consequently PS function, which may diminish surface tension-reducing capabilities—resulting in atelectasis—and may lead ultimately to altered ventilation. Fibroblasts are important cells in lung tissue development and maintenance however long-term effects of DNA damage due to toxin exposure may not be evident for many years. Further to that, fibroblasts respond to injury and inflammation through proliferation and fibrotic tissue development. Therefore it is intriguing to speculate whether chronic exposure to *S. chartarum* spore/toxins may lead ultimately to development of pulmonary fibrosis.

Taken together, the current studies contributed to better understanding of the pulmonary system in terms of alterations to lung cell biochemistry, changes to surface tension-reducing properties of PS, and consequences of exposure to pulmonary toxins. Better understanding of reversible and non-reversible respiratory conditions may lead to better prevention and intervention strategies.